Appendix A

Plume Evaluation Field Sampling Plan for Operable Unit 3-13, Group 5 Snake River Plain Aquifer

DOE/ID-10784
Revision 1

[The document that is the subject of this appendix was provided as an attachment to the original deliverable.]

Appendix B

Long-Term Monitoring Plan for Operable Unit 3-13, Group 5 Snake River Plain Aquifer

DOE/ID-10783
Revision 1

[The document that is the subject of this appendix was provided as an attachment to the original deliverable.]

Appendix C

Groundwater Numerical Modeling Support for the Idaho Nuclear Technology Engineering Center, Operable Unit 3-13 Group-5 Interim Action

TABLE OF CONTENTS

LIST OF FIGURES

LIST OF TABLES

Appendix C

Groundwater Numerical Modeling Support for the Idaho Nuclear Technology Engineering Center, Operable Unit 3-13 Group-5 Interim Action

1 INTRODUCTON

Modeling of the Snake River Plain Aquifer for the WAG-3 (Waste Area Group 3) Operable Unit (OU) 3-13 Remedial Investigation/Baseline Risk Assessment (RI/BRA) (DOE-ID, 1997) predicted a risk beyond the year 2095 to groundwater users due to groundwater concentrations of I-129 and Sr-90 predicted to remain in the low-hydraulic conductivity HI sedimentary interbed. However, only a limited amount of empirical data is available to confirm the physical properties of the HI interbed as assumed in the OU 3-13 RI/BRA model and there is no data regarding the presence or absence of contaminants in the interbed. Empirical evidence of the HI interbed contamination and permeability is required to verify the model predictions and refine the model parameterization.

Sensitivity of the model parameterization was performed to identify key data needs and support field activities to collect empirical data. The Iodine 129 isotope (I-129) was chosen as the indicator contaminant for model sensitivity because it is long lived and it was predicted to present the greatest long term risk within the interbed. A refined and recalibrated model was then used to determine if contamination within the HI interbed still presents a risk to groundwater users. The refined and recalibrated model represents a first effort in updating the WAG-3 conceptual model with more recent data. However, the new model needs to incorporate data from the HI interbed sampling/characterization effort before the predictive simulations can be relied upon.

The tasks performed to refine the model and to assess sensitivity were: (1) review of the OU 3-13 RI/BRA model, (2) review of the I-129 source term in the model, (3) review of the existing HI interbed thickness and elevation data, (4) rediscretization of the OU 3-13 RI/BRA (hereafter referred to as "rediscretized") model to include all the existing interbed data, (5) sensitivity analysis of HI interbed discretization, (6) review of the HI interbed permeability data, (7) sensitivity analysis of HI interbed permeability, (8) recalibration of the rediscretized model (hereafter referred to as "updated"), and (9) predictive simulations with the updated model for the beta/gamma radiation emitting contaminants of concern (COCs) identified in the RI/BRA. The predictive simulations were performed to assess the cumulative aquifer risk and estimate concentrations of other radionuclides, which may need to be addressed if remediation is needed.

The results of performing these tasks are documented in this report. Section 2 presents a review of the RI/BRA aquifer model and the I-129 simulations. Section 3 presents the sensitivity analysis of the HI interbed parameterization. Section 4 presents the updated model calibration and predictive simulations. Section 5 presents modeling data needs, and Section 6 provides a modeling path forward.

2 REVIEW OF THE WAG-3 OU 3-13 RI/BRA AQUIFER MODEL

The OU 3-13 RI/BRA modeling was performed using the TETRAD multi-purpose simulator (Vinsome and Shook, 1993). Two separate models were used to represent the vadose zone and aquifer beneath the Idaho Nuclear Technology Engineering Complex (INTEC). The basis for these two conceptual models are briefly presented here. A detailed description of the OU 3-13 RI/BRA models can be found in Appendix F, DOE-ID (1997).

2.1 OU 3-13 RI/BRA Aquifer Model Parameterization

The physical and hydrogeologic setting of the INTEC is highly complex, consisting of layers of basalt and sediments. In the vadose zone, the sedimentary interbeds are often saturated, forming perched water zones. The geology of the aquifer region is more uniform in the vertical direction than the geology of the vadose zone. The aquifer basalt structures tend to be thicker, and the sedimentary interbeds are fewer in number. USGS studies (Anderson, 1991) indicate that aquifer in the region north of the INTEC and extending south of the RWMC is comprised primarily of the H basalt flow, the HI interbed, and the I basalt flow. The I basalt flow is significantly thicker (Anderson, 1991) and may have a lower permeability than the H basalt flow because the high permeability inter-flow rubble zones represent a smaller fraction of the total flow thickness. The HI interbed separates the two basalt flows.

The RI/BRA aquifer model incorporated the I basalt flow, the HI interbed, and the H basalt flow. The aquifer model domain extends from approximately 2.5 km north of the INTEC facility to the southern INEEL boundary in the north-south direction and approximately 6.5 km east of the INTEC facility to slightly west of the RWMC facility in the east-west direction. The model was discretized into 400 x 400 x 7.6 m grid blocks as shown in Figures 2-1 and 2-2. Local refinement corresponding to the discretization level applied in the vadose zone model is used for the footprint of the INTEC (200 x 200 m grid) and also in the vicinity of TRA. This local refinement was only in the top 7.6 m of the aquifer model.

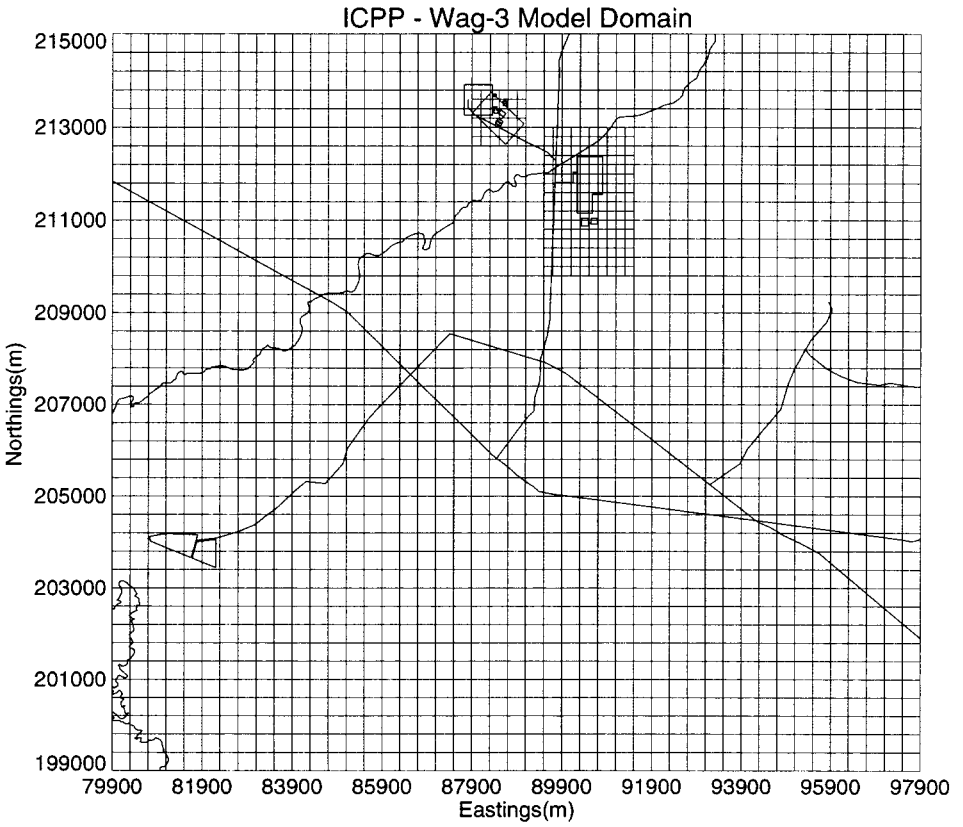

Figure 2-1 Aquifer model domain.

The vertical aquifer domain extends downward from an elevation of 1,360 m to 1,284 m. This total depth was chosen to be below the completion intervals of the primary INTEC pumping and injection wells and from the effective aquifer thickness estimated by Robertson (1974).

The aquifer model used four distinct stratigraphic types. These include an upper I basalt unit, a lower I basalt unit, the HI interbed, and the H basalt. The upper I basalt structure was assigned permeabilities representative of those obtained from aquifer testing of the INTEC pumping and injection wells. The lower I basalt and H basalt structure used regional permeabilities taken from the WAG-10 modeling effort (McCarthy et al., 1995). The H basalt structure in the vicinity of the vadose zone foot print was assigned local INTEC permeabilities from the pumping tests.

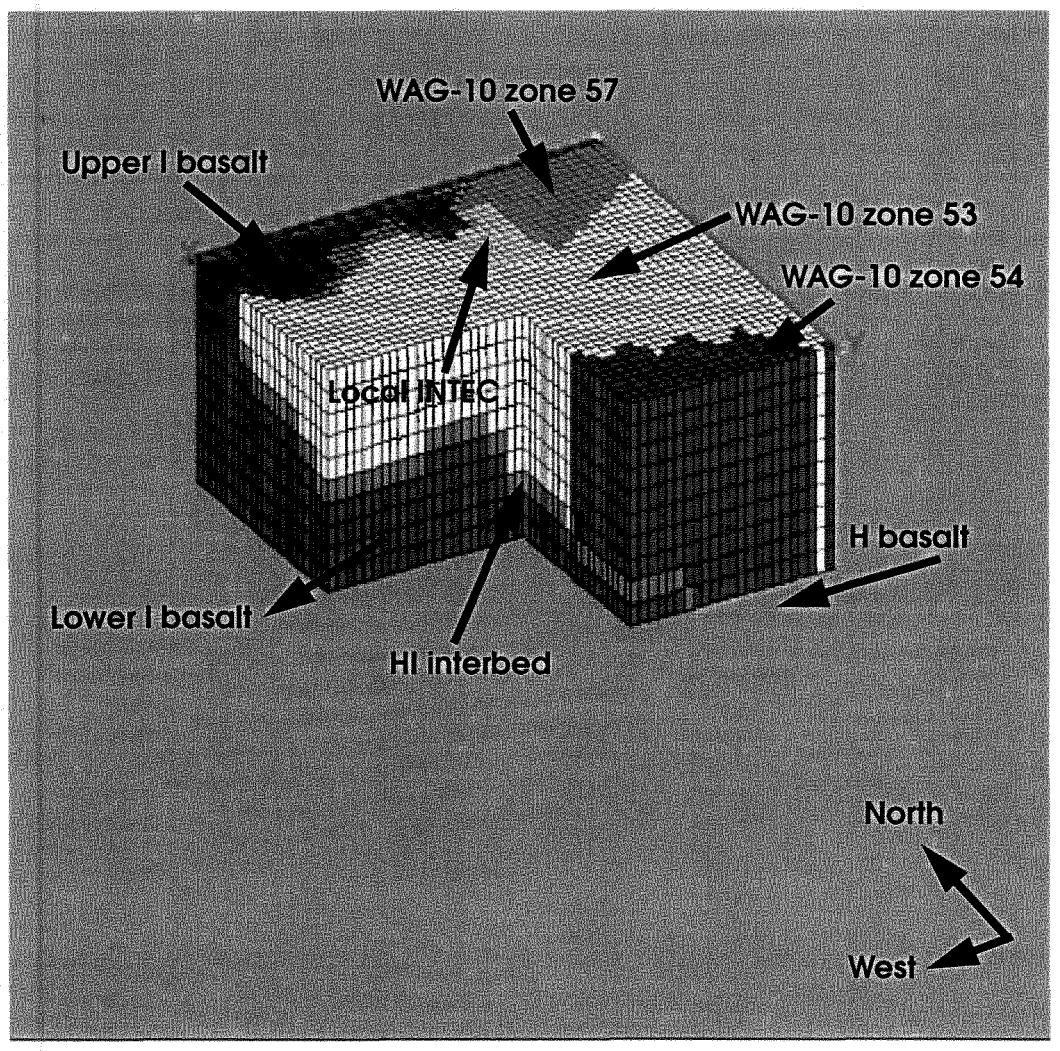

Figure 2-2 3-D Aquifer model representation

The I basalt flow, HI interbed and H basalt unit were combined into a three-dimensional domain by preserving the I basalt flow top and assumed thickness to the bottom of our modeling domain. As illustrated in Figure 2-2, the I basalt flow rises above the water table along the north to northwest boundary. The slope of the I basalt flow near the north west of the region shown is steeply angled downward. High dip angles may be associated with more fractures which means that the top of the I basalt flow will exhibit higher permeability, with the permeability decreasing in the flatter regions to the south. This distinction between an upper and lower I basalt region is indicated by dark blue and violet shades in Figure 2-2, respectively. The turquoise shade region represents the HI sedimentary interbed. The vertical discretization throughout the model is uniform at a spacing of 7.6 m. The uniform vertical discretization fixes the HI interbed to be 7.6 m thick.

The hydraulic conductivities used in the aquifer model were first interpolated onto the WAG-3 model grid from the WAG 10 regional groundwater flow model. This model used an Eastern Snake River Plain regional water balance to define the boundaries in order to ensure a water mass balance through the Eastern Snake River Plain aquifer. The permeabilities used in the WAG 10 model are shown in Figure 2-3 and given for the INTEC region in Table 2-1.

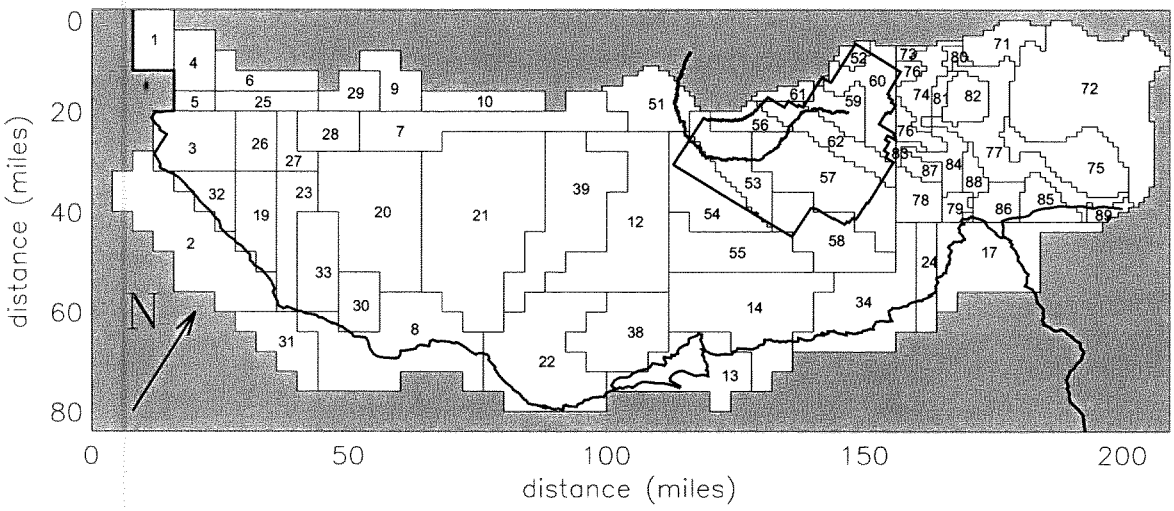

Figure 2-3 Wag 10 hydraulic conductivity zones and model domain.

Table 2-1 WAG-10 permeability and hydraulic conductivity in the vicinity of the INTEC.

WAG 10 K Zone	Permeability (mD)	Hydraulic Conductivity (ft/day)	Comment
53	170,000	459	INTEC is in this zone
54	1,800,000	4,925	This zone is south of the INTEC.
57	370,000	1,002	This zone is east of the INTEC.

The upper I basalt unit, lower I basalt unit, and the HI interbed are the dominant stratigraphic features in the saturated zone. It is hypothesized that the upper I basalt flow and lower I basalt flow differ hydraulically because the I basalt flow dips steeply near the north to northwest boundary of our model domain. This dip means that the top of that basalt flow is probably more highly fractured and thus exhibits higher permeability, with the permeability decreasing in the flatter regions to the south. Distinguishing an upper and lower I basalt region was done by assigning a value representative of the permeabilities taken from pumping tests of wells CPP-01, CPP-02, and CPP-3 to the upper I basalt region, and assigning one half of the lowest WAG-10 INTEC permeability (8.5e4 mDarcy) to the lower I basalt region. These values replaced the WAG-10 permeabilities in grid blocks containing the I basalt flow.

To be consistent with the sediment properties used in the vadose zone interbeds, a permeability of 4 mD (0.01ft/day) and porosity of 0.487 was assigned to the first layer of grid blocks overlying the I basalt flow. The vadose zone interbed permeability was determined by calibrating to perched water depth in the vadose zone. Assigning sediment properties uniformly over the I flow assumed that the HI interbed is 7.6 m thick and exists everywhere the I basalt flow is below the water table. The porosity for the aquifer model basalt was 0.0625. This value was derived from calibration of the aquifer model to tritium disposal records and the corresponding tritium sampling results from wells in the vicinity of and down gradient of the INTEC.

The final level of refinement for basalt hydraulic conductivities in the INTEC aquifer model was to incorporate INTEC local scale field data. These local scale hydraulic conductivities were initially applied

throughout the vertical profile defined by the footprint of the vadose zone model. These values were then slightly adjusted by setting a minimum value at 18,000 mD to prevent excessive mounding beneath the Big Lost River.

The Big Lost River flows across the aquifer model domain and infiltration from the Big Lost River was applied directly in the aquifer model outside the area of the vadose zone footprint. Infiltration within the footprint was accounted for indirectly through the water flux from the vadose zone model. In addition to the Big Lost River, there are three other primary water sources influencing the aquifer heads. These were pumping from CPP-01, CPP-02 and CPP-04; reinjection into CPP-03; and recharge from percolation ponds. The pumping and injection wells were simulated in the aquifer model. Water from the percolation ponds was accounted for indirectly from the vadose zone model flux.

The boundary conditions for the aquifer model were specified flux at the surface, which included the water sources discussed above, no flux at the bottom, and specified heads on the sides. The specified heads were interpolated from the WAG-10 model.

2.2 OU 3-13 RI/BRA Aquifer Model Calibration

The OU 3-13 RI/BRA aquifer flow model relied on the WAG-10 model calibration (McCarthy et al., 1994) and the hydraulic parameters were not adjusted in the transport calibration process. Calibration of the transport model parameters (porosity and dispersivity) used the tritium disposal history in the CPP-03 injection well. The tritium disposed in CPP-03 provided fair calibration data because the inventory disposed to the injection well is fairly well defined and there is a long historical record (1953-present) from USGS wells located down gradient. Figure 2-4 illustrates the CPP-3 injection well tritium disposal history used in the RI/BRA aquifer model calibration. A more detailed description of the RI/BRA tritium calibration can be found in Appendix F, DOE-ID (1997).

The match between RI/BRA simulated hydraulic head and tritium concentrations and the observed values was evaluated with both qualitative and quantitative criteria. The RI/BRA model agreement with observed values has been assessed to provide a standard for calibration of the updated aquifer model. The qualitative criteria included simulated contour maps of the spring 1999 hydraulic head measurements with observed data plotted on the maps, and simulated tritium breakthrough curves at USGS observation wells with observed tritium concentrations overplotted on the curves. The spring 1999 hydraulic head measurements were chosen to evaluate the flow model because this data set is more comprehensive for a single time period than the data sets available when the RI/BRA modeling was performed.

Three quantitative indicators were chosen to measure the agreement between field data and simulation results: (1) the root mean square (RMS) error, (2) a modified version of the root mean square (ModRMS) error, and (3) the correlation coefficient. The RMS error was used to evaluate the match between observed and simulated hydraulic head. The RMS error provides a good estimation of the average error throughout the data set and is defined as:

$$RMS = \sqrt{\frac{\sum_{i=1}^{k} (s_i - f_i)^2}{k}} \qquad (1)$$

where

f_i = field data point

s_i = simulation data point

k = number of comparison points.

The ModRMS error was used to evaluate the match between observed and simulated tritium concentrations. The modification was to divide the RMS error by the average measured tritium concentration at each observation well, over the observation period at each well. The modification allows distal wells with much lower tritium concentrations to have a similar weight on the overall RMS error as the near wells which have tritium concentrations several orders of magnitude higher. The more traditional relative mean square error (i.e., the error term s_i-f_i in Equations 1 and 2 is replaced by $(s_i$-$f_i)/f_i)$ could not be used because tritium concentrations are zero before and after the breakthrough and result in division by zero. Smaller values of the ModRMS error indicate a better agreement between simulated and observed values. The ModRMS error is most useful for comparing the performance of the updated model with the RI/BRA model. The ModRMS is defined as:

$$ModRMS = \frac{\sqrt{\frac{\sum_{i=1}^{k}(s_i - f_i)^2}{k}}}{\frac{\sum_{i=1}^{k} f_i}{k}}. \qquad (2)$$

The correlation coefficient was used to evaluate the agreement of the simulated and observed tritium breakthrough curve shape. The correlation coefficient measures the degree to which there is a linear correlation between two data sets. A perfectly linear relationship between data sets would result in a correlation coefficient of 1. Independent data sets would have a correlation coefficient of 0. Data sets which have a linear relationship, but trend in different directions will have a negative correlation coefficient. The correlation coefficient (r) is defined as:

$$r = \frac{k\sum_{i=1}^{k} s_i f_i - \sum_{i=1}^{k} s_i \sum_{i=1}^{k} f_i}{\sqrt{\left[k\sum_{i=1}^{k} s_i^2 - \left(\sum_{i=1}^{k} s_i\right)^2\right]\left[k\sum_{i=1}^{k} f_i^2 - \left(\sum_{i=1}^{k} f_i\right)^2\right]}}. \qquad (3)$$

The RI/BRA model's hydraulic head RMS error over all wells within the model domain was 1.6 m. The RI/BRA model's steady-state flow field with spring 1999 measured hydraulic head is presented in Figures 2-5 and 2-6. The RI/BRA model's tritium breakthrough average ModRMS error over all monitoring wells was 1.98 and the average correlation coefficient of all the calibration wells was 0.239. The ModRMS and correlation coefficient were calculated at the model grid block closest to the well screen center. Figures 2-7 and 2-8 illustrates the locations of the tritium breakthrough calibration wells and Figure 2-9 illustrates model predicted breakthrough and observed tritium concentrations for each well. Wells outside of the observed CPP-3 injection well tritium plume and wells with less than observed 2 data points were excluded from the ModRMS error and correlation coefficient calculation and Figure 2-9. Four data sets are plotted on each well's breakthrough plot: (1) observed concentration (thin black line with a cross data symbol), (2) simulated well screen center (thick red line), (3) simulated concentration at the aquifer top (thin dashed green line), and (4) simulated concentration at the aquifer bottom (thin blue line).

Two problems can be seen in the tritium disposal and breakthrough data sets. The first problem is tritium disposal prior to 1962 was reported as an annual average and the disposal data after 1962 suggests there may have been significant monthly variation in tritium disposal. The second problem is the highest observed tritium concentration in wells nearest the injection well (USGS-47, USGS-43, and USGS-41) occurs in 1962

while the disposal history indicates very little tritium was disposed during this time. Given the close proximity of these wells to the CPP-3 injection well and relatively high aquifer velocity, tritium disposal spikes should be almost immediately seen in the nearest down gradient wells.

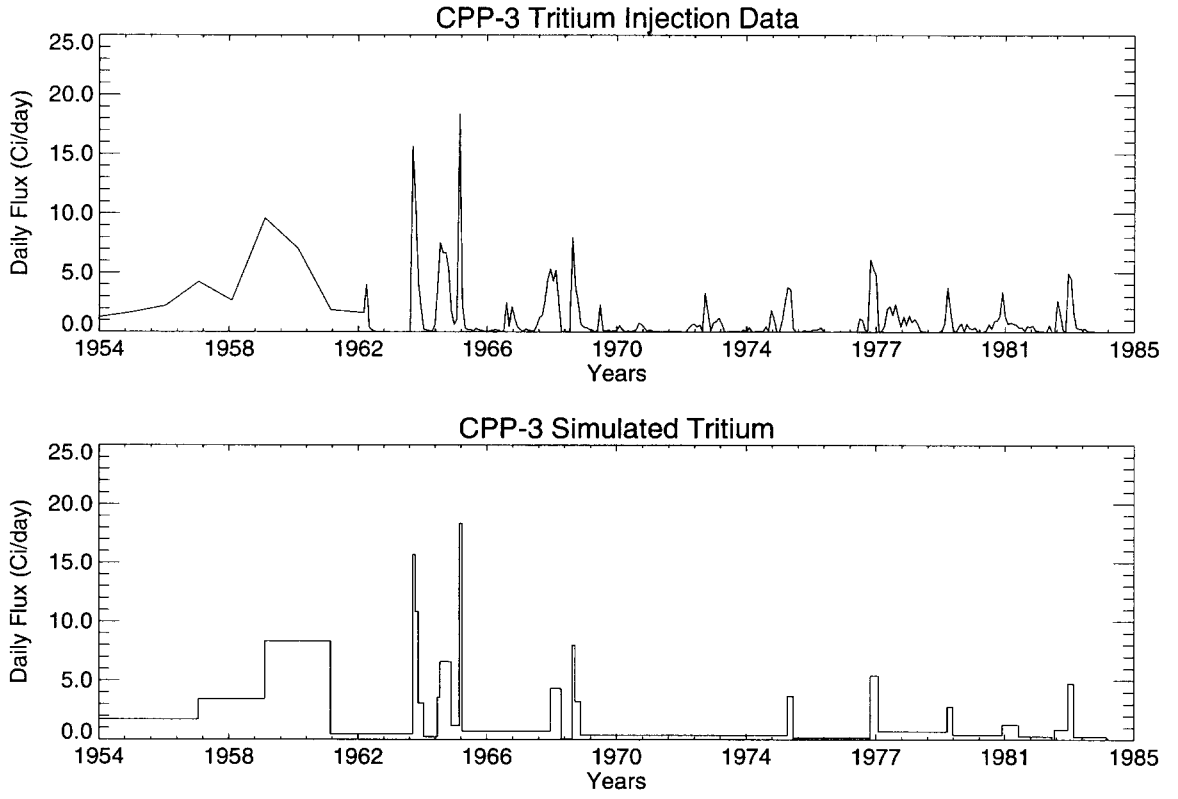

Figure 2-4 CPP-3 injection well actual and simulated tritium disposal data.

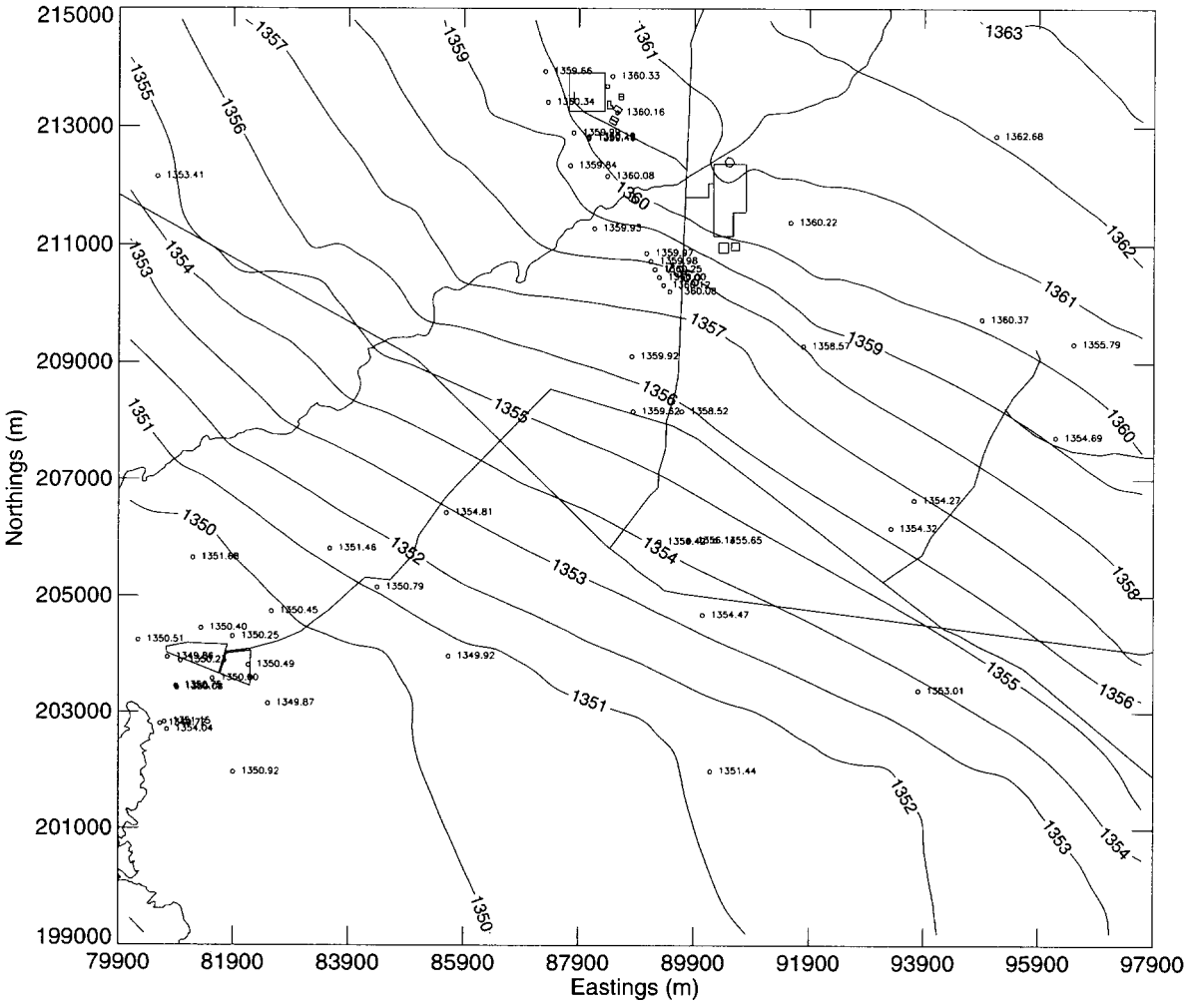

Figure 2-5 RI/BRA simulated hydraulic head (m) with spring 1999 observations.

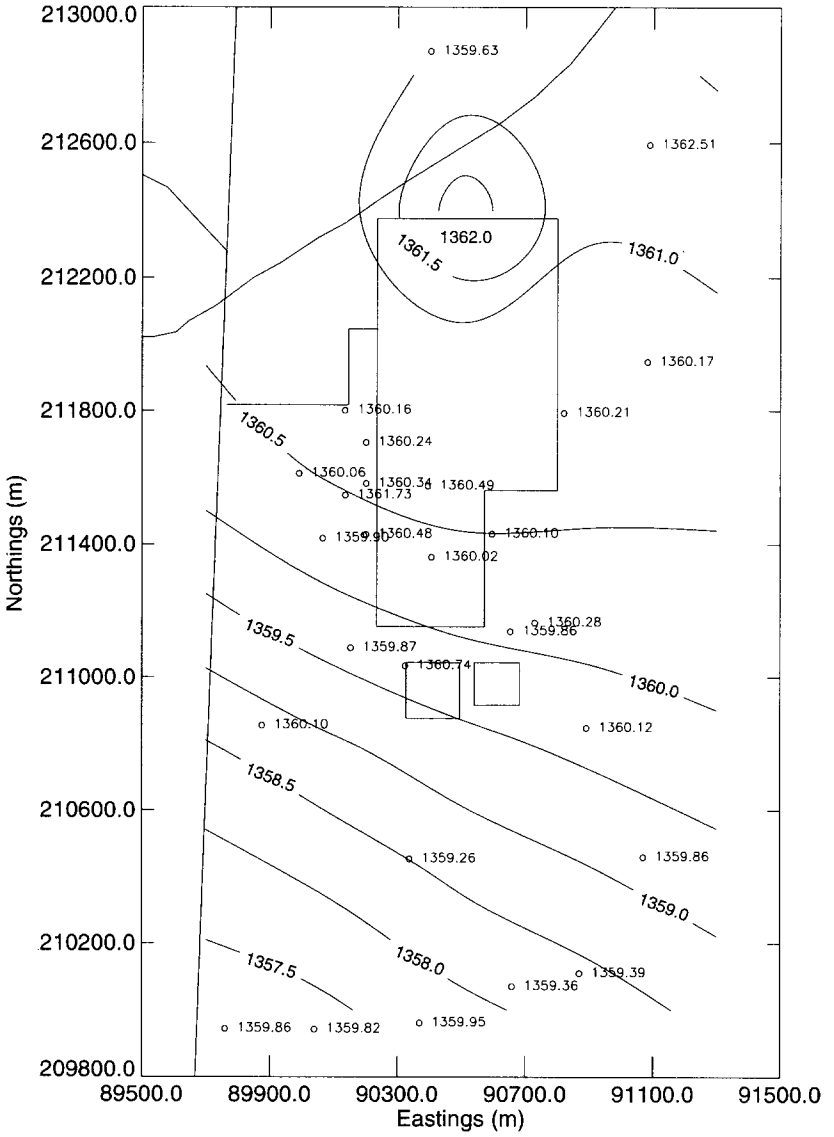

Figure 2-6 RI/BRA simulated hydraulic head (m) with spring 1999 observations near the INTEC.

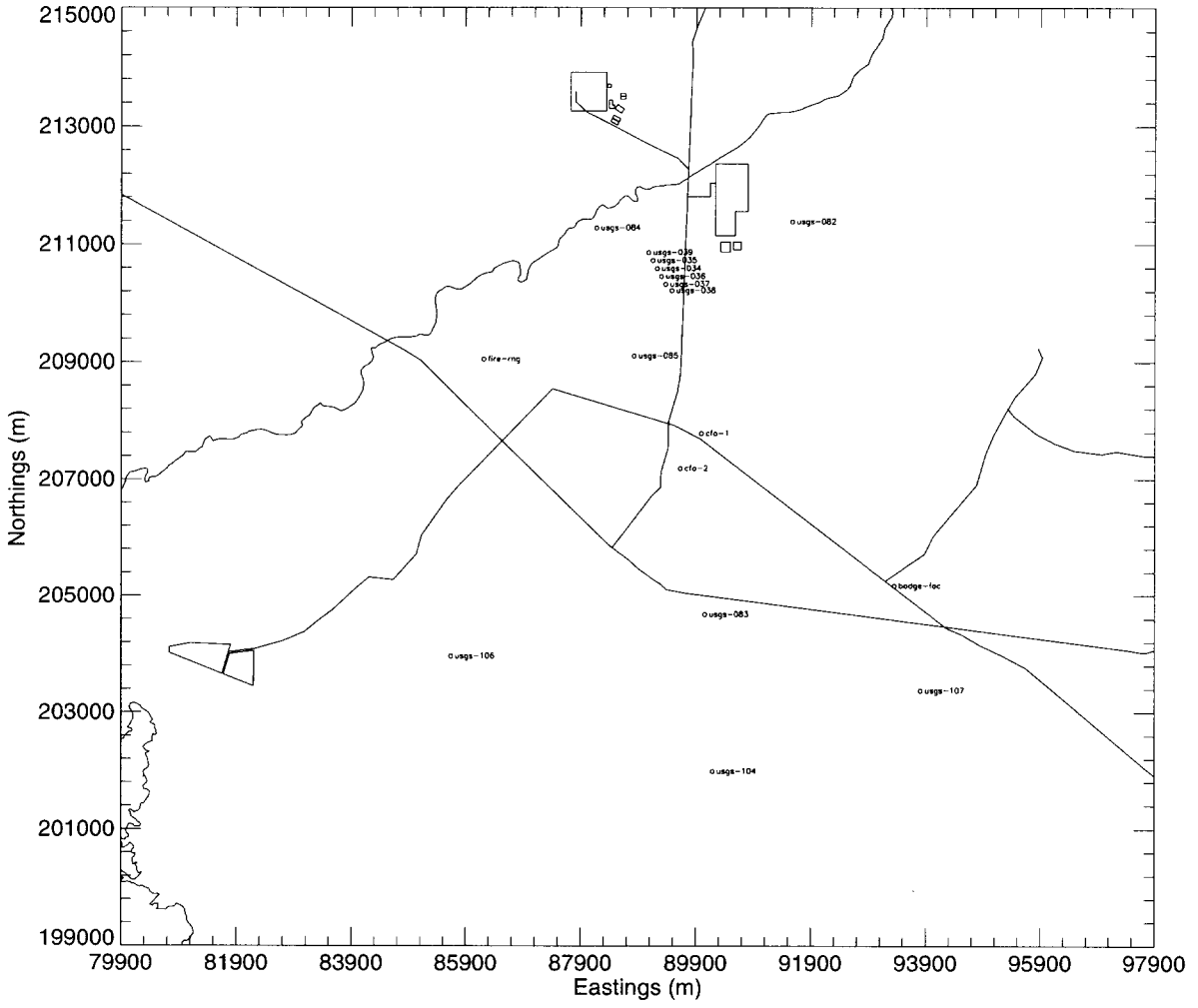

Figure 2-7 Locations of RI/BRA tritium calibration wells.

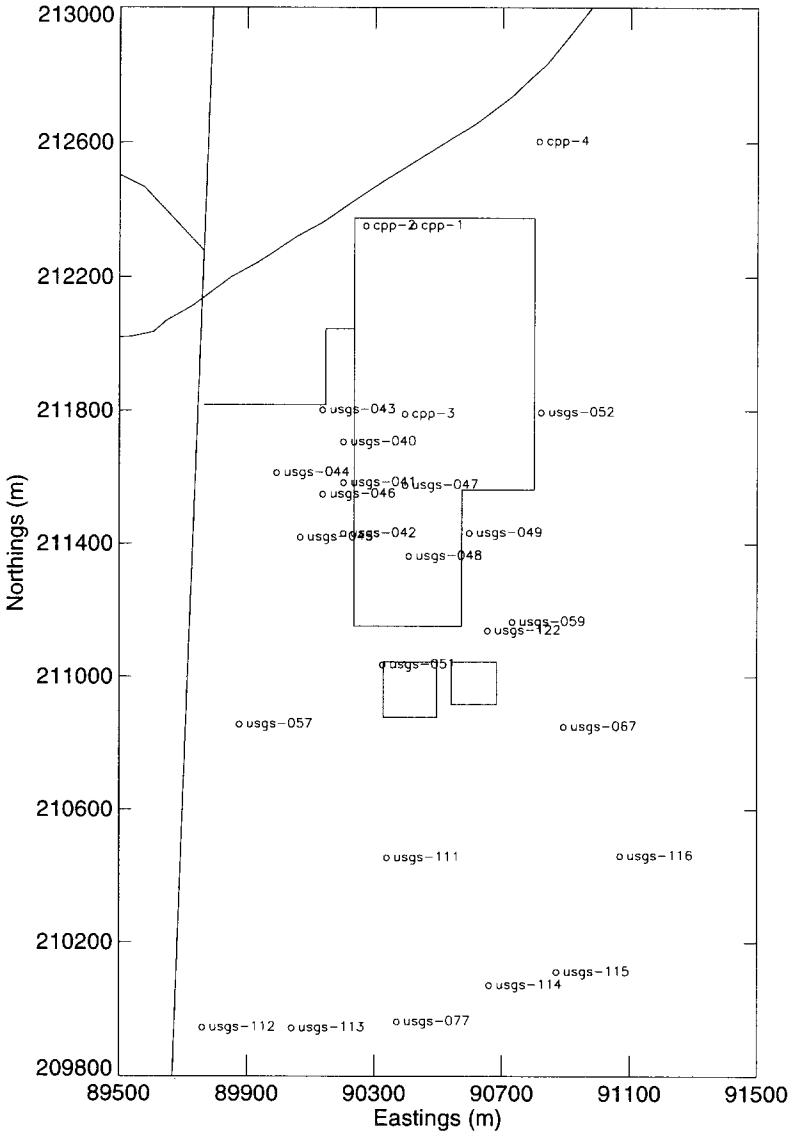

Figure 2-8 Locations of RI/BRA tritium calibration wells near INTEC.

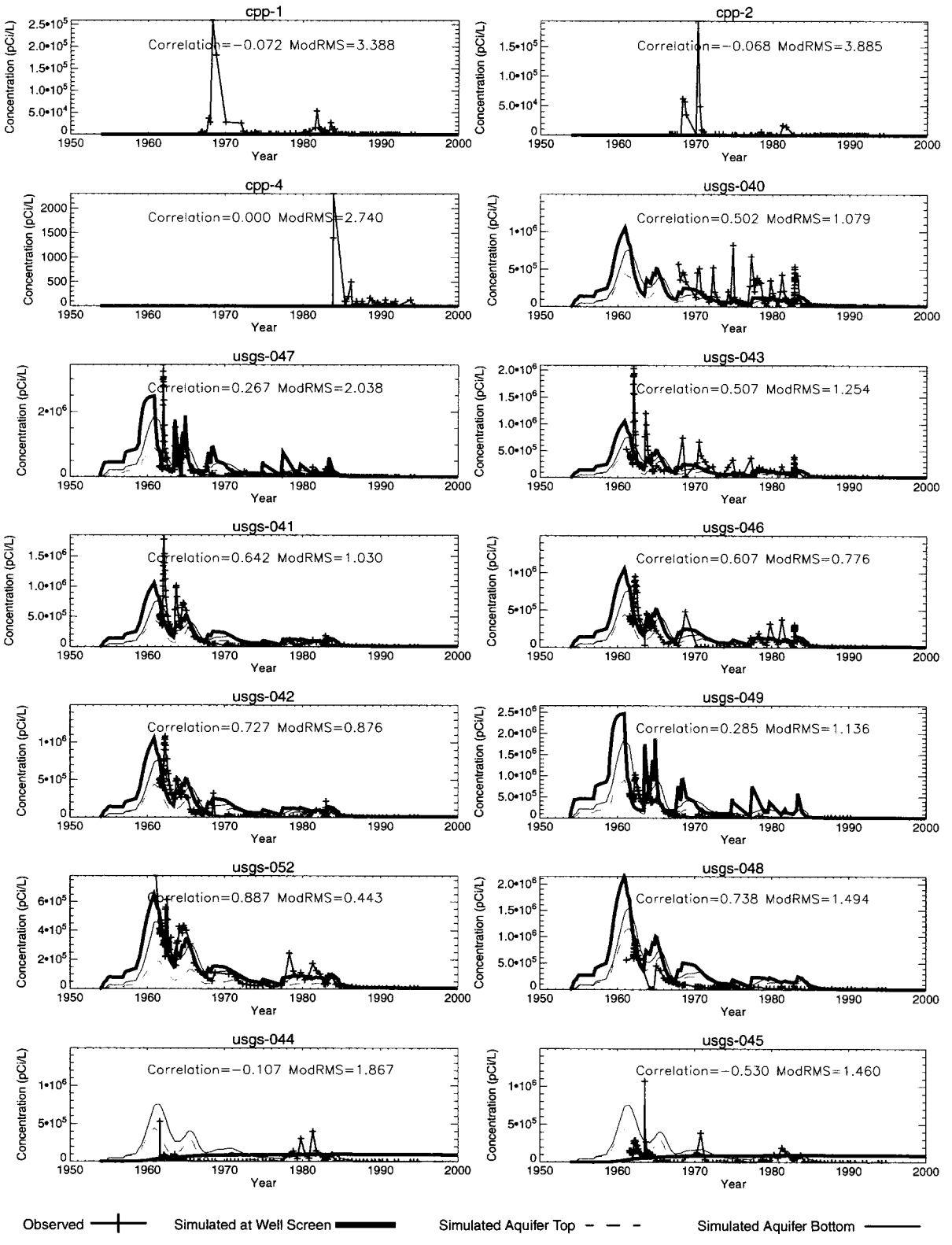

Figure 2-9 RI/BRA model tritium calibration wells breakthrough.

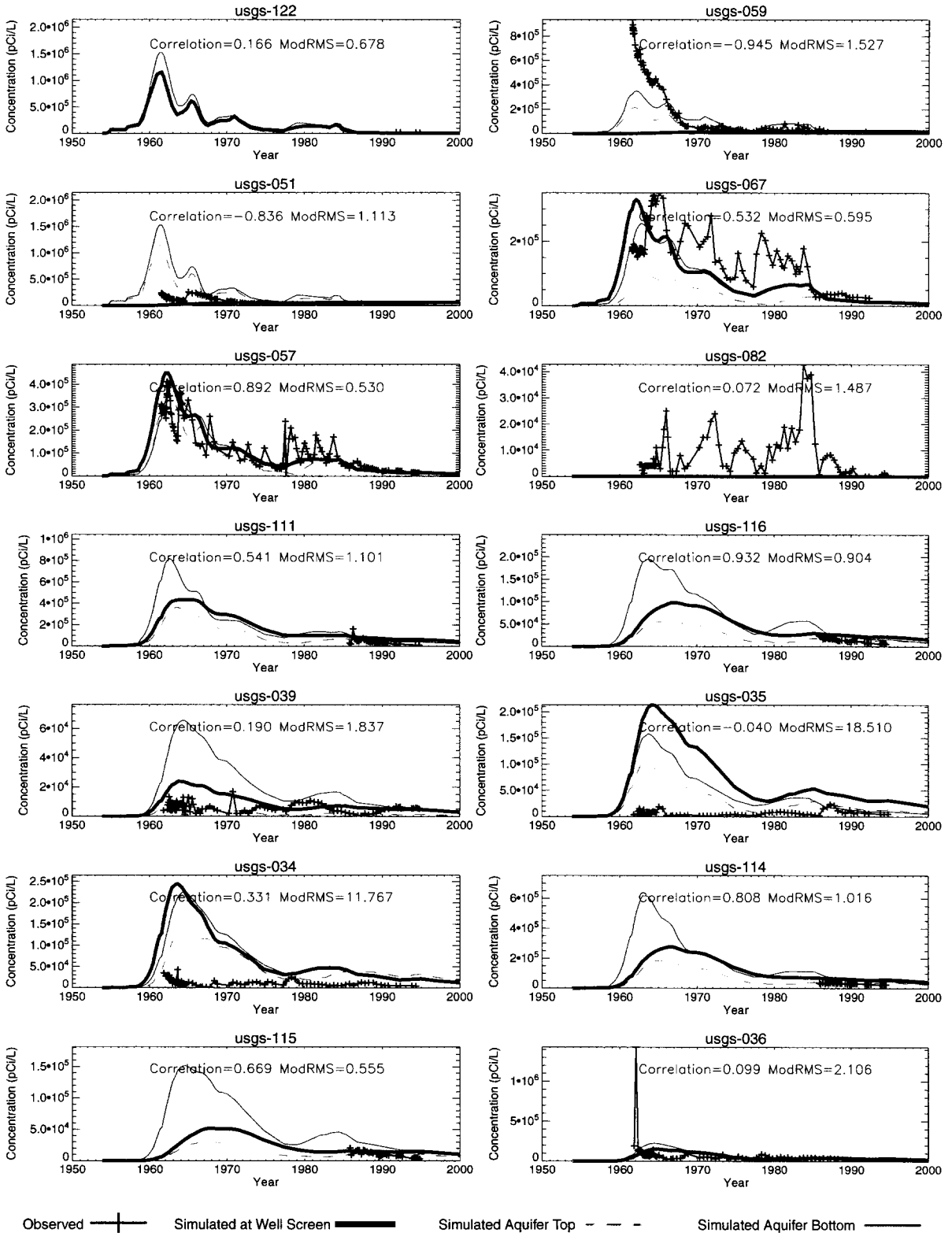

Figure 2-9 continued RI/BRA model tritium calibration wells breakthrough.

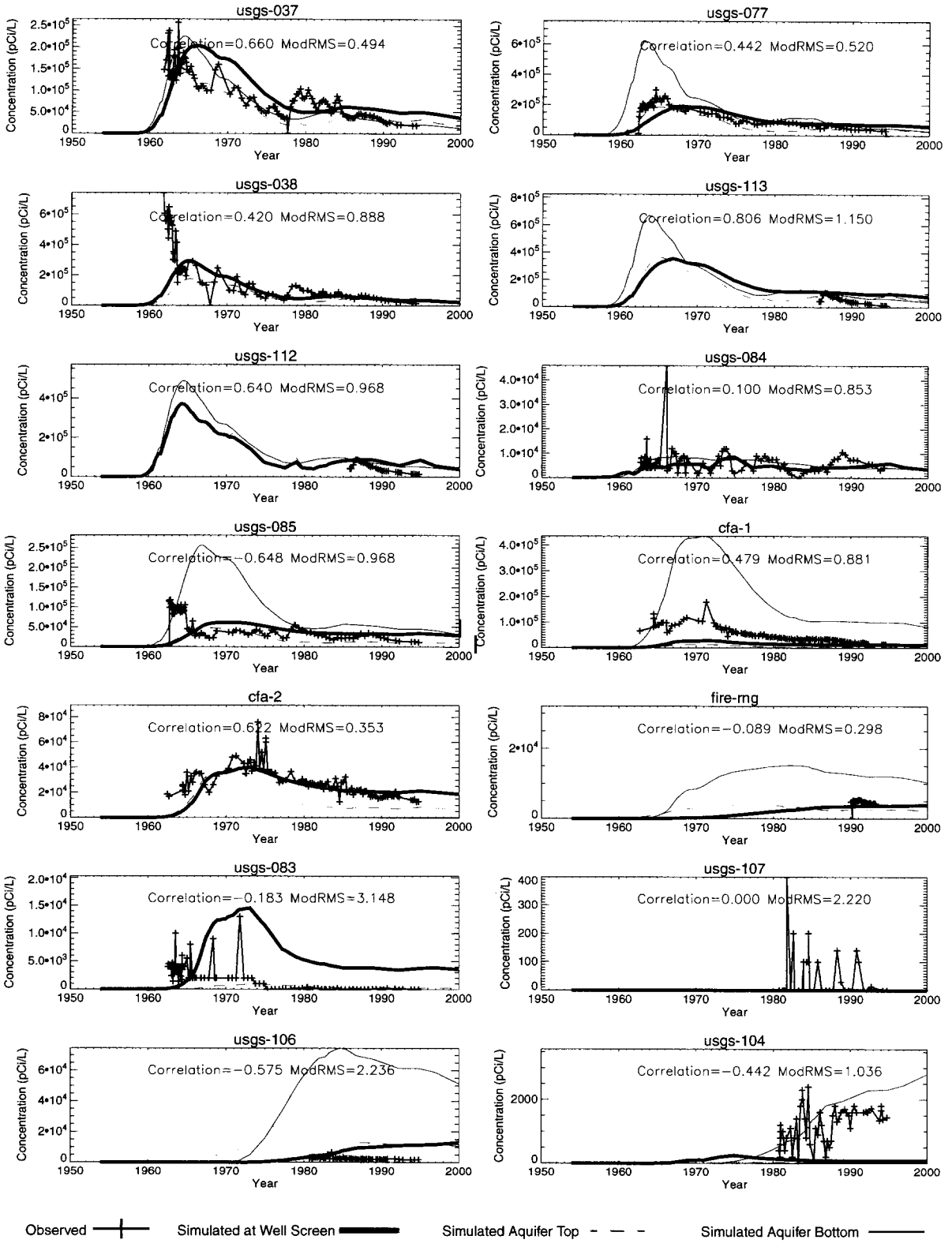

Figure 2-9 continued RI/BRA model tritium calibration wells breakthrough.

2.3 Review of Iodine-129 Source Term

The historical I-129 source term at the INTEC is described in Chapters 5 and 6 of Appendix F of the WAG-3 OU 3-13 RI/BRA report (DOE-ID, 1997). For the RI/BRA study, the INTEC releases were defined as one of three types: (1) known releases, (2) service waste releases, or (3) soil contamination releases. The contaminant sources evaluated in the OU 3-13 study are listed below.

Known releases - The I-129 from known releases were assumed to come from accidental liquid releases in the Tank Farm area. There have been three major releases identified. They are defined as the CPP-28, CPP-31, and 1986 releases.

- It was assumed that the CPP-31 and the 1986 releases contained I-129. The CPP-31 release occurred over 30 days during the month of November, 1972.
- 1986 release occurred over 26 days during the month of July, 1986.
- The CPP-28 release occurred over the period of 1956 through 1974, however, it was assumed not to contain I-129. This is clearly not true, however, as will be shown later, the estimated inventory of I-129 disposed to the injection well is far larger than that released at the Tank Farm, therefore, this source omission was assumed to be insignificant.

Service Waste Releases - There were two primary service waste releases.

- Injection well - This well was drilled to discharge the service waste water directly to the aquifer. The injection well operated from 1953 through 1986. During the period of Jan. 1968 - Sep. 1970, the well casing corroded and collapsed, discharging the service wastewater directly to the vadose zone.
- Service Waste Ponds (SWPs) - These ponds were constructed to replace the injection well. A portion of the service waste water was discharged to the ponds starting in 1984 and all the service waste water has been discharged to the ponds since 1986.

Soil Contamination Releases - Soil contaminated with I-129 throughout the INTEC area was assumed to be available in 1992 for transport through the vadose zone to the aquifer.

The flux of I-129 to the aquifer was estimated based on service waste disposal records for the injection well. For the other sources, a vadose zone flow and transport numerical model was used to calculate the I-129 flux to the aquifer. Figures 2-10 and 2-11 show the I-129 flux to the aquifer from the injection well and to the vadose zone when the injection well failed. Figure 2-12 shows the I-129 flux to the aquifer predicted by the vadose zone model from the vadose zone sources. The simulated flux in Figure 2-12 includes the I-129 from the injection well that was discharged to the vadose zone during the periods when the injection well failed (shown in Figure 2-11), as well as the I-129 from the known releases and soil contamination.

As shown in Figure 2-10, the injection well flux to the aquifer was assumed to be a relatively constant 1.2e-8 pCi/d for approximately 20 years. A similar flux to the vadose zone is shown in Figure 2-11 when the injection well failed. In Figure 2-12, the flux to the aquifer shows a sharp rise to about 3.5e+7 pCi/d when the injection well fails, after which, the flux falls off to approximately 1e+7 pCi/d for the next 50 years. The daily flux during the years of direct injection to the aquifer is significantly higher than the simulated flux from the vadose zone.

Table 2-2 is a summary of the I-129 sources assumed in the OU 3-13 RI/BRA report (DOE-ID, 1997) and each source is explained in greater detail below.

- The I-129 source from the Tank Farm releases is based on estimates of the liquid release volumes and the average I-129 concentrations in the liquid release. The I-129 contribution from the Tank Farm is essentially zero (0.5% of the total).
- The I-129 source from the injection well is significantly larger than the other sources accounting for 91.5% of the total I-129 source to the aquifer. The injection well source term was estimated from data in the RWMIS database. Data was available for the period May 1976 through April 1985. It was assumed that the average I-129 flux during this period is representative of the entire period of injection well operation.
- The I-129 source from the SWPs is approximately 5.4% of the total I-129 source to the aquifer. It was assumed that all of the I-129 from the SWP was in the SWP disposals between 1984 through 1990. After 1990, the SWP water was assumed to have no I-129.
- The I-129 source from the soil contamination was calculated to be approximately 2.5% of the total I-129 source to the aquifer. Although all of the I-129 in the soil was assumed to be available for transport at the same time (January 1992), the I-129 is distributed across the INTEC facility and the leaching water will be diluted and the I-129 dispersed as it moves through the vadose zone. Therefore, the I-129 soil contamination had little influence on the I-129 concentrations in the aquifer.

Table 2-2 Summary of the I-129 sources and time frame of environmental and aquifer flux. (From Table 5-42 in the Appendix F of the OU 3-13 RI/BRA, DOE-ID, 1997).

I-129 Source	Source Activity		Primary Time Frame	
	Total (Ci)	% of Total	Flux to Vadose Zone	Flux to Aquifer
Tank Farm	0.007	0.5%	11/1/72-11/30/72	No aquifer flux
Injection Well	1.39	91.6%	1/68 - 9/70*	1/53 - 12/67 10/70 - 3/86
SWPs	0.08	5.4%	4/84 - 1/90	No aquifer flux
Soil Contamination	0.04	2.6%	1/92	No aquifer flux
* Injection well collapse resulting in deep vadose zone contamination.				

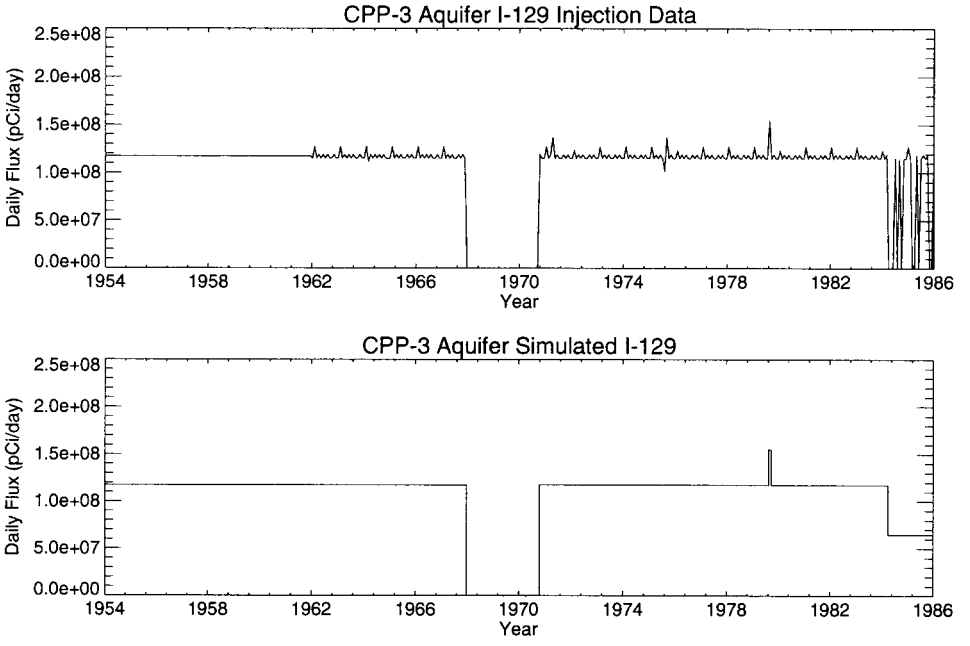

Figure 2-10 I-129 actual and simulated disposal history to the aquifer from the CPP-3 injection well.

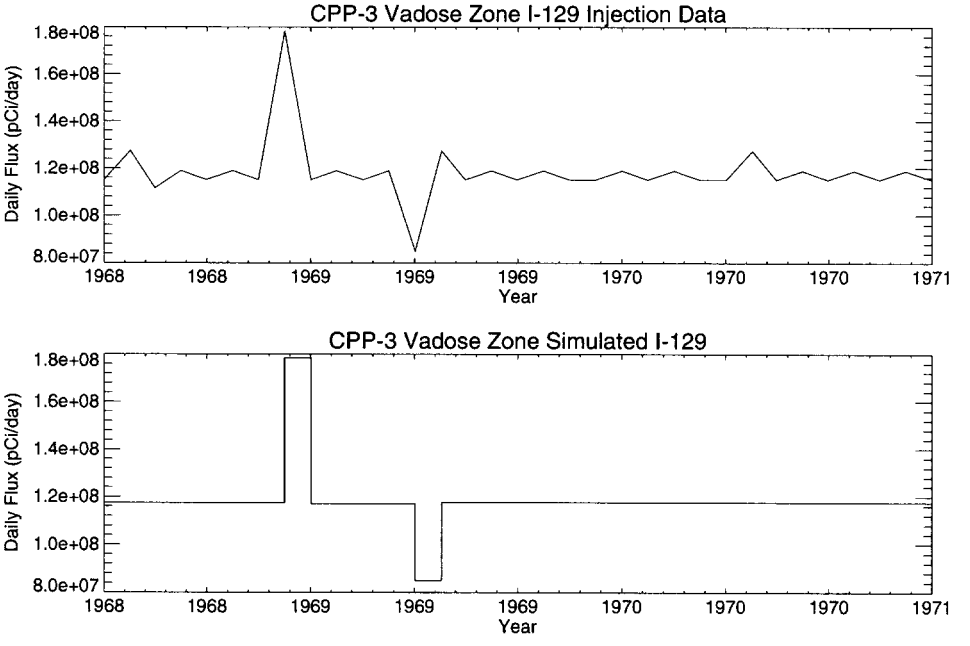

Figure 2-11 I-129 actual and simulated disposal history to the vadose zone from the CPP-3 injection well.

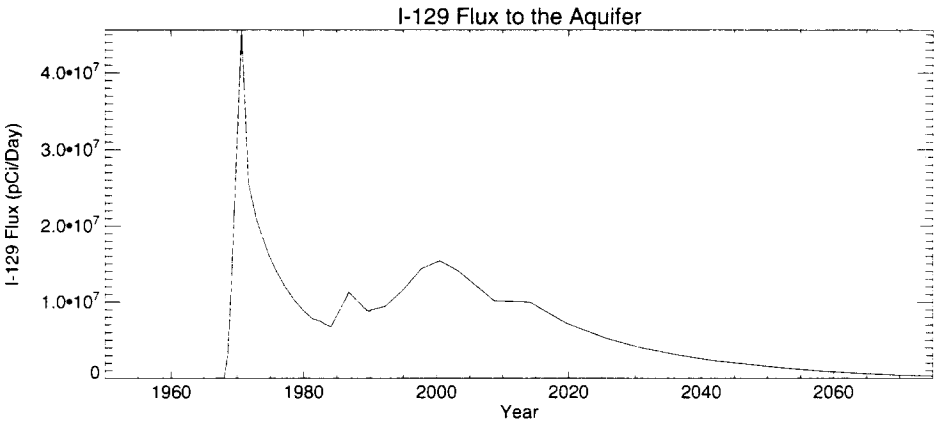

Figure 2-12 I-129 simulated mass flux from the vadose zone.

2.4 Review of OU 3-13 RI/BRA Iodine-129 Simulation Results

The OU 3-13 RI/BRA modeling predicted a relatively large area of the Snake River Plain Aquifer will have I-129 concentrations greater than the 1 pCi/L MCL in the year 2095. Two areas of the HI interbed contained I-129 at concentrations above the MCL in 2095. The first area is immediately southwest of the INTEC and has a peak concentration of 3.0 pCi/L. The second area is west of Lincoln Boulevard and north of State Highway 20 and has a peak concentration of 1.4 pCi/L. All grid blocks with concentrations over 1pCi/L are located within the HI interbed.

These values are different from those presented in Appendix F of the OU 3-13 RI/FS. The Appendix F peak was 4.7 pCi/L. The difference is due to a coding error in TETRAD version 12.2. All the RI/BRA fate and transport simulations were performed from a common set of initial conditions, which were read from a restart file. The restart file option in TETRAD allows a simulation to be stopped and restarted at any time without a loss of simulation information. However in TETRAD version 12.2, different simulation results were obtained when the simulation was run with and without stopping the simulation after initial conditions were obtained. TETRAD version 12.7 was used to verify the OU 3-13 simulations and identical results were obtained with or without using the restart option. Figures 2-13 through 2-22 presents a layer by layer comparison of TETRAD version 12.2 and 12.7 simulation results for 5 times (1959, 1972, 1992, 2025, and 2095). The version 12.7 results plotted in red over the version 12.2 results in black. A summary of peak I-129 concentration in each layer at the 5 times is provided in Table 2-3.

The TETRAD coding error in version 12.2 is due to TETRAD failing to maintain the specified dispersivity value. Upon a restart, the TETRAD code reset the simulation dispersivity value to 0m from the specified 5 m value. As can be seen in Figures 2-13 through 2-22 and Table 2-3, the peak concentrations between the two versions 12.2 and 12.7 are initially very similar. However as simulation time progresses, the attenuation from the specified dispersion increasingly lowers the simulated peak value in each layer.For comparison. The differences between TETRAD version 12.2 and 12.7 are provided in Appendix C-1.

Figure 2-23 illustrates the plume axis as predicted by the RI/BRA model in year 2000 and 2095. Figures 2-24 and 2-25 illustrate a vertical cross sections of the rediscretized model's plume axis for the years 1954, 1965, 1981, 2000, 2025, 2058, 2074 and 2095. The 0.01, 0.1, and 1.0pCi/L isopleths are illustrated by a thin dashed, thin, and thick black lines, respectively. The aquifer bottom is shown as a thick red line and the HI interbed is denoted by dashed lines. The CPP-3 injection well was simulated as a fully screened well extending 40 m below the water table and is shown in Figures 2-24 and 2-25 as a vertical blue line in the upper left corner of each cross-section. The CPP-03 injection well is screened across the HI interbed, which is present

approximately 25 m below the water table. I-129 disposal begins in 1954 and by 1965, the down gradient migration of I-129 in the HI interbed lags behind that in the surrounding basalt. However in the year 2058, clean water movement through the contamination area lags in the interbed and isolated high concentrations of I-129 persist in the interbed where aquifer velocity is low.

Table 2-3 Maximum I-129 concentrations predicted with TETRAD version 12.2 and 12.7.

Layer	Maximum I-129 Concentration (pCi/L)									
	5/1959		11/1972		4/1992		3/2025		10/2095	
	TETRAD Version 12.2	TETRAD Version 12.7	TETRAD Version 12.2	TETRAD Version 12.7	TETRAD Version 12.2	TETRAD Version 12.7	TETRAD Version 12.2	TETRAD Version 12.7	TETRAD Version 12.2	TETRAD Version 12.7
1	28.2	28.1	22.9	22.8	4.6	4.6	2.6	2.6	0.3	0.3
2	33.4	33.2	31.8	31.2	4.8	4.8	2.4	2.4	0.4	0.3
3	35.3	35.5	31.9	32.1	7.0	6.8	1.8	1.8	1.3	0.9
4	22.9	22.6	16.7	16.6	14.3	13.2	5.7	4.9	1.2	1.7
5	32.5	32.3	30.0	29.8	13.7	13.4	9.0	8.4	4.7	3.0
6	32.8	32.8	30.4	30.4	14.3	13.2	7.2	5.7	2.8	1.5
7	33.0	33.0	30.4	30.4	11.8	10.1	4.2	3.3	1.1	1.1
8	31.8	31.6	29.5	29.3	10.3	10.1	4.2	3.5	1.5	1.4
9	30.0	29.7	28.1	27.7	12.2	12.1	4.5	4.3	1.3	1.1
10	26.7	26.5	23.8	23.5	13.2	13.0	5.8	5.5	0.4	0.4
Maximum for All Layers	35.3	35.5	31.9	32.1	14.3	13.2	9.0	8.4	4.7	3.0

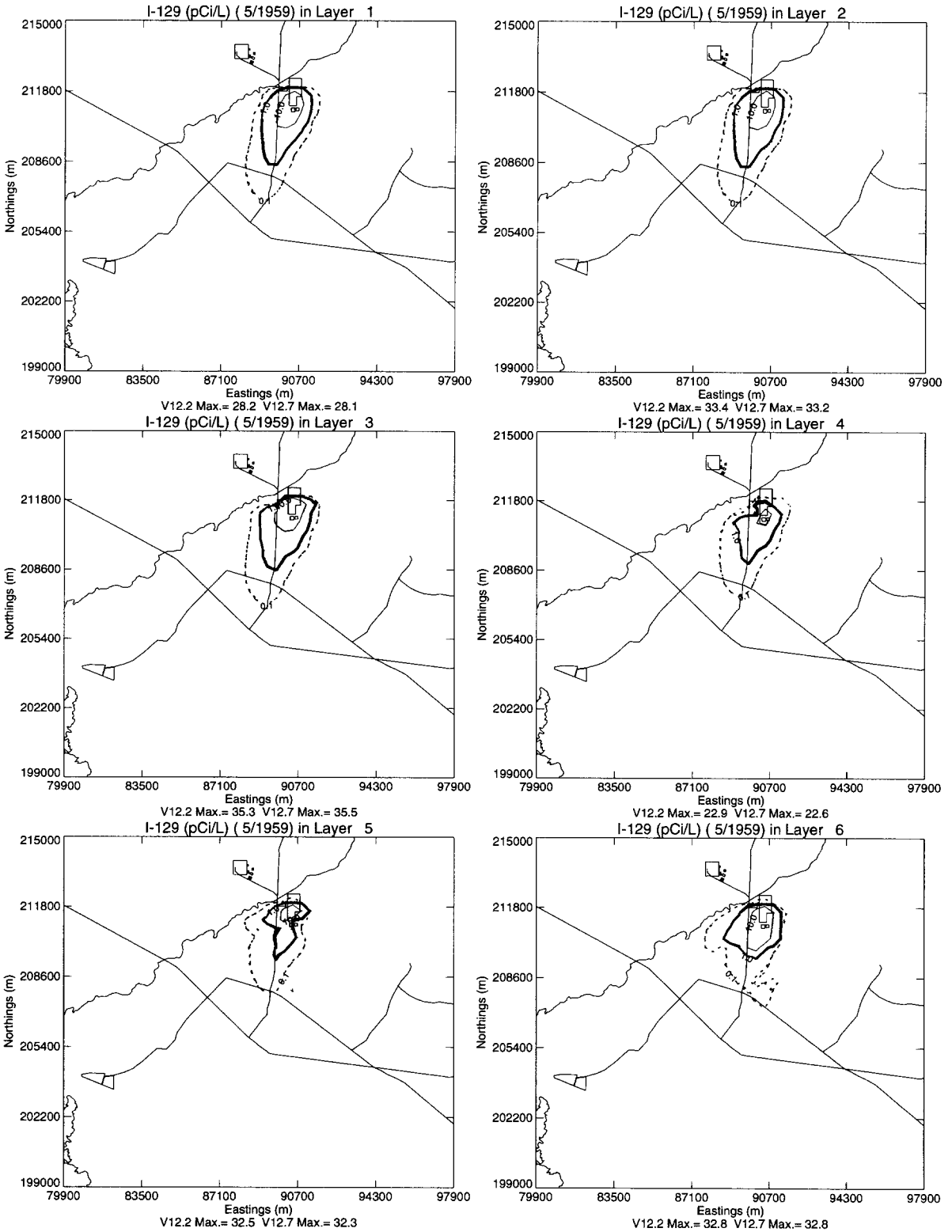

Figure 2-13 RI/BRA model I-129 concentrations, TETRAD version 12.2 (black) vs. 12.7 (red) for layers 1-6 in 5/1959.

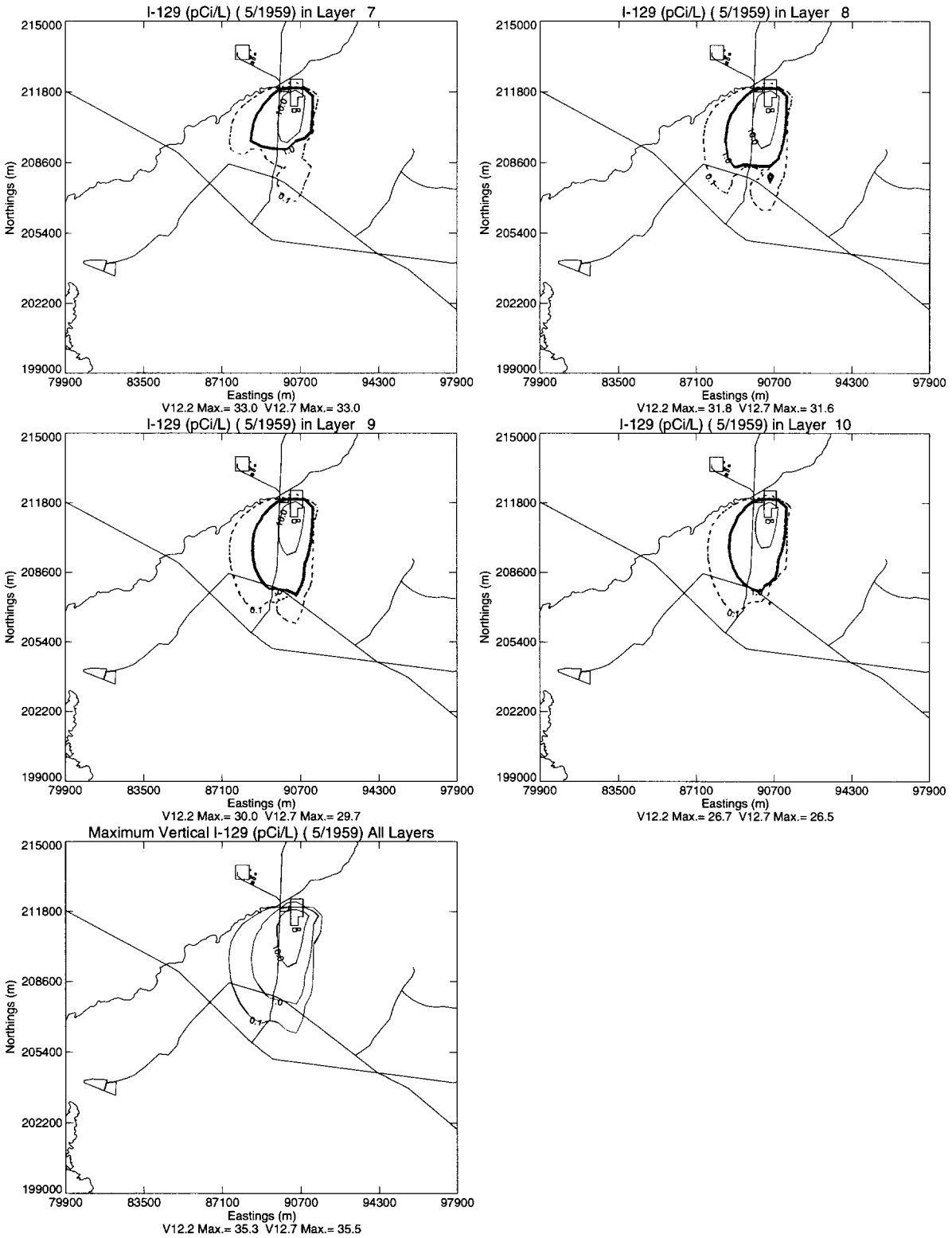

Figure 2-14 RI/BRA model I-129 concentrations, TETRAD version 12.2 (black) vs. 12.7 (red) for layers 7-10 in 5/1959.

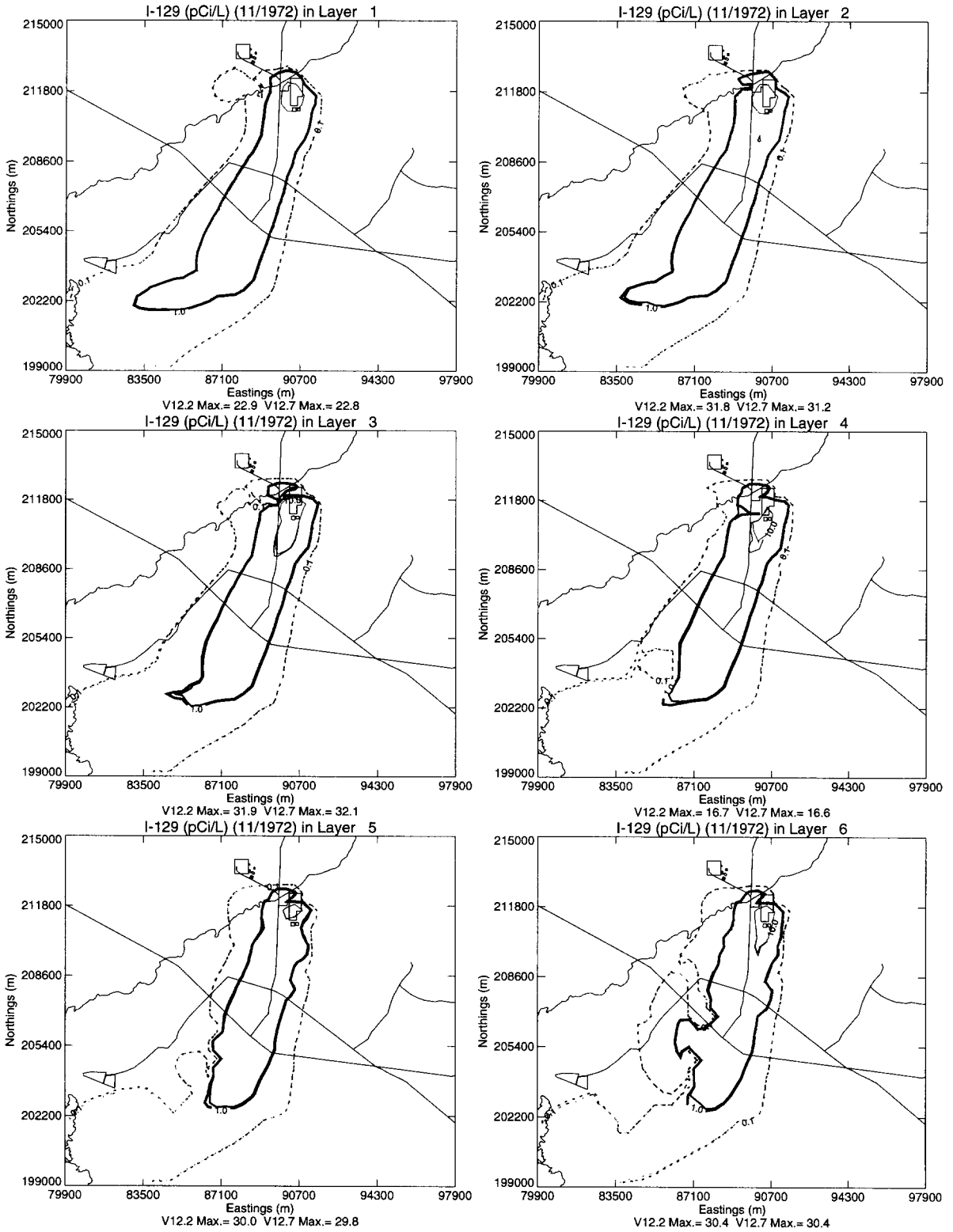

Figure 2-15 RI/BRA model I-129 concentrations, TETRAD version 12.2 (black) vs. 12.7 (red) for layers 1-6 in 11/1972.

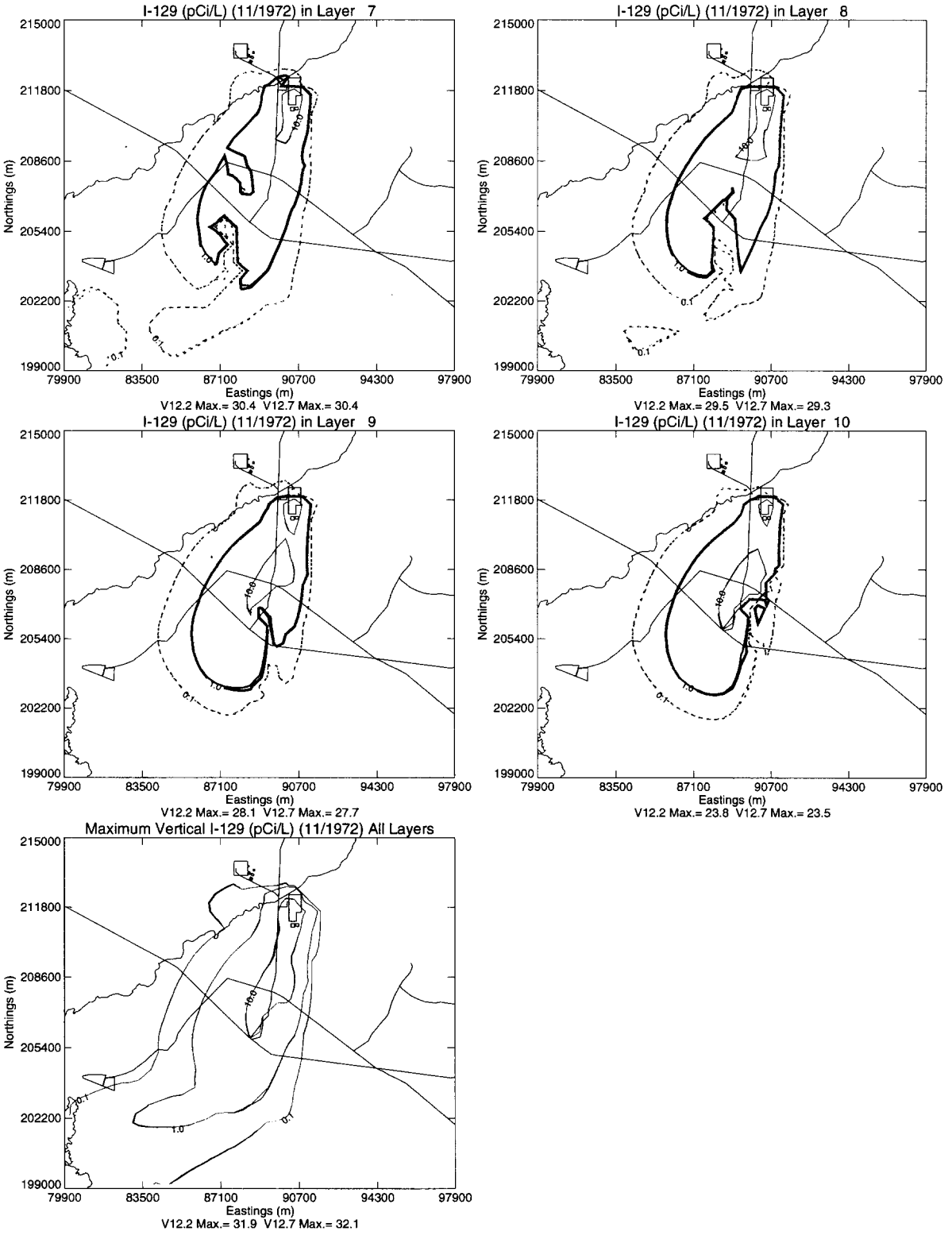

Figure 2-16 RI/BRA model I-129 concentrations, TETRAD version 12.2 (black) vs. 12.7 (red) for layers 7-10 in 11/1972.

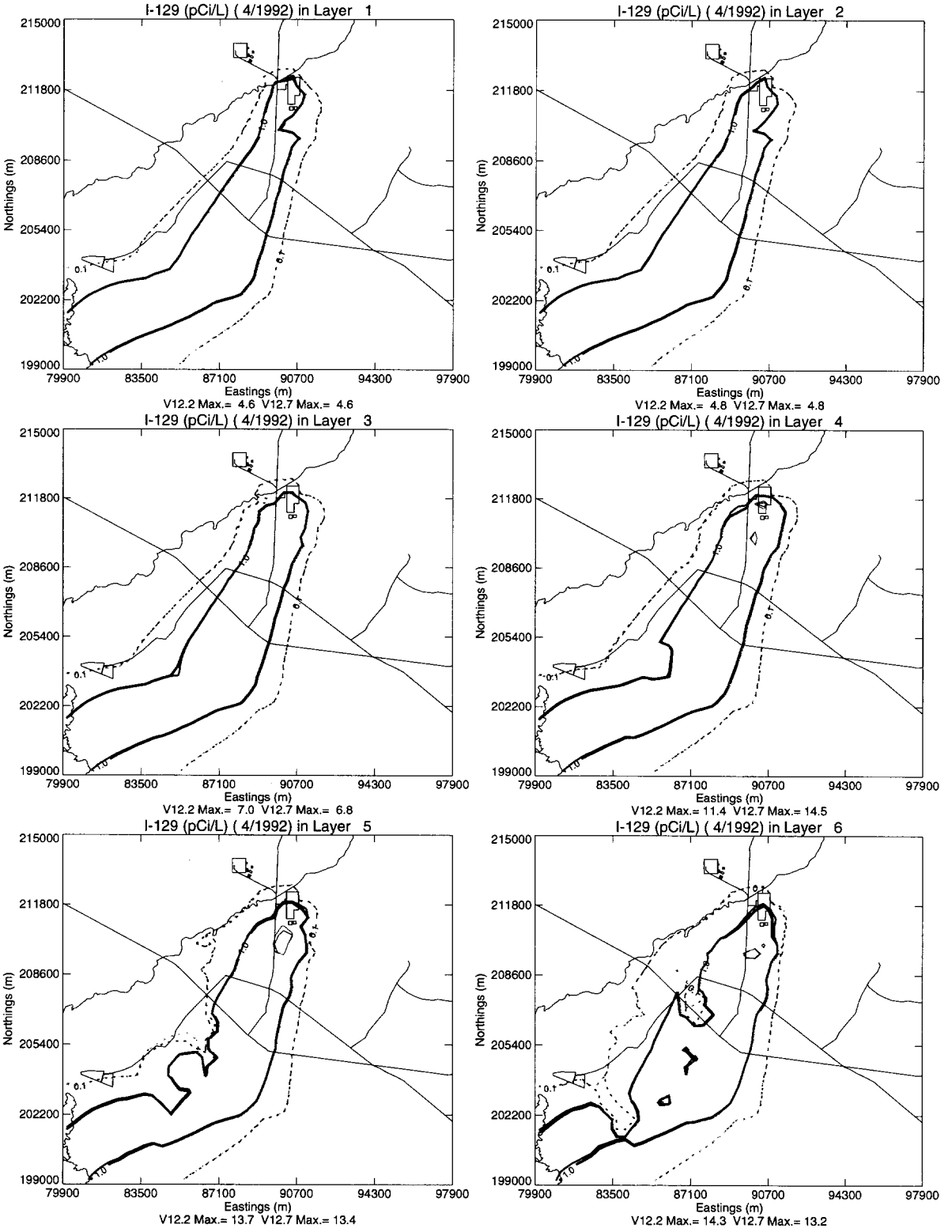

Figure 2-17 RI/BRA model I-129 concentrations, TETRAD version 12.2 (black) vs. 12.7 (red) for layers 1-6 in 4/1992.

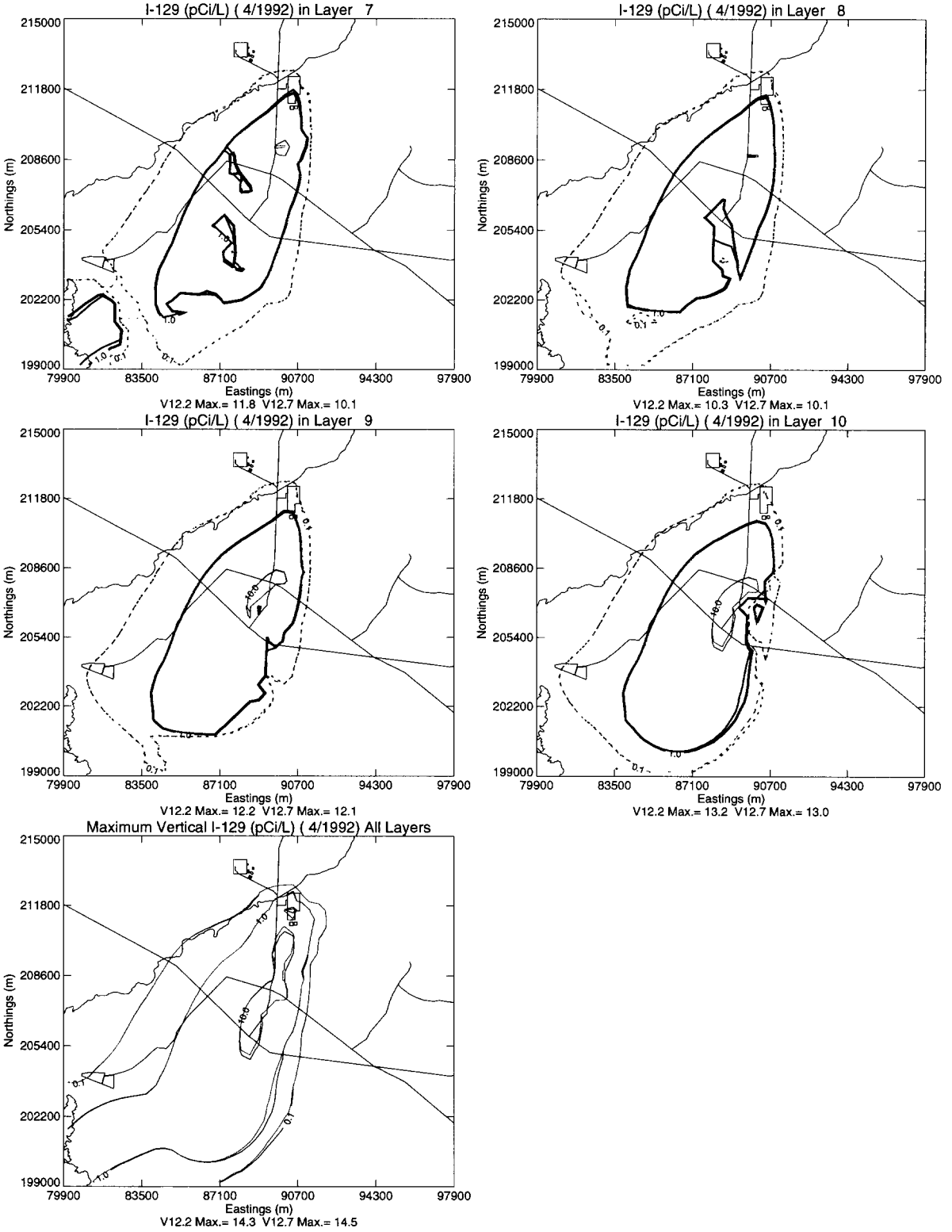

Figure 2-18 RI/BRA model I-129 concentrations, TETRAD version 12.2 (black) vs. 12.7 (red) for layers 7-10 in 4/1992.

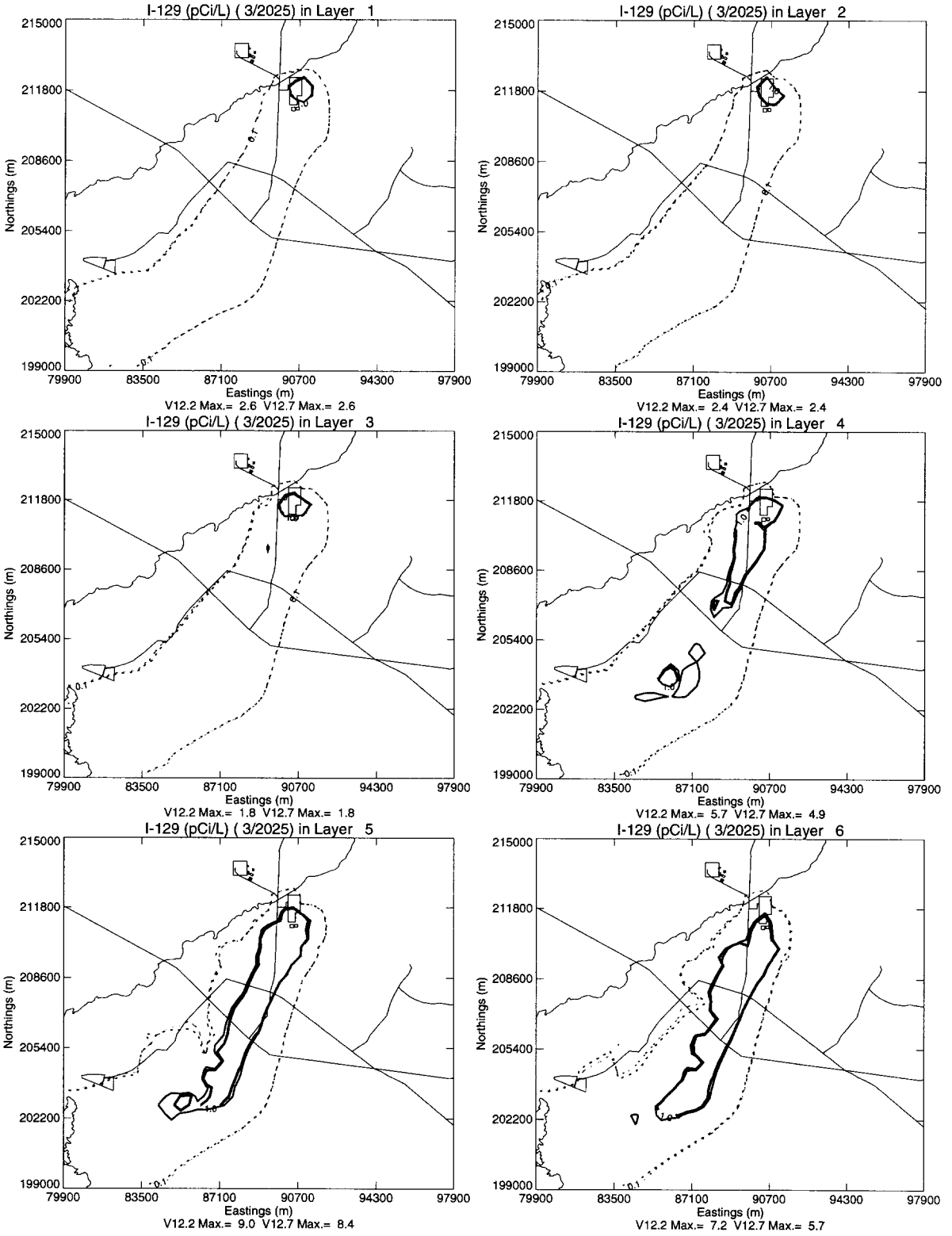

Figure 2-19 RI/BRA model I-129 concentrations, TETRAD version 12.2 (black) vs. 12.7 (red) for layers 1-6 in 3/2025.

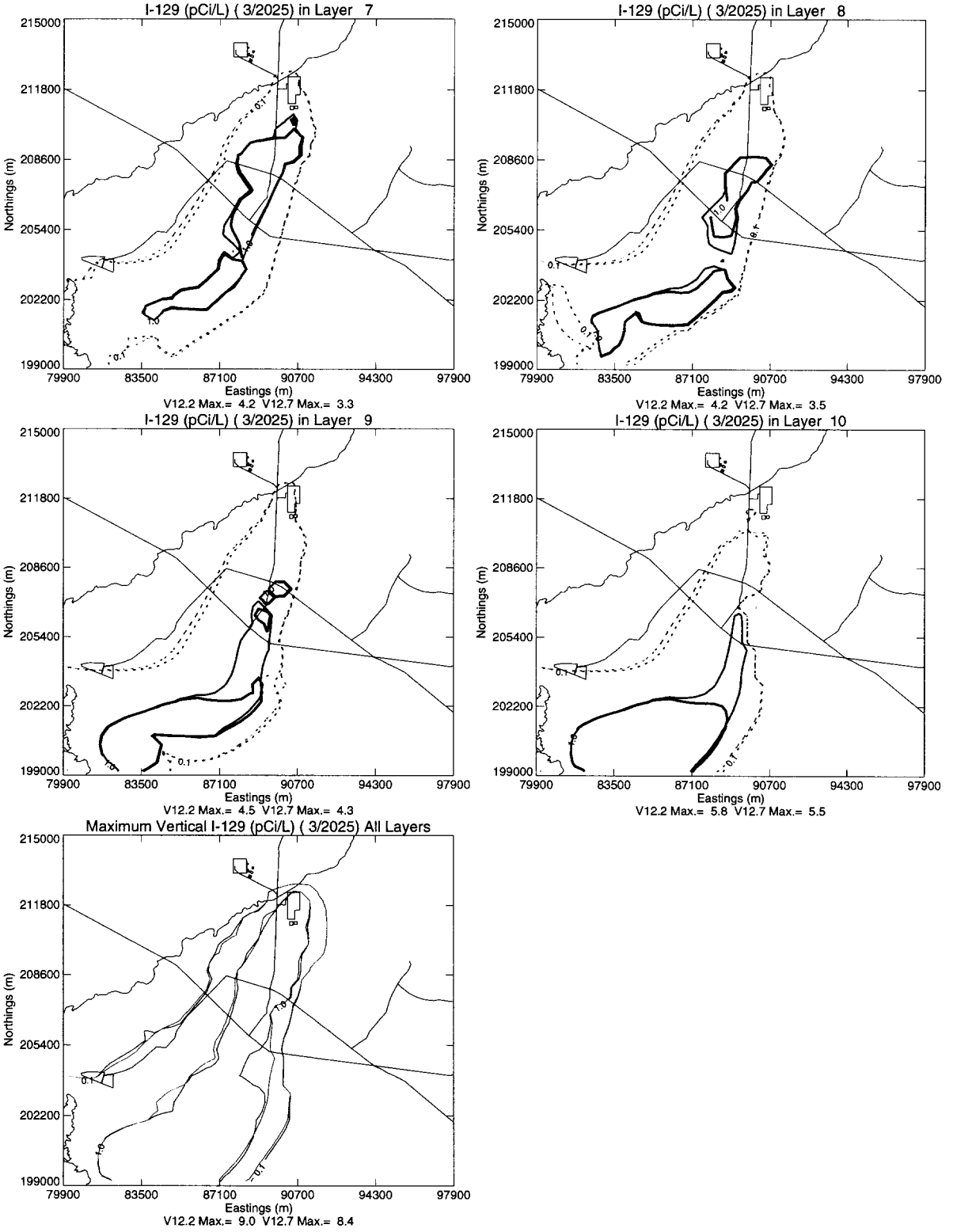

Figure 2-20 RI/BRA model I-129 concentrations, TETRAD version 12.2 (black) vs. 12.7 (red) for layers 7-10 in 3/2025.

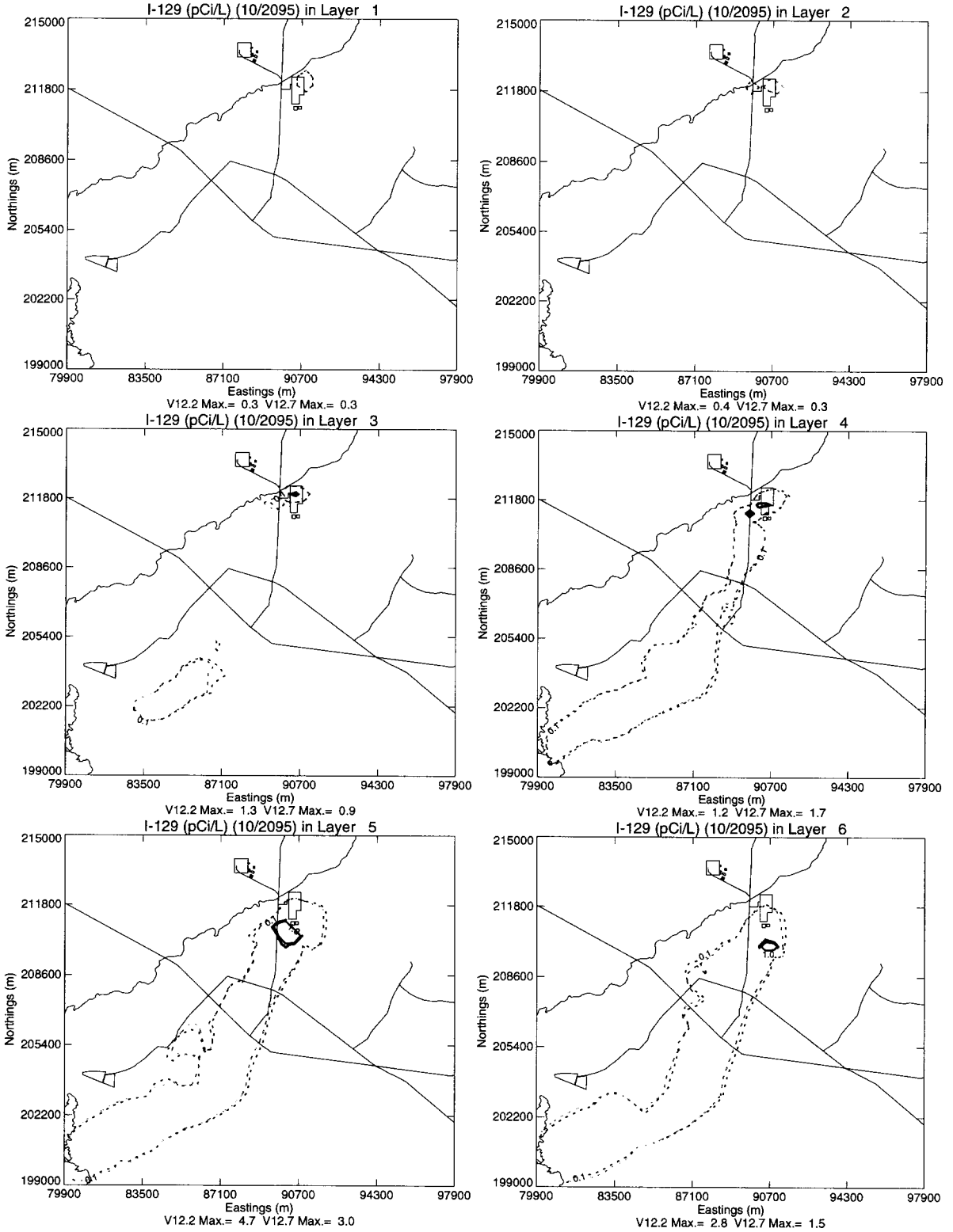

Figure 2-21 RI/BRA model I-129 concentrations, TETRAD version 12.2 (black) vs. 12.7 (red) for layers 1-6 in 10/2095.

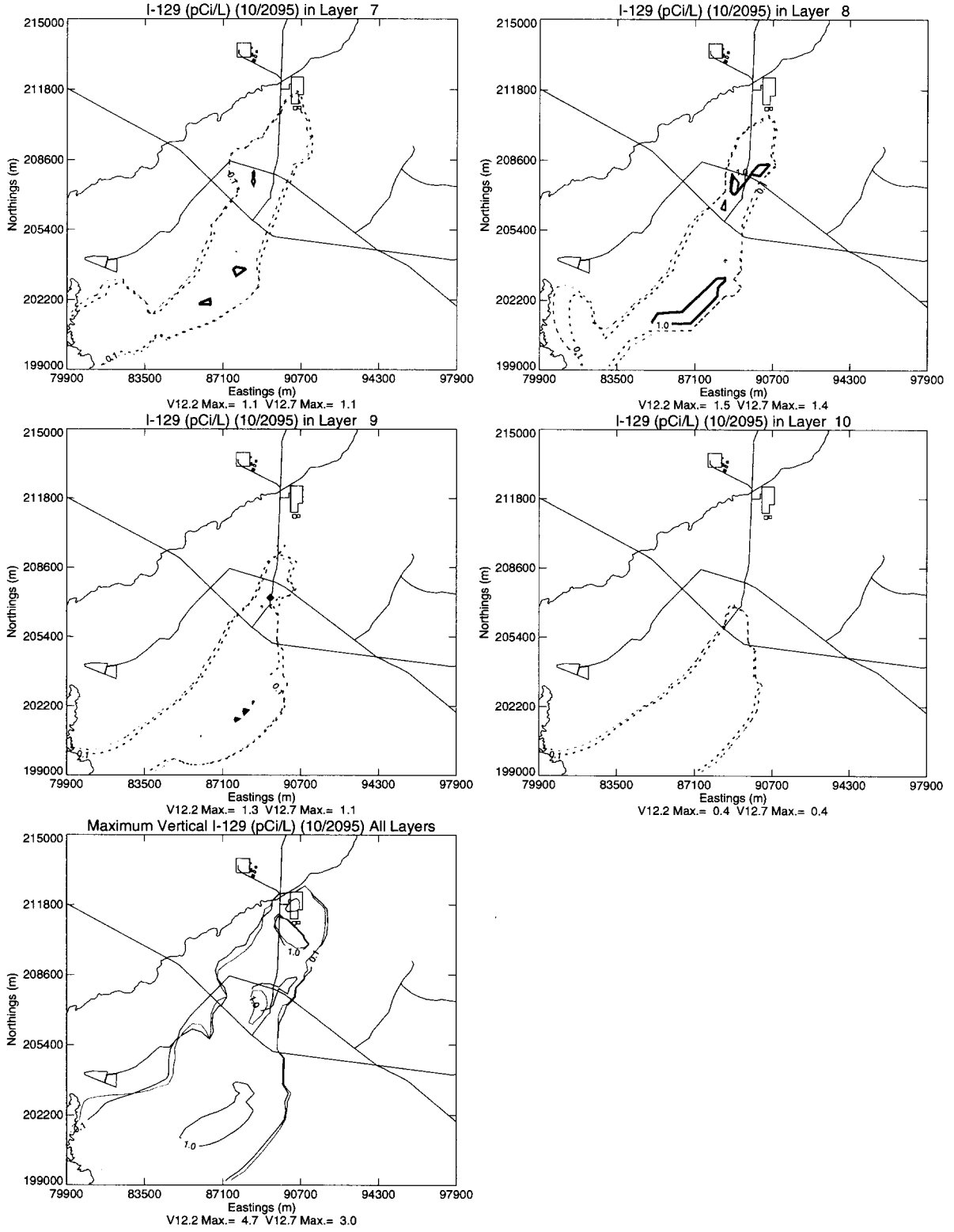

Figure 2-22 RI/BRA model I-129 concentrations, TETRAD version 12.2 (black) vs. 12.7 (red) for layers 7-10 in 10/2095.

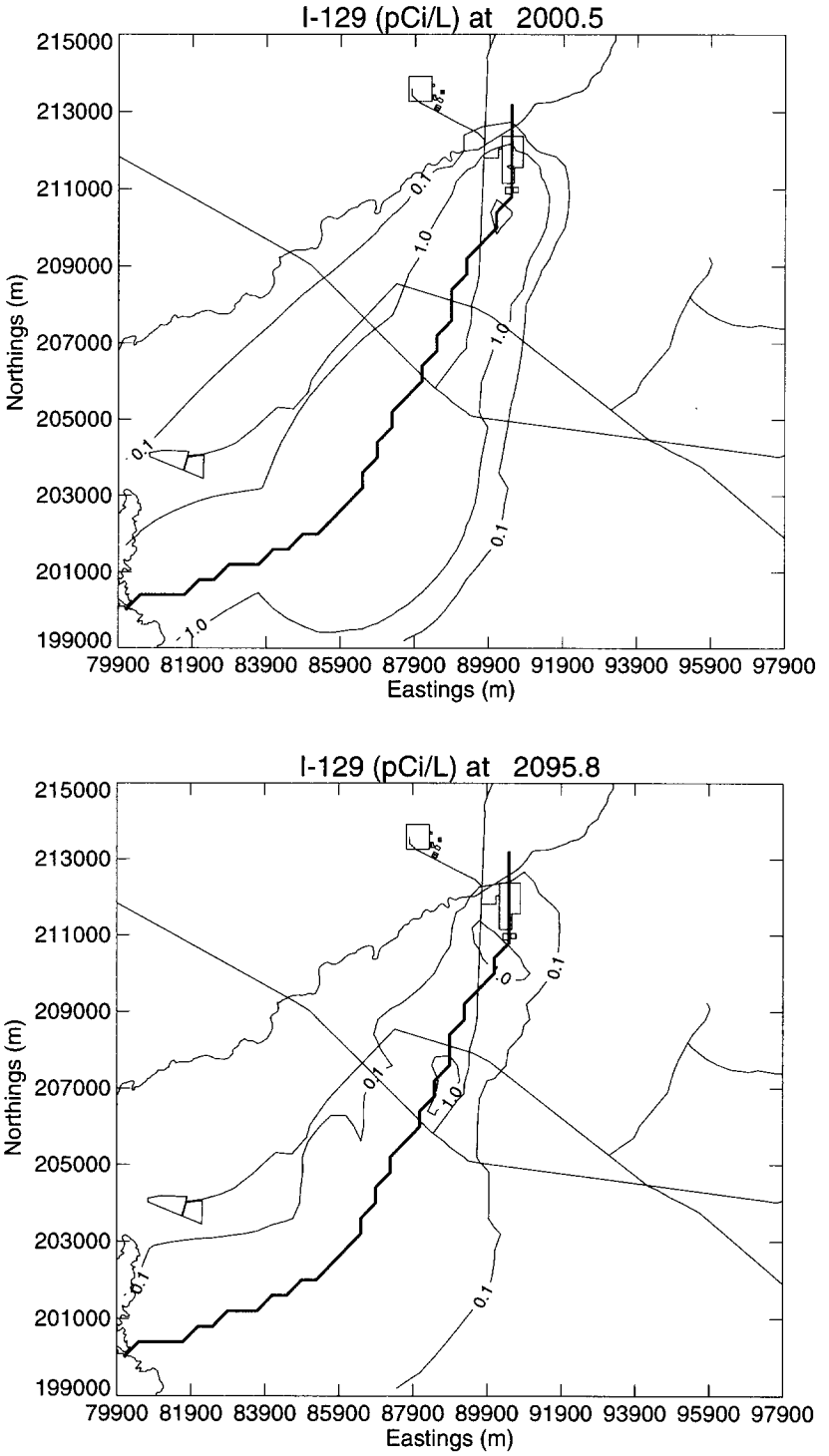

Figure 2-23 RI/BRA model maximum I-129 concentrations in 2000 and 2095 with plume axis (blue).

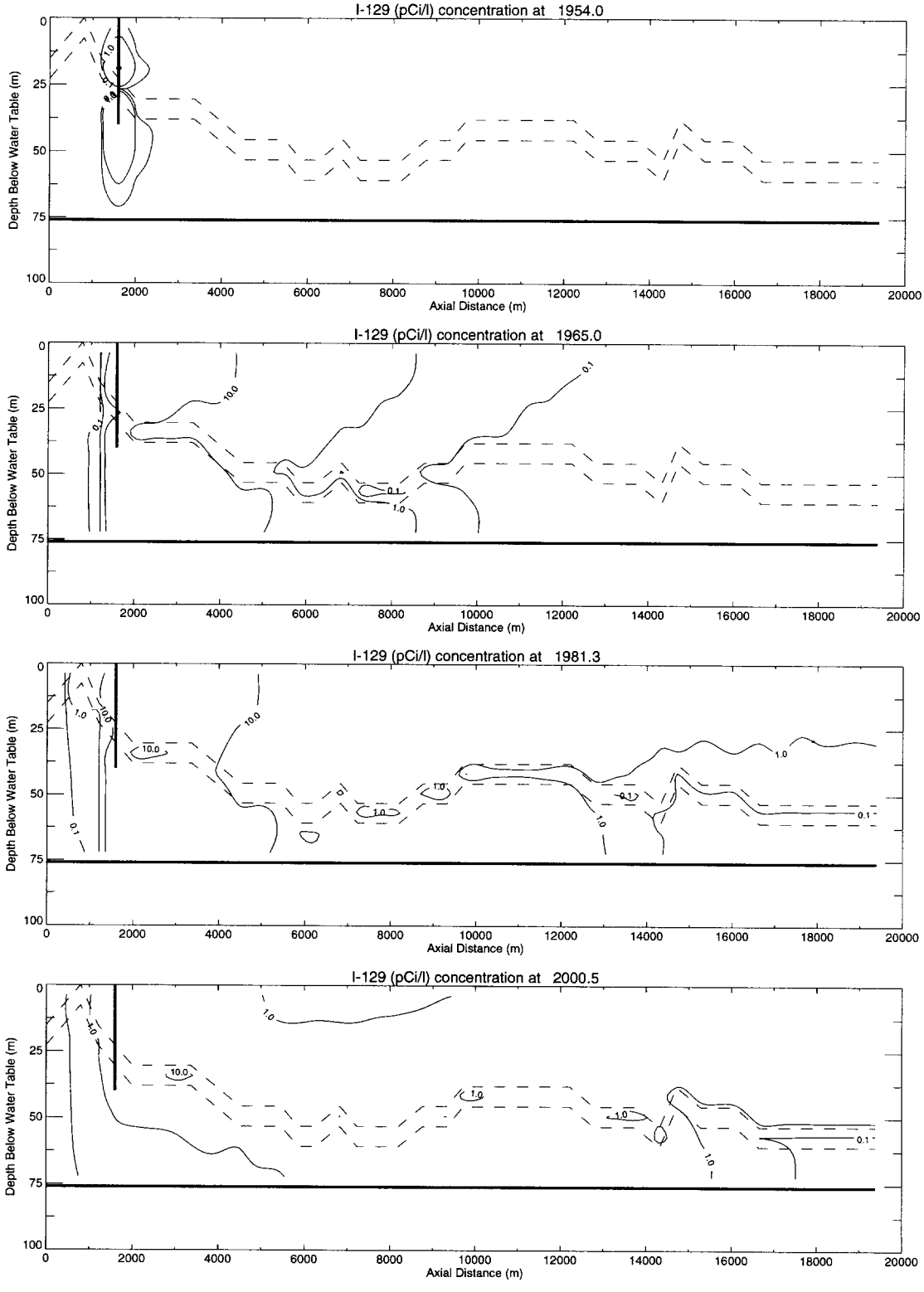

Figure 2-24 RI/BRA model plume axis vertical I-129 concentrations in 1954, 1965, 1981, and 2000 (the injection well is blue, the model bottom is red, and the long dashed black line represents the interbed).

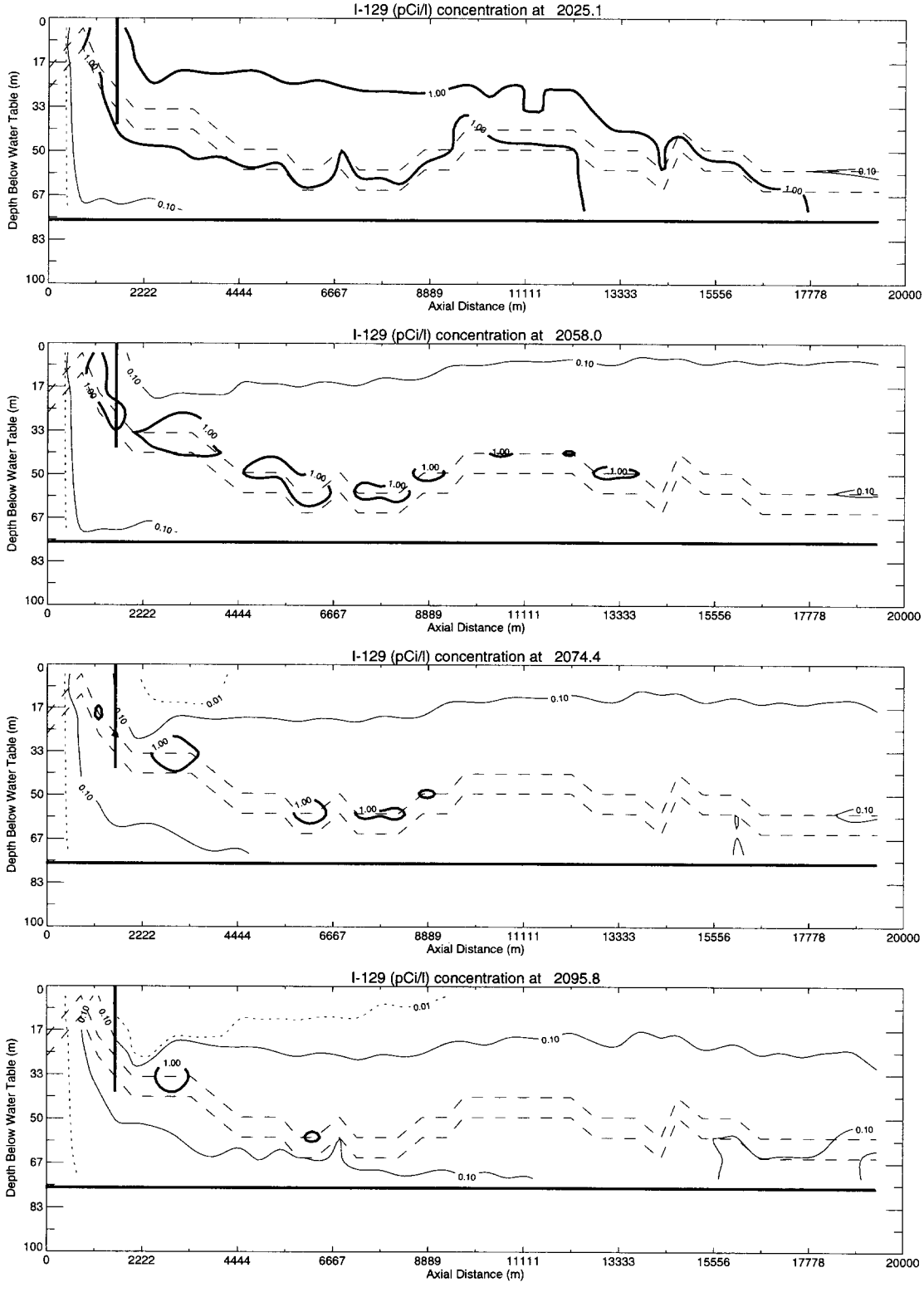

Figure 2-25 RI/BRA model plume axis vertical I-129 concentrations in 2025, 2058, 2074, and 2095 (the injection well is blue, the model bottom is red, and the long dashed black line represents the interbed).

3 WAG-3 OU 3-13 RI/BRA AQUIFER MODEL SENSITIVITY TO INTERBED PARAMETERIZATION

Only a limited amount of empirical data is available to confirm the physical properties of the HI interbed as assumed in the OU 3-13 RI/BRA model and there is no data regarding the presence or absence of contaminants in the interbed. Empirical evidence of the HI interbed contamination and permeability is required to verify the model predictions and refine the model parameterization. In the event that observed concentrations exceed the action levels defined in the WAG-3 Record of Decision, an updated numerical model will be used to guide remediation efforts. Sensitivity of the model parameterization was performed to identify key data needs, support field activities to collect empirical data, and help estimate the uncertainty of the RI/BRA model.

3.1 HI Interbed Discretization Sensitivity

The OU 3-13 aquifer model has been rediscretized to determine the RI/BRA model's sensitivity to the simulated aquifer depth and the number of model layers used to represent the HI interbed. The OU 3-13 RI/BRA simulations indicated the HI interbed was primarily responsible for maintaining elevated I-129 concentrations. The RI/BRA model treats the vertical component of the HI interbed as a single numerical grid block of constant (7.6 m) thickness. This one grid block discretization averages concentrations throughout the entire depth of the interbed and does not allow a vertical concentration gradient to exist in the interbed. This effect may allow an artificially large amount of mass to enter the interbed. As a general rule, lithological structures of very different hydrologic properties should be represented by at least 3 model layers.

The OU 3-13 aquifer model also used a uniform 76 m total thickness, which placed the model's bottom surface either above or below the interbed. Placement of the OU 3-13 model's bottom surface above the HI interbed's lowest point presents potential for erroneous low or high velocity areas due to extreme confining conditions, which are the result of the numerical grid. The updated model's bottom surface was created from flowing aquifer thickness estimates provided by Dr. Smith (personal communication, 2000). Dr. Smith used deep well temperature logs to estimate flowing aquifer thickness. The isothermal temperature gradient in the temperature logs suggest cold recharge water is moving fast enough to overcome the geothermal gradient and identify the actively flowing portion of the aquifer. The number of deep wells which fully penetrate the aquifer is limited and a large amount of interpolation was needed to create the model's bottom surface. Figure 3-1 illustrates deep well locations and the flowing aquifer thickness at each well. The updated model's bottom surface is below the HI interbed at all locations within the simulation domain and does not present the possibility of extreme confining conditions. The temperature log from well UGSG-22 indicates the aquifer is not moving at this location and the effective thickness is zero. Figure 3-2 illustrates the simulated aquifer thickness in the updated model. The surface illustrated in Figure 3-2 is one of many possible realizations of the active aquifer depth in the vicinity of the INTEC.

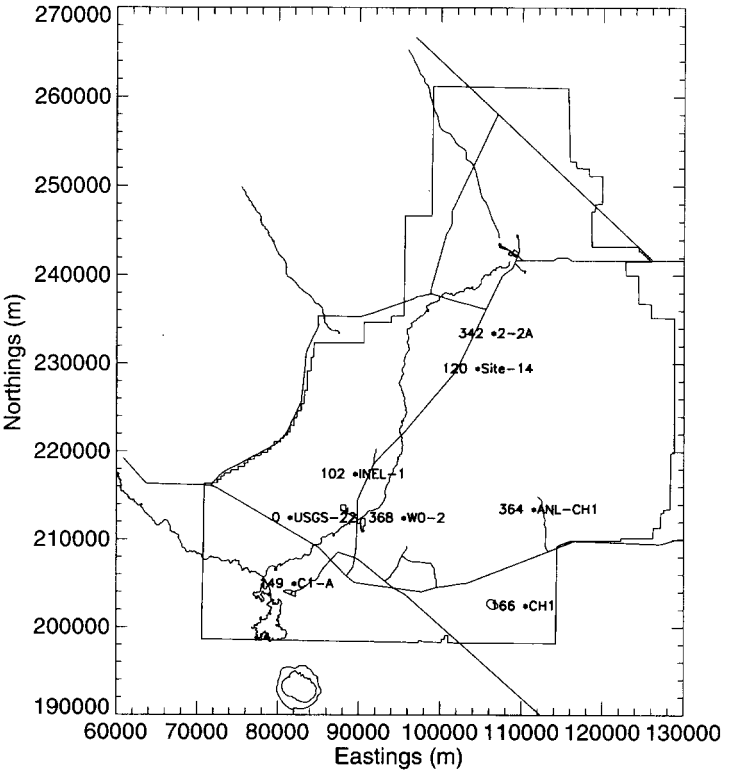

Figure 3-1 INEEL deep wells locations with flowing aquifer depth (m).

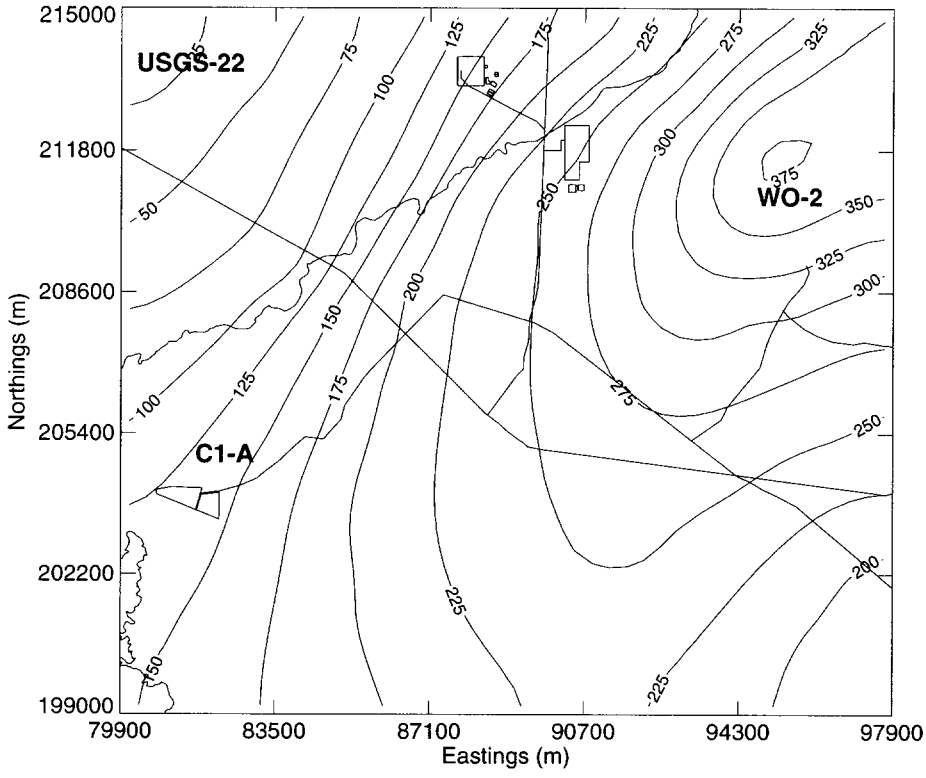

Figure 3-2 Updated aquifer model thickness (m).

3.1.1 HI Interbed Placement

HI interbed elevation and thickness data for placement of the HI interbed were reviewed and incorporated into the updated aquifer model.

3.1.1.1 HI Interbed Depth and Thickness

The HI interbed is a widespread layer of clay and silt overlying basalt flow group I. The interbed tends to dip in the south-east direction when viewed from a large scale (OU 3-13 RI/BRA aquifer model domain) and the interbed tends to become thicker and more continuous in the south-east direction. Well logs from wells SPERT-IV and Site-09 (south-east of INTEC) indicate the interbed can be approximately 27 m thick in some areas.

Data from 51 wells were used to described the HI interbed thickness and surface elevation. Planes were fitted through both surface elevation and thickness data sets. Detrended data sets of the surface and thickness were created by subtracting the fitted planes. Variogram models describing spatial correlation were then fitted to the detrended data and Kriging was used to create the model HI interbed structure. The data used to create the HI interbed is contained in Table 3-1. Figures 3-3 and 3-4 illustrate interbed thickness and Figures 3-5 and 3-6 illustrate interbed elevation surfaces. Figures 3-3 through 3-6 include the data used to create the thickness and elevation surfaces. The correlation length of the thickness data was approximately 5,000 m, but the correlation among the data was not strong. This was especially the case at smaller distances. The weak

correlation and the large grid block size (several observations in one grid block) resulted in the interpolated surfaces departing from the observed data in some locations.

Table 3-1 HI interbed elevation and thickness data.

Well	Easting* (ft)	Northing* (ft)	Well Surface Elevation (m)	Depth to HI Interbed Top (m)	Hi Interbed Thickness (m)
cfa-1	295268	681593	1502.	190.	15.
cpp-3	296574	694817	1498.	158.	2.
cpp-4	297949	697486	1496.	159.	0.
lf2-09	294198	682901	1503.	190.	4.**
lf2-10	294274	682831	1503.	189.	15.
mtr-test	290310	701522	1499.	107.	0.
npr-test	312210	698222	1504.	169.	13.
ow-1	264794	665336	1537.	231.	2.
ow-2	264932	664910	1537.	238.	2.
rwmc-m04d	265512	667255	1531.	222.	1.
site-09	309853	677319	1502.	221.	26.
site-19	286464	701784	1502.	141.	2.
spert-IV	315027	685745	1501.	255.	27.
tra-06a	288954	698077	1501.	149.	2.
tra-07	288106	698380	1503.	151.	2.**
usgs-020	301200	686506	1499.	186.	20.**
usgs-034	292744	690801	1502.	181.	1.
usgs-038	293579	689569	1503.	182.	2.
usgs-039	292261	691692	1503.	173.	1.
usgs-040	295939	694541	1498.	161.	1.
usgs-041	295940	694140	1499.	162.	1.
usgs-042	295936	693637	1499.	167.	0.
usgs-043	295723	694859	1498.	157.	1.
usgs-044	295251	694237	1499.	159.	0.
usgs-045	295490	693598	1500.	165.	3.
usgs-046	295726	694027	1498.	165.	2.
usgs-047	296576	694114	1498.	162.	2.
usgs-048	296612	693414	1499.	167.	1.
usgs-049	297232	693640	1497.	165.	1.
usgs-051	296345	692344	1499.	171.	1.
usgs-052	297972	694833	1496.	160.	2.
usgs-057	294871	691753	1500.	173.	2.
usgs-058	290594	699503	1499.	104.	2.
usgs-059	297685	692760	1498.	169.	1.
usgs-065	288960	698169	1501.	149.	2.**
usgs-066	292672	697345	1500.	111.	2.
* Coordinates are: State Planar, Zone 3701, Datum NAD27					
** Well did not Fully Penetrate Interbed					

Table 3-1 continued HI interbed elevation and thickness data.

Well	Easting* (ft)	Northing* (ft)	Well Surface Elevation (m)	Depth to HI Interbed Top (m)	Hi Interbed Thickness (m)
usgs-067	298205	691728	1498.	174.	5.
usgs-076	290029	695977	1503.	161.	1.
usgs-079	286622	700079	1503.	148.	1.
usgs-082	300453	693410	1496.	170.	3.
usgs-083	295467	671394	1507.	218.	11.**
usgs-085	291436	685932	1505.	192.	2.**
usgs-104	295916	662585	1521.	210.	4.**
usgs-106	280997	669060	1529.	199.	0.
usgs-121	296600	698363	1496.	158.	2.
usgs-123	295776	692519	1500.	170.	1.
C-1A	269793	671707	1533.	213.	2.
EOCR	306147	677081	1507.	294.	10.
NPR_WO-2	312178	698359	1503.	174.	8.
S5G-Test	301655	722940	1478.	213.	8.
WS-INEL-1	294334	713220	1487.	204.	9.
* Coordinates are: State Planar, Zone 3701, Datum NAD27					
** Well did not Fully Penetrate Interbed					

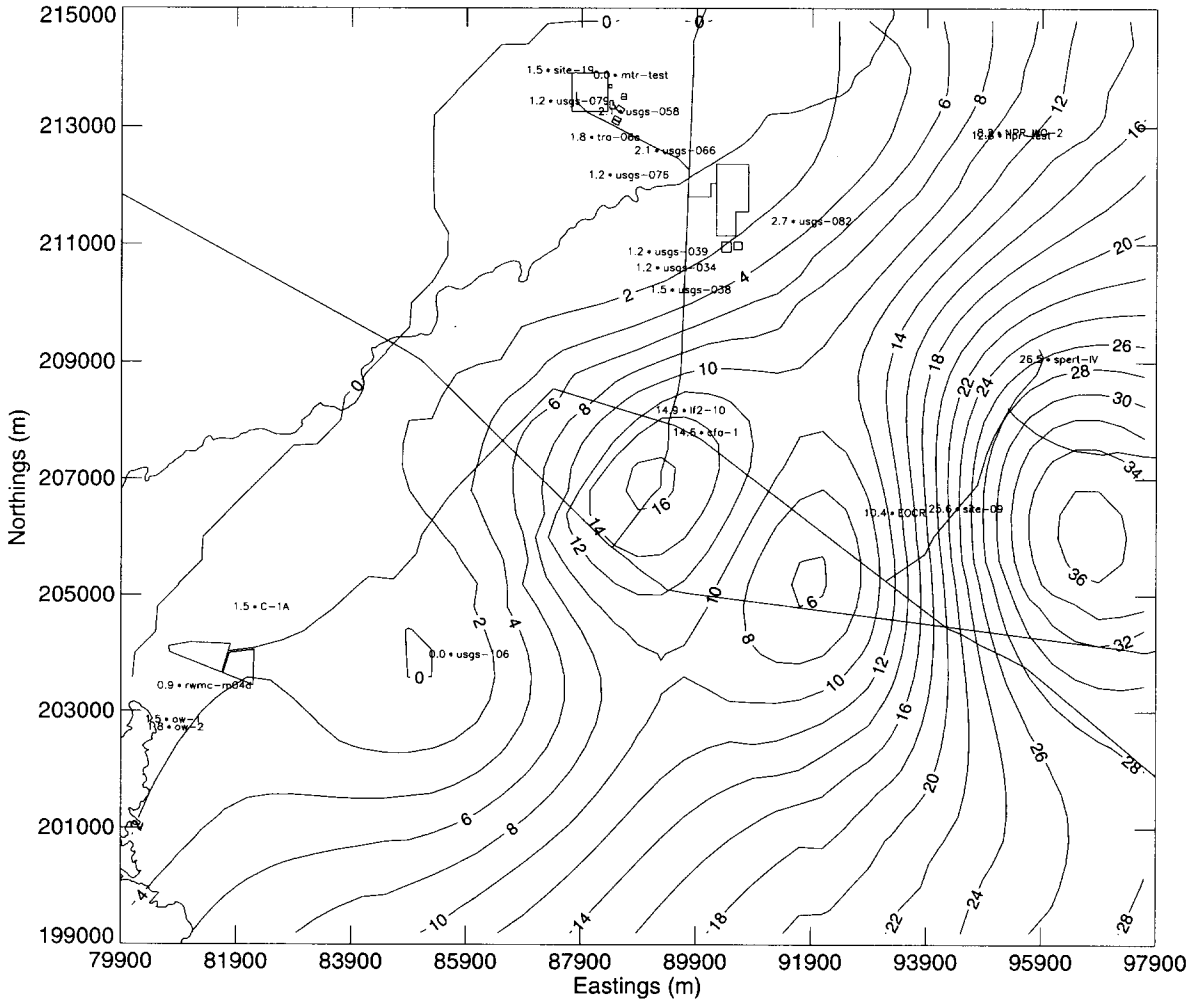

Figure 3-3 Simulated HI interbed thickness surface (m).

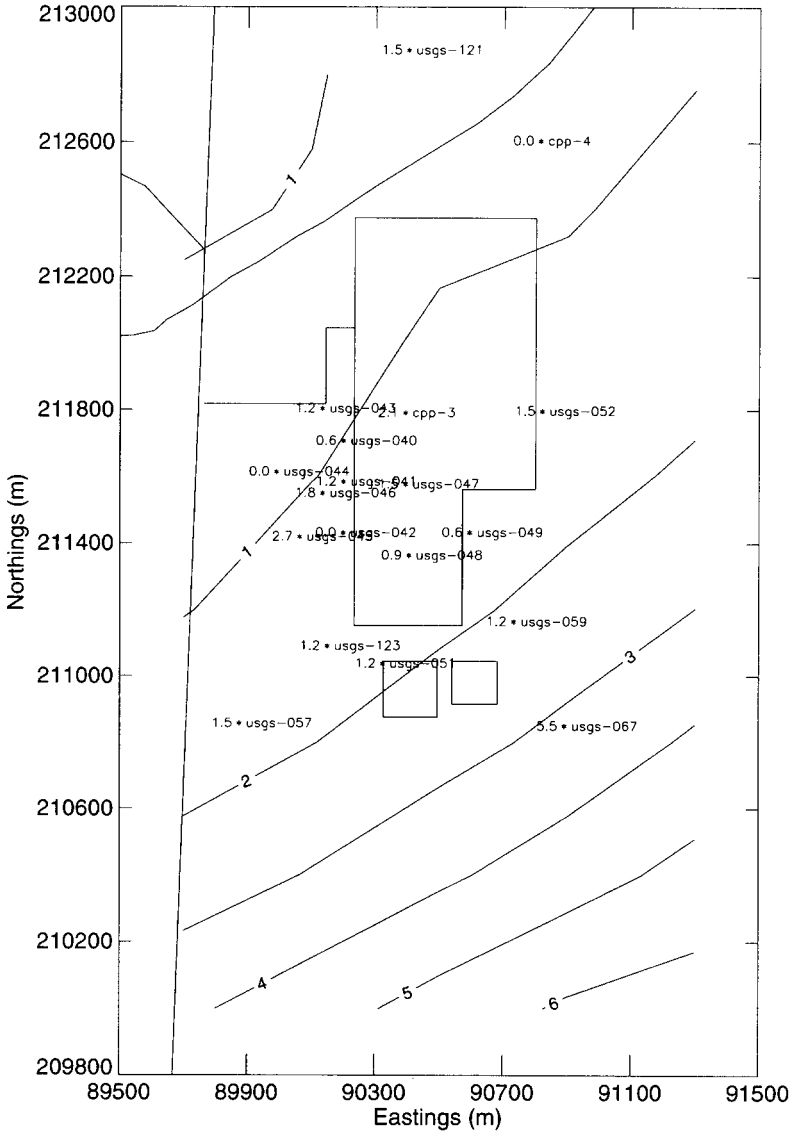

Figure 3-4 Simulated HI interbed thickness surface (m) in the INTEC vicinity.

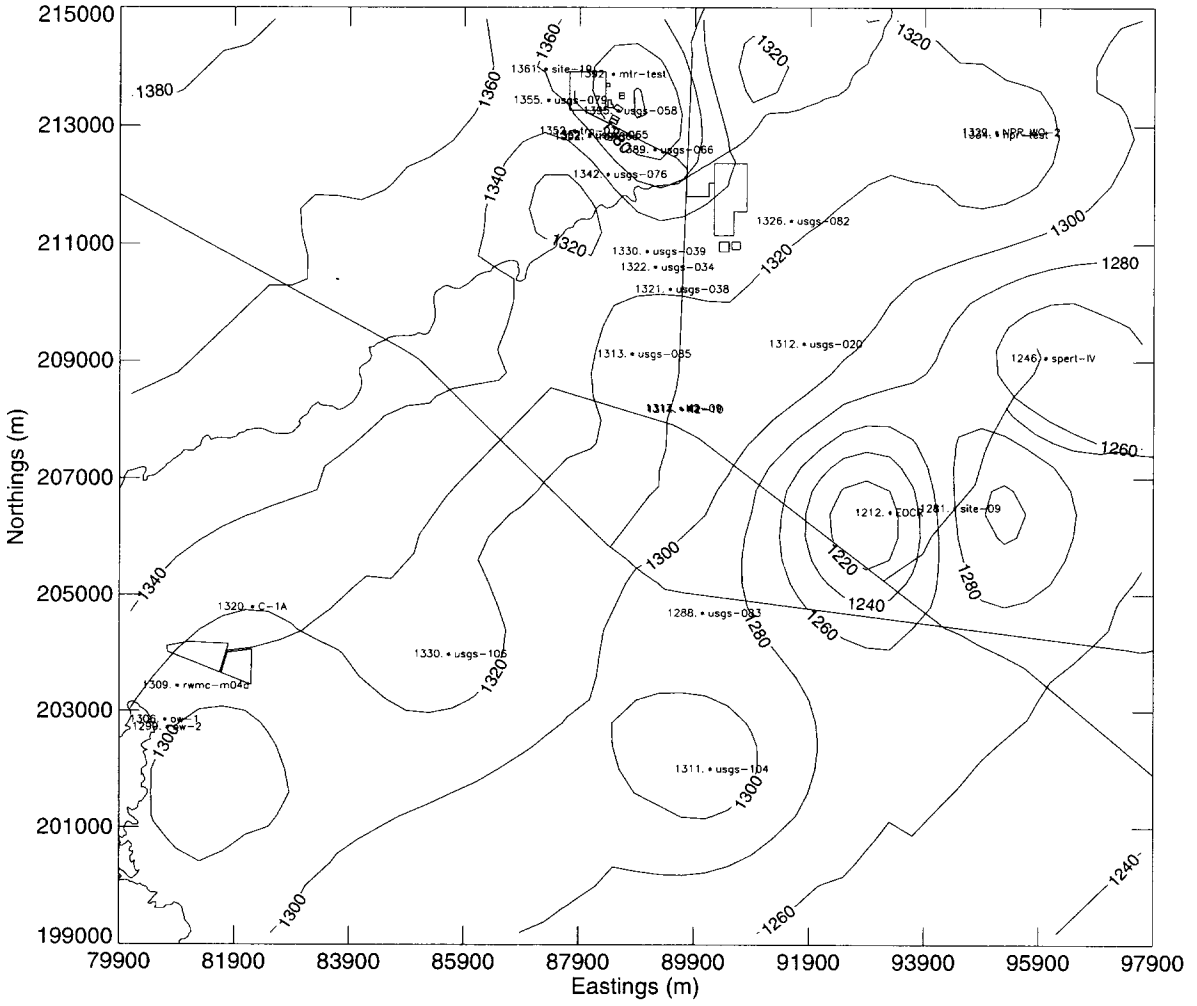

Figure 3-5 Simulated HI interbed surface elevation (m).

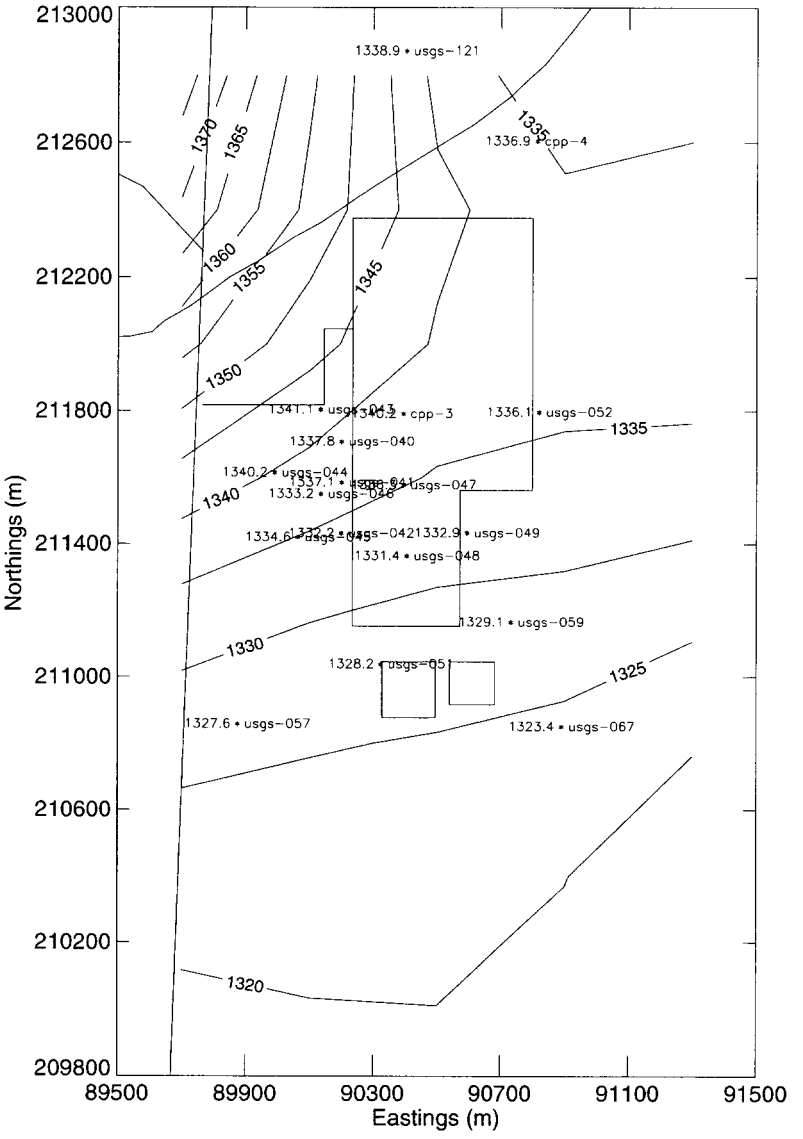

Figure 3-6 Simulated HI interbed surface elevation (m) in the INTEC vicinity.

3.1.2 HI Interbed Rediscretization

The updated model's vertical discretization follows the HI interbed to place more computational nodes in and around the HI interbed. Adapting the grid to follow the HI interbed also allows fewer computational nodes while adequately representing the complex lithology of the interbed. The interbed is represented by an average of four model layers, and the minimum thickness is 2 m. In some locations where the interbed is less than 6 m thick, fewer than 3 grid block are used to represent the interbed. This area is generally located northwest of a line between the SDA and INTEC percolation ponds. The need to maintain appropriate grid block aspect ratios (ratio of vertical to horizontal length) does not allow grid blocks less than 2 m thick. The grid block thickness increases with distance above and below the interbed and the updated model consisted of

18 layers. The vertical discretization is shown in Figure 3-7. The simulated HI interbed is illustrated by the red grid blocks.

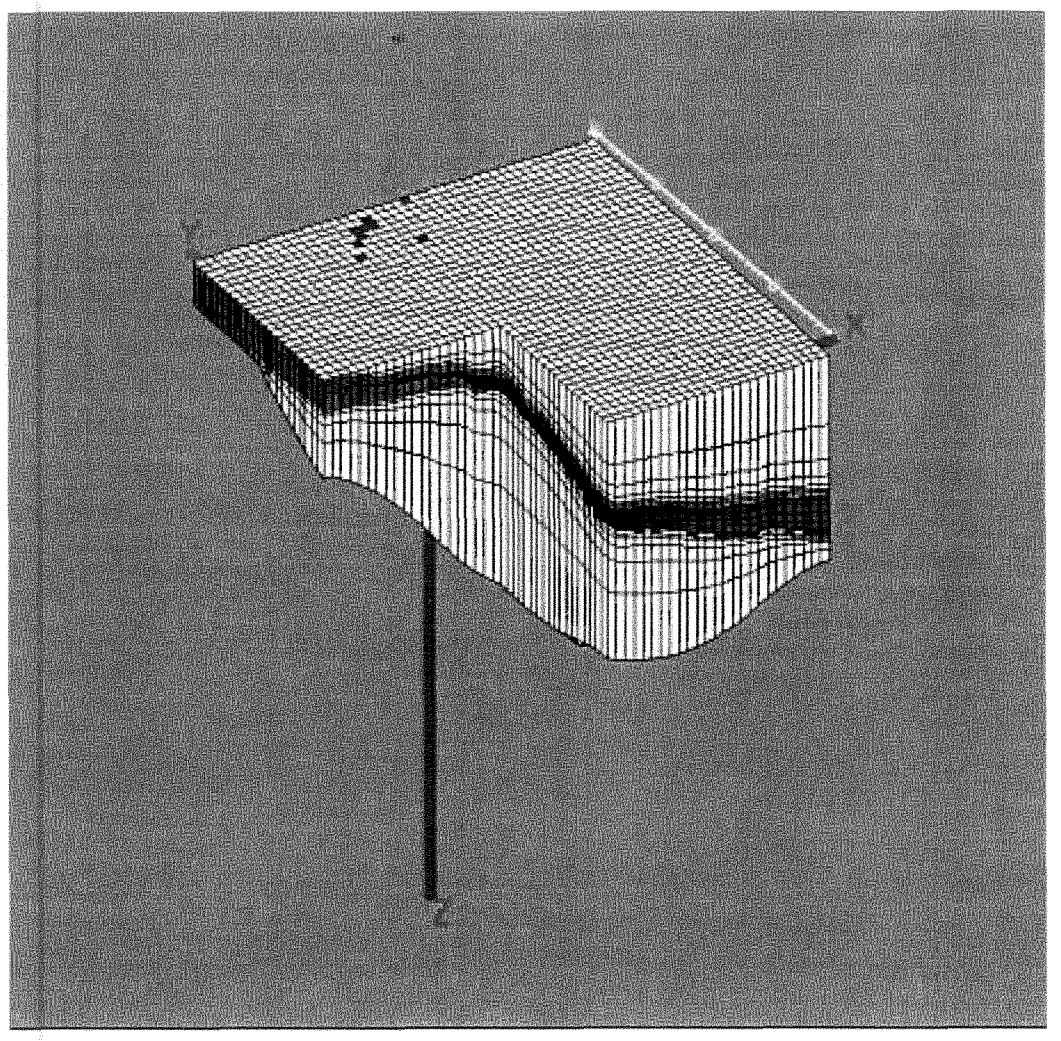

Figure 3-7 Updated aquifer model vertical discretization with vertical exaggeration.

3.1.3 Model Discretization Sensitivity Results

The discretization sensitivity simulations used the updated model's grid, but did not use the recalibrated model's hydrologic parameters. Parameterization of the rediscretized model, apart from the vertical discretization, was identical to the RI/BRA model. The rediscretized model predicts the peak aquifer I-129 concentration will be 0.26 pCi/L in the year 2095. This is in contrast to the OU 3-13 RI/BRA model, which predicted the peak concentration would be 3.0 pCi/L in the year 2095 and large area of the HI interbed south of the INTEC would remain above the 1 pCi/L beyond 2095. This is primarily due to the rediscretization of the HI interbed and placing the model bottom below the HI interbed. I-129 still persists in the rediscretized model's HI interbed, but to a lesser extent of that in the RI/BRA model. In both models, the I-129 takes a relatively long time to enter and exit the interbed compared to basalt. This is because of the low permeability (4 mD (0.01 ft/day) for the interbed vs. approximately 1.e+5 mD (243 ft/day) for the basalt) and high porosity (0.487 for the interbed vs. 0.0625 for the basalt). In the RI/BRA model, I-129 persists longer within and above the HI interbed because of low velocity areas created by the different HI interbed placement. It is important to note that the rediscretized model has not been calibrated to tritium disposal and breakthrough as the RI/BRA

model was. The I-129 plumes in both models are comparable. However, the axis of the rediscretized model's plume has shifted slightly westward.

Figure 3-8 illustrates the maximum vertical I-129 concentrations and the plume axis as predicted by the rediscretized model in year 2000 and 2095. Figures 3-9 and 3-10 illustrate vertical cross sections of the rediscretized model's plume axis for the years 1954, 1965, 1981, 2000, 2025, 2058, 2074 and 2095. The aquifer bottom is shown as a thick red line and the HI interbed is denoted by dashed lines. The 0.01, 0.1, and 1.0 pCi/L isopleths are illustrated by a thin dashed, thin, and thick black lines, respectively. The CPP-3 injection well was simulated as a fully screened well extending 40 m below the water table and is shown in Figures 3-9 and 3-10 as a vertical blue line in the upper left corner of each cross-section. The CPP-03 injection well is screened across the HI interbed, which is present approximately 25 m below the water table. Figures 3-9 and 3-10 use a 300 m vertical scale instead of the 100 m scale presented in the RI/BRA cross sections because of the increased rediscretized model's depth.

I-129 disposal begins in 1954 and by 1965, as with the RI/BRA model, the down gradient migration of I-129 in the HI interbed lags behind that in the surrounding basalt. However in the year 2058, clean water movement through the contamination area lags in the interbed and isolated high concentrations of I-129 persist in the interbed where aquifer velocity is low.

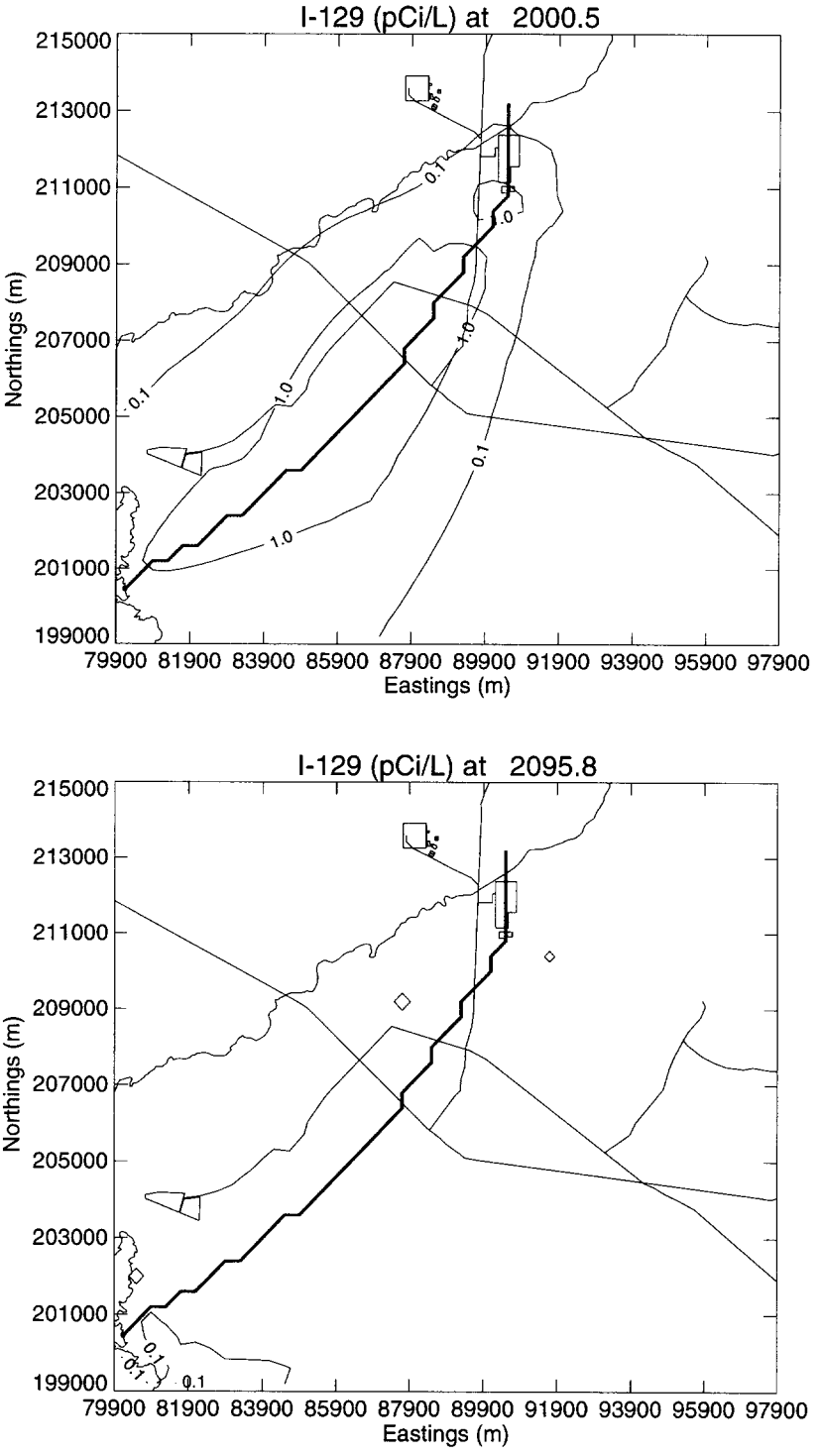

Figure 3-8 Rediscretized model maximum I-129 concentrations in 2000 and 2095 with plume axis (blue).

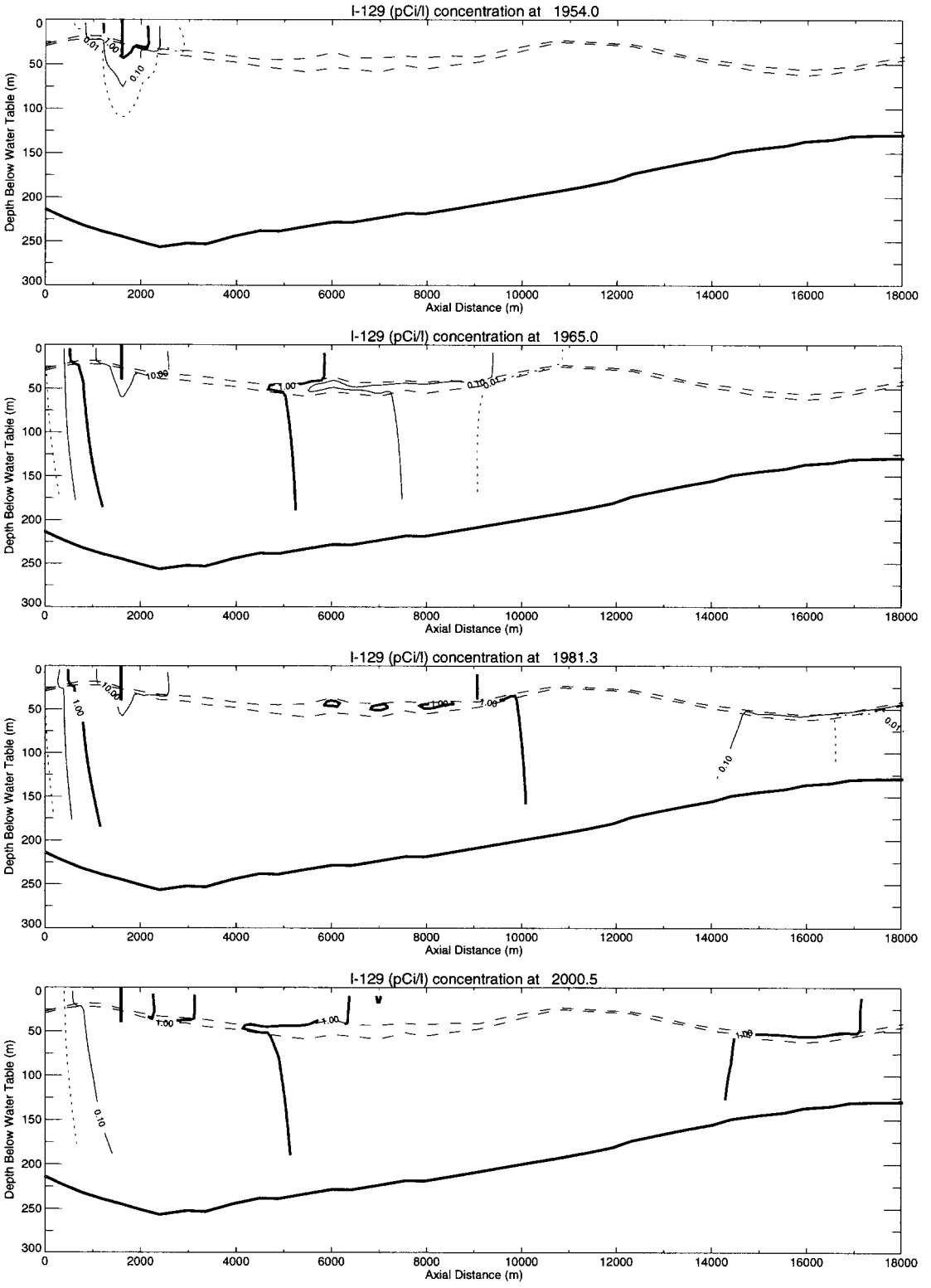

Figure 3-9 Rediscretized model plume axis vertical I-129 concentrations in 1954, 1965, 1981, and 2000 (the injection well is blue, the model bottom is red, and the long dashed black line represents the interbed).

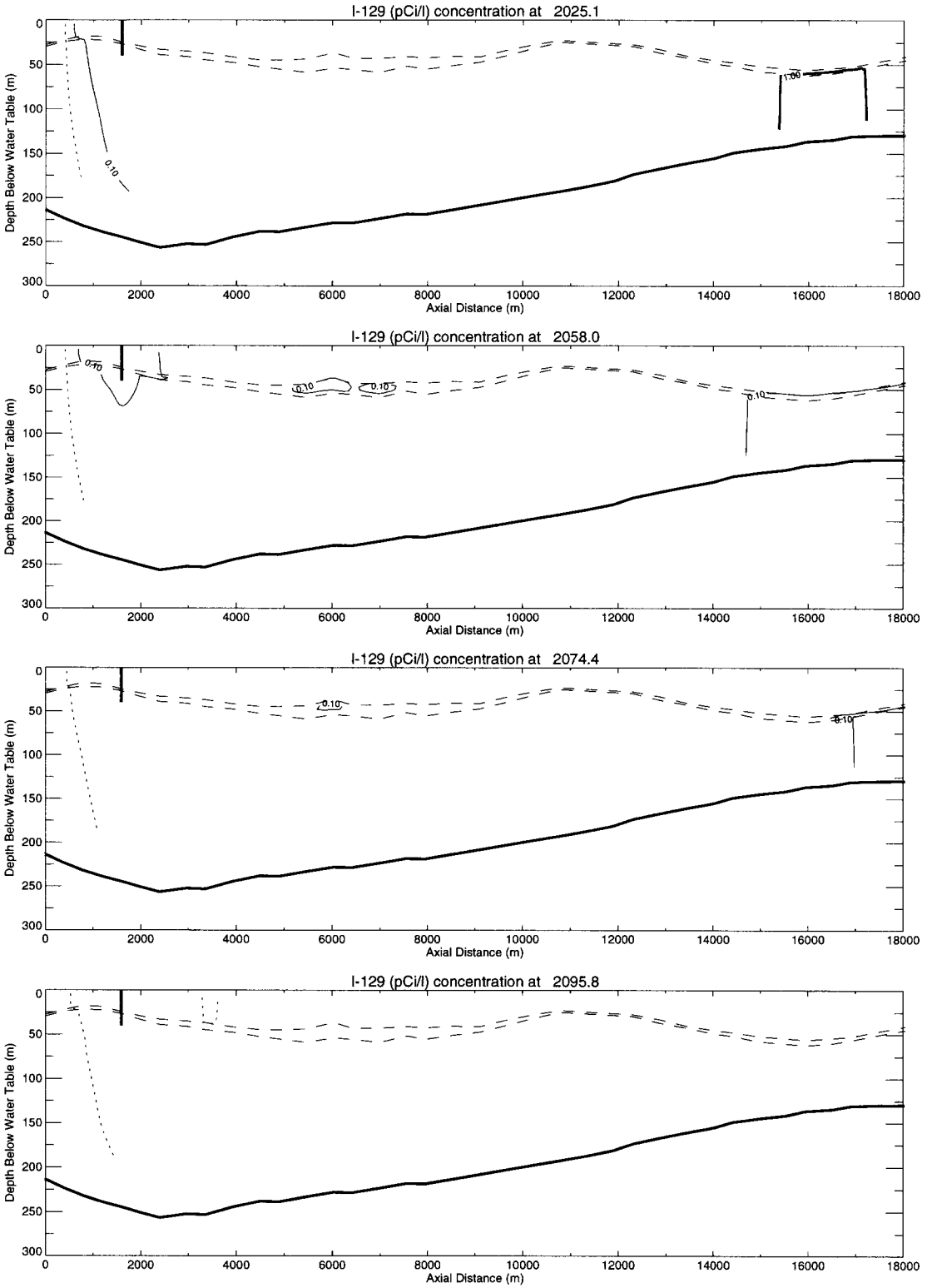

Figure 3-10 Rediscretized model plume axis vertical I-129 concentrations in 2025, 2058, 2074, and 2095 (the injection well is blue, the model bottom is red, and the long dashed black line represents the interbed).

3.2 Model Sensitivity to HI Interbed Permeability

The low permeability of the HI interbed is primarily responsible for maintaining elevated I-129 concentrations in the simulated Snake River Plain Aquifer. There is very little data available on the permeability of the HI interbed. The OU 3-13 RI/BRA aquifer modeling used a 4 mD (0.01 ft/d) interbed permeability from the RI/BRA vadose zone model calibration to perched water bodies beneath the INTEC. There is little confidence that vadose zone calibration adequately represents the HI interbed permeability within the aquifer. The existing permeability data for the HI interbed was reviewed and most representative permeability value along with reasonable bounds for the interbed permeability were estimated. The sensitivity of the RI/BRA and rediscretized model to HI interbed permeability using bounding values was evaluated to determine the value of gathering HI interbed permeability data.

3.2.1 Permeability Data Review

There is very little information available on the hydraulic conductivity of the HI interbed and the following tables include information available regarding other interbeds. WAG-3 OU 3-13 RI/BRA (DOE-ID, 1997) contained three tables with interbed hydraulic properties. The hydraulic conductivity information in those tables has been summarized, converted to permeability in millidarcies (mD) and presented in Table 3-2. In addition, in Table 3-3 is a summary of HI interbed hydraulic conductivities estimated by model calibration of pumping test results performed by the State of Idaho (Fredrick and Johnson, 1996). These pumping tests were done using packers to isolate the interbed from the surrounding basalt and are the only hydraulic conductivity information available specifically for the HI interbed.

Based on these interbed permeabilities, the 4 mD (0.01 ft/d) used for the WAG 3-13 modeling is relatively low. The HI interbed model calibration results shown in Table 3-2 (Frederick and Johnson, 1996) suggest the range is 37 mD (0.09 ft/d) to 100 mD (0.24 ft/d). Therefore, the 4 mD (0.01 ft/d) used for the WAG 3-13 modeling is at least an order of magnitude low. The other interbed permeability information ranges from 0.05 mD (0.0001 ft/d) to 3,500 mD (8.5 ft/d). An average permeability of 40 mD (0.10 ft/d) is on the low end of a the most appropriate permeability value. The 4 mD (0.01 ft/d) used in the RI/BRA modeling represents a low bounding value and 200 mD (0.49 ft/d) represents a high bounding value. A 200 mD (0.49 ft/d) permeability is approximately double the geometric mean all interbed permeability data provided in Table 3-2 and double the highest value in Table 3-3.

Table 3-2 Summary of interbed hydraulic conductivity data from the OU 3-13 RI report (DOE-ID,1997).

Well	Material	Average Permeability (mD)	Range of Permeability (mD)		Reference
MW-2	Sandy clay interbed	1.86E+03	Single Value		OU 3-13 RI, Table 2-17
MW-4	Silty sand and gravel interbed	4.04E+01	Single Value		OU 3-13 RI, Table 2-17
MW-6	Silty sand, fine grained inter-bed	1.35E+03	Single Value		OU 3-13 RI, Table 2-17
MW-3	Silty clay	9.21E+01	Single Value		OU 3-13 RI, Table 2-18
MW-4	Silty sand and gravel	1.66E+01	Single Value		OU 3-13 RI, Table 2-18
MW-8	Clay with silt	1.14E+01	Single Value		OU 3-13 RI, Table 2-18
MW-10	Sandy silt	1.04E+01	Single Value		OU 3-13 RI, Table 2-18
MW-11	Silty sand	1.24E+01	Single Value		OU 3-13 RI, Table 2-18
MW-4	Silt	3.31E+01	Single Value		OU 3-13 RI, Table 2-18
MW-4	Silt	6.94E+01	Single Value		OU 3-13 RI, Table 2-18
Arithmetic mean		1.45E+03			
Geometric mean		8.86E+01			

Table 3-2 continued Summary of interbed hydraulic conductivity data from the OU 3-13 RI report (DOE-ID,1997).

Well	Material	Average Permeability (mD)	Range of Permeability (mD)	(mD)	Reference
MW-6	Clay	3.11E-01	Single Value		OU 3-13 RI, Table 2-18
MW-9	Clay with silt	2.17E+04	Single Value		OU 3-13 RI, Table 2-18
MW-11	Clay	5.38E-02	Single Value		OU 3-13 RI, Table 2-18
MW-3	silty clay	8.59E+02	Single Value		OU 3-13 RI, Table 2-18
MW-6	silty clay	2.28E+03	Single Value		OU 3-13 RI, Table 2-18
MW-9	silt with clay	3.52E+03	Single Value		OU 3-13 RI, Table 2-18
MW-1	sand with silt	3.42E+02	Single Value		OU 3-13 RI, Table 2-18
CD interbed		3.83E+01	3.11E-01	1.35E+03	OU 3-13 RI, Table 2-19
D interbed		1.35E+02	5.38E-02	3.52E+03	OU 3-13 RI, Table 2-19
deep interbed		3.42E+02	3.42E+02	3.42E+02	OU 3-13 RI, Table 2-19
TRA		1.45E+00	1.76E-02	1.45E+03	OU 3-13 RI, Table 2-19
RWMC		7.87E+01	7.87E+01	7.87E+01	OU 3-13 RI, Table 2-19
Arithmetic mean		1.45E+03			
Geometric mean		8.86E+01			

Table 3-3 Summary of calibrated HI interbed permeability values from Fredrick and Johnson, 1996.

Well	Permeability (mD)	Reference
USGS-44	9.99E+01	Fredrick and Johnson, 1996, Table 11
USGS-45	7.89E+01	Fredrick and Johnson, 1996, Table 11
USGS-46	7.89E+01	Fredrick and Johnson, 1996, Table 11
USGS-59	3.68E+01	Fredrick and Johnson, 1996, Table 11
arithmetic mean	73.62	
geometric mean	69.17	

3.2.2 Permeability Sensitivity Results

HI interbed permeability in the RI/BRA and rediscretized model was varied from 4 to 200 mD (0.01 to 0.5 ft/day) and peak concentrations and the size of the I-129 plume in 2095 were compared. The area of the remaining plume in 2095 is very sensitive to permeability and monotonically decreases in size with increasing permeability for both models. The RI/BRA model area of the 0.1pCi/L plume decreased from 70.6 to 45.4 Km^2 for the 4 and 200 mD (0.01 to 0.49 ft/day) interbed permeability, respectively. The rediscretized model 0.1 pCi/L area decreased from 4.32 to 0 Km^2 for the 4 and 200 mD (0.01 to 0.49 ft/day) simulations. The peak concentrations in the year 2095 did not monotonically decrease with increasing permeability. The RI/BRA model's peak values ranged from 2.1 pCi/L for the 8 mD (0.02 ft/day) permeability to 3.4 pCi/L for the 40 mD (0.1 ft/day) permeability simulation. The rediscretized model's peak values ranged from 0.09 pCi/L for the 200 mD (0.49 ft/day) simulation to 0.50 pCi/L for the 8 mD simulation. The varied peak concentrations in 2095 for the different interbed permeabilities indicate flow field substantially changes with different interbed permeabilities, which results in different areas retaining high I-129 concentrations. Only the RI/BRA 4 mD (0.01 ft/day) interbed permeability simulation was calibrated to tritium disposal in CPP-3 and breakthrough in down gradient wells. Table 3-4 provides maximum concentrations and the area of the I-129 plume with concentrations above 0.1 and 1.0 pCi/L.

Table 3-4 Permeability sensitivity year 2095 I-129 maximum concentrations and areal extent.

HI Interbed Permeability Sensitivity Simulation	RI/BRA Model			Rediscretized Model*		
	Maximum 2095 Concentration (pCi/L)	2095 Areal Extent of 0.1 pCi/L Plume (km^2)	2095 Areal Extent of 1 pCi/L Plume (km^2)	Maximum 2095 Concentration (pCi/L)	2095 Areal Extent of 0.1 pCi/L Plume (km^2)	2095 Areal Extent of 1 pCi/L Plume (km^2)
4mD	3.0	70.6	1.92	0.26	4.32	0.
8mD	2.1	64.8	0.80	0.50	2.08	0.
40mD	3.4	51.2	0.32	0.24	0.64	0.
200mD	3.1	45.4	0.96	0.09	0.	0.
*The rediscretized model used identical hydrologic properties as the RI/BRA. Only the model discretization was changed.						

4 WAG-3 UPDATED AQUIFER MODEL CALIBRATION AND PREDICTIVE SIMULATIONS

The conceptual model of the HI interbed used to evaluate the RI/BRA model's sensitivity to HI interbed parameterization is used as the basis for the updated aquifer model. The updated model was recalibrated to flow and transport with the goal of achieving or exceeding the same degree of model calibration as that of the RI/BRA model. The updated model was then used as a predictive tool to reassess the beta/gamma radiation emitting contaminants of potential concern (COPCs) identified in the RI/BRA. The simulated contaminants included: iodine-129, cobalt-60, cesium-137, tritium, plutonium-241, strontium-90, and technetium-99.

4.1 Updated Model Calibration

The updated model used the same discretization as the rediscretized RI/BRA model used for the HI interbed parameter sensitivity analysis presented in Section 3.1. As with the RI/BRA model, the updated model incorporated a H basalt, HI interbed, upper I basalt, and lower I basalt structure. The upper I basalt was located north-west of the INTEC where the HI interbed is more steeply angled downward and is defined in approximately the top 25 m of the I basalt. Initial permeability values for the updated model's H basalt were created from a spatial correlation analysis of pumping test hydraulic conductivity values in INEEL wells. Initial permeability values for the updated model's HI interbed and I basalt were taken from the RI/BRA model. Initial estimates of model transport parameters (porosity and dispersivity) were also taken from the RI/BRA model. Figure 4-1 illustrates the initial H basalt hydraulic conductivity field and includes the pumping test data.

The boundary conditions for the rediscretized model were specified flux at the surface from the Big Lost River and the RI/BRA vadose zone model, zero flux at the model bottom, and specified pressure head on the model sides. Initial values for the specified head boundary conditions were created from performing a spatial correlation analysis on the 1999 head data set and interpolating these values onto the model perimeter. These initial model parameter estimates were then adjusted during model calibration.

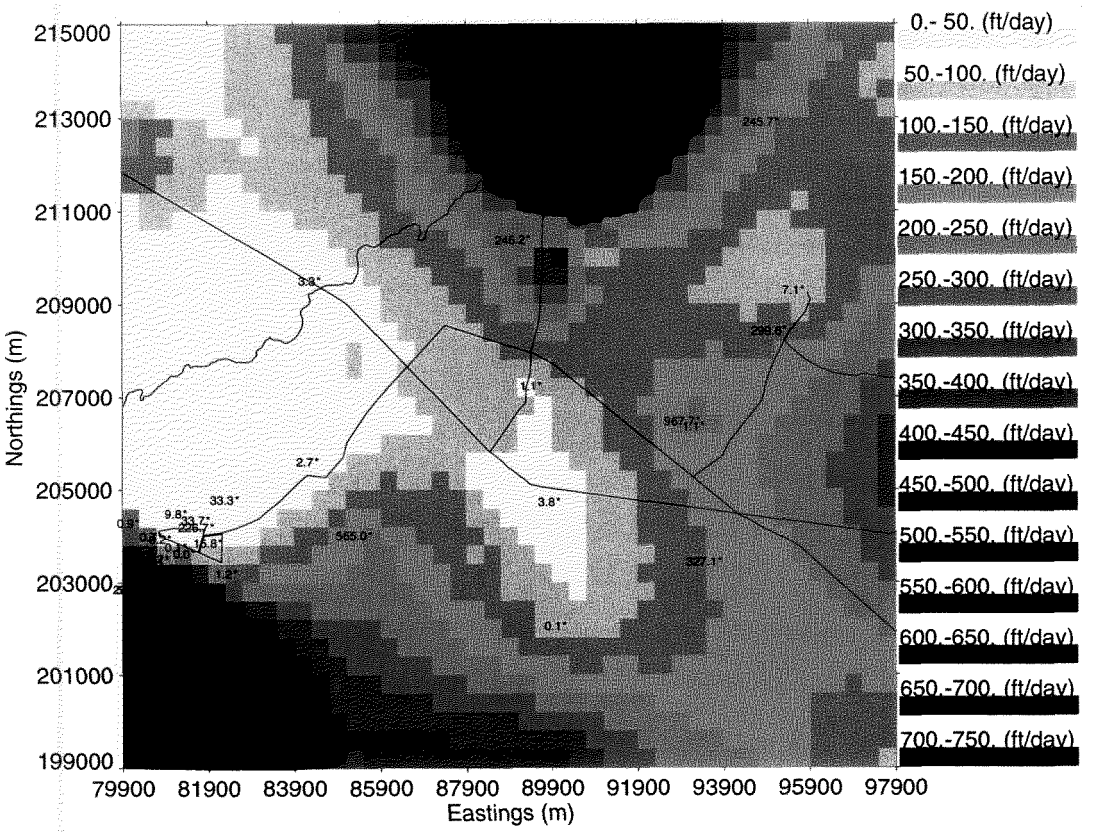

Figure 4-1 Initial H basalt hydraulic conductivity estimate.

4.1.1 Aquifer Hydraulic Head Calibration

The best agreement with the spring 1999 hydraulic head data was obtained by slightly adjusting the model's southeast specified head boundary condition and setting the H basalt minimum permeability to 1,000 mD (2.4 ft/day). A minimum H basalt permeability was needed to prevent extreme mounding from Big Lost River recharge. The updated model's hydraulic head RMS error over all wells within the simulation domain was 1.1 m. The updated model's steady-state flow field with spring 1999 measured hydraulic head is presented in Figures 4-2 and 4-3. It is interesting to note that recharge from the spreading areas located southwest of the Radioactive Waste Management Complex (southwest corner of the simulation domain) may be creating sufficient groundwater mounding to locally reverse the gradient. The average hydraulic head of four wells immediately east of the spreading area (RWMC-MA65, USGS-120, RWMC-MA66, and RWMC-MA13) is 1351.5 m and average hydraulic head of six wells immediately south of the RWMC (RWMC-M01S, USGS-17, USGS-88, RWMC-M04D, USGS-119, and RWMC-M06S) is 1350.1 m suggesting water is flowing towards the SDA from the spreading area.

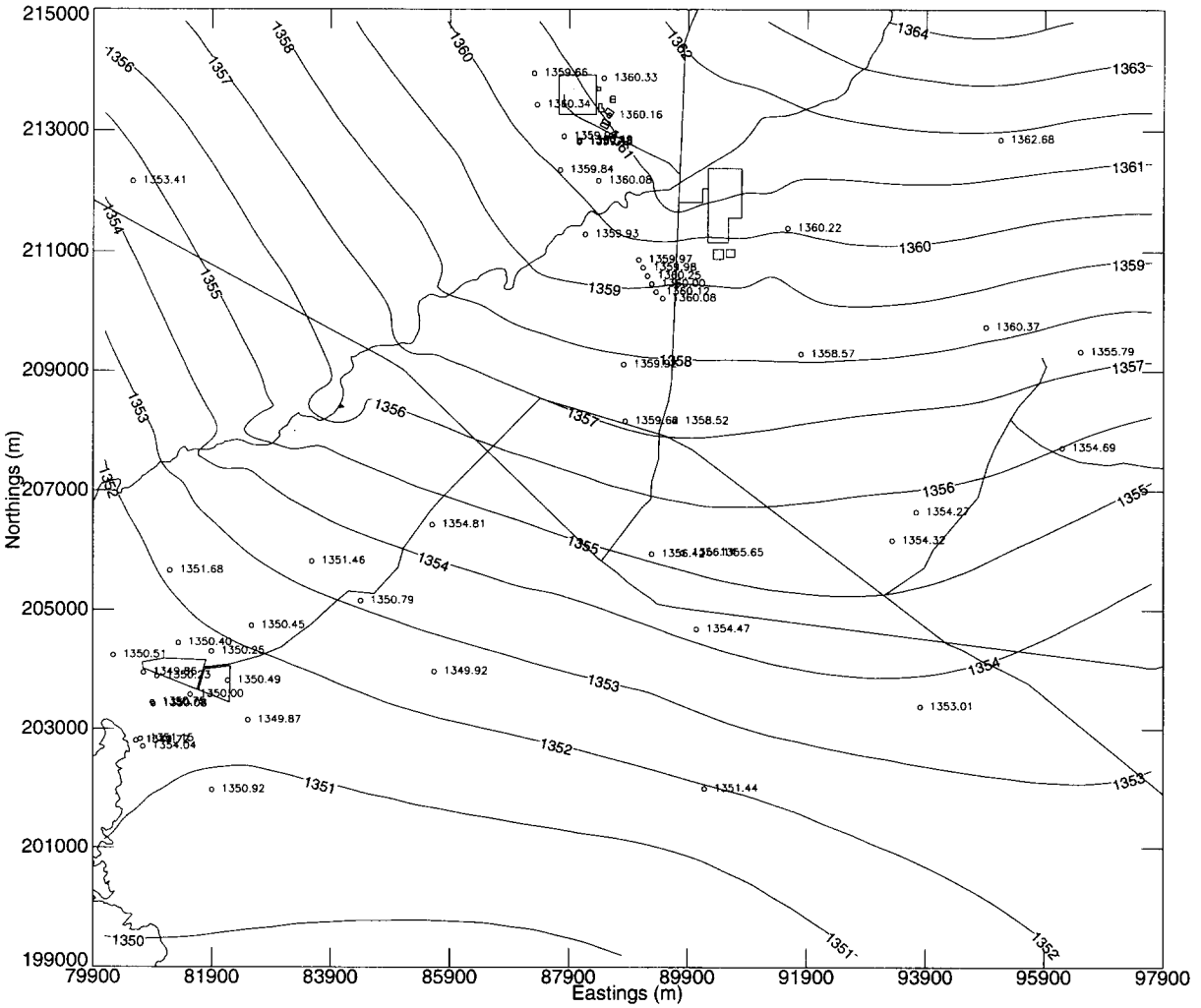

Figure 4-2 Rediscretized model hydraulic head (m) with spring 1999 observations.

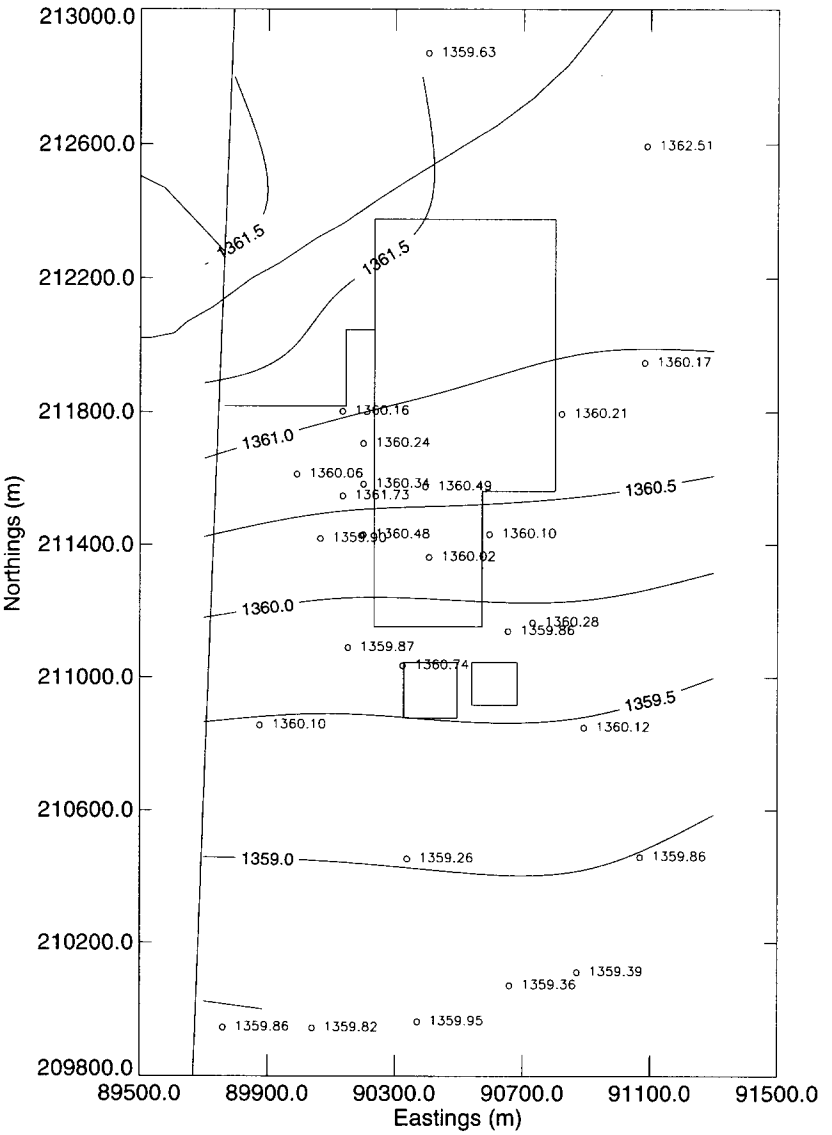

Figure 4-3 Rediscretized model hydraulic head (m) with spring1999 observations near the INTEC.

4.1.2 CPP-3 Injection Well Tritium Disposal Calibration

The best agreement between simulated and observed tritium concentrations was obtained by decreasing basalt porosity to 3% and decreasing the initial basalt permeability estimates by a factor of two. Increasing the HI interbed permeability from 4 mD (0.01 ft/day) to 70 mD (0.17 ft/day) and increasing the dispersivity to 20 m in the longitudinal direction 10 m in the transverse direction also improved the calibration. 70 mD (0.17 ft/day) was the average permeability obtained by pumping tests of the HI interbed (Frederick and Johnson, 1996).

The rediscretized model's calibrated porosity was similar to the value needed to simulate the trichloroethene plume at the Test Area North (TAN) (Martian, 1997). Both the updated model and the TAN

model departed from previous groundwater modeling of the INEEL by using a variable thickness aquifer based on hydrogeologic data. The QR interbed provided the effective bottom of the contaminated aquifer at TAN and deep well temperature logs provided estimates the actively flowing aquifer below the INTEC. Inverse modeling of a large scale infiltration/tracer test at the INEEL (Magnuson, 1995) also produced an approximately 3% large scale effective porosity for the fractured basalt.

Figure 4-4 illustrates the model predicted breakthrough and observed tritium concentrations for each calibration well. The updated model's ModRMS error was 1.86 and the average correlation coefficient was 0.496 for all wells. The updated model's hydraulic head calibration was significantly improved over the RI/BRA calibration. The RMS error was decreased from 1.6 m to 1.1 m. However, the magnitude of the tritium calibration error was not significantly improved. The ModRMS error decreased from 1.98 to 1.86 m. The correlation coefficient was significantly improved over the RI/BRA model's value. The correlation coefficient increased from 0.239 to 0.496. Both the RI/BRA and the updated model greatly overpredict tritium concentrations in wells USGS-39, USGS-35, and USGS-34 (upper crescent wells) and match concentrations in wells USGS-36, USGS-37, and USGS-38 (lower crescent wells). The order of magnitude decrease in observed tritium concentration between the upper and lower crescent wells suggests permeability may be lower near the upper crescent wells or local recharge from the Big Lost River may be changing the local gradient and diluting aquifer concentrations. In either case, hydrologic data is not available to explain the different tritium concentrations. Pumping tests of the crescent wells could assist in explaining the very different tritium concentrations seen between wells USGS-34 and USGS-36.

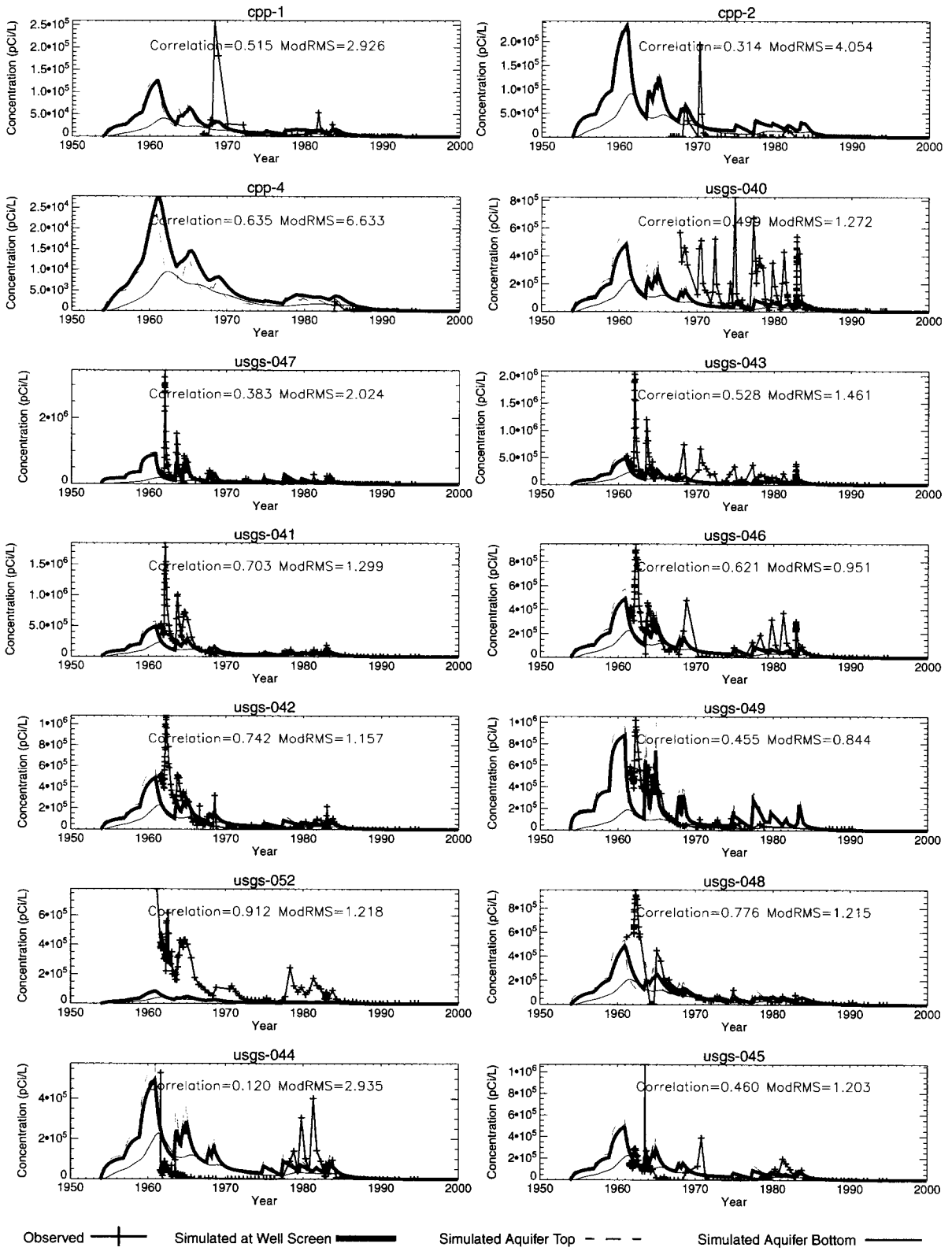

Figure 4-4 Updated model tritium calibration wells breakthrough.

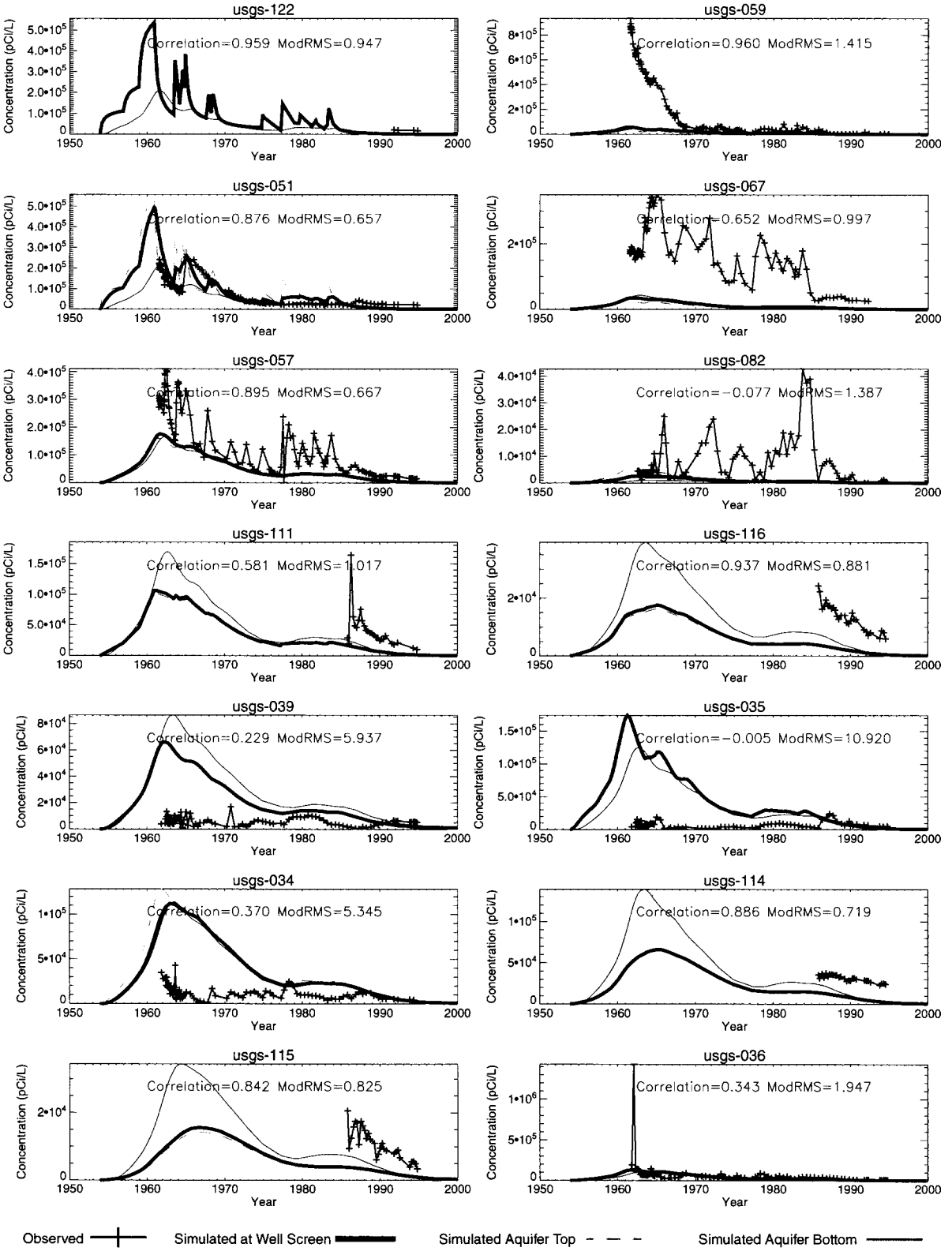

Figure 4-4 continued Updated model tritium calibration wells breakthrough.

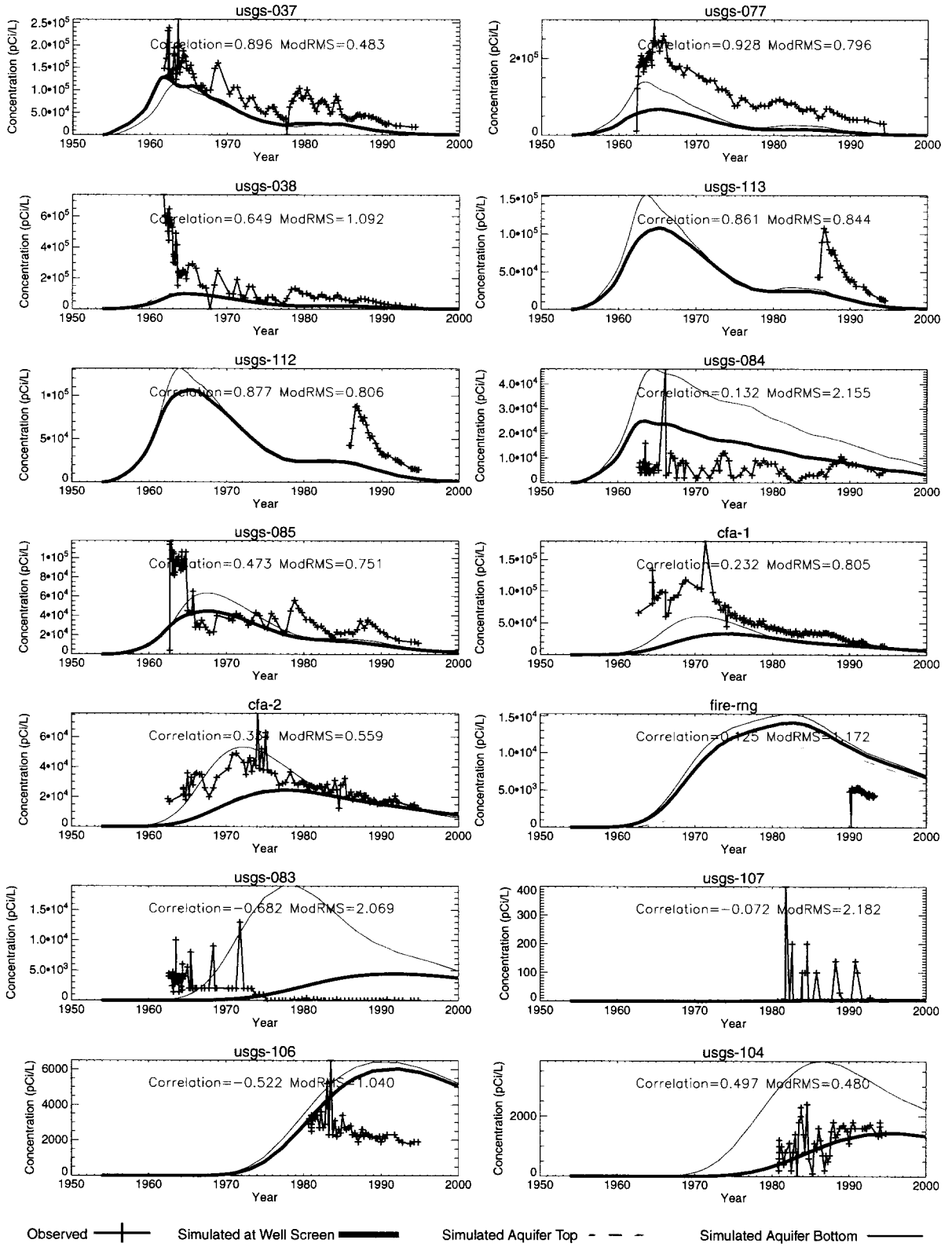

Figure 4-4 continued Updated model tritium calibration wells breakthrough.

4.2 Updated Model Predictive Simulations

The beta/gamma radiation emitting COPCs identified in the RI/BRA were simulated with the updated and recalibrated model. The simulated contaminants included: iodine-129, cobalt-60, cesium-137, tritium, plutonium-241, strontium-90, and technetium-99. Table 4-1 lists each COPC, the half-life, the partition coefficients (K_d), the 10^{-6} risk concentration, and the federal drinking water standard (MCL) concentration. The partition coefficient are those used in the RI/BRA analysis. The simulations used the water and COPC flux from the RI/BRA vadose zone simulations as the upper boundary condition. This upper boundary condition represents the soil contamination and backed up injection well sources. A complete description of contaminant sources can be found in the RI/BRA (DOE-ID, 1997).

The updated model simulation results are presented as peak contaminant concentration anywhere in the aquifer over the simulation period and as aquifer breakthrough concentrations at observation wells. Observed concentrations are graphically compared to simulated concentrations by overplotting the data on the breakthrough curves. Comparison of Pu-241 concentrations is not presented because the Pu-241 isotope has not been reported in the aquifer. Individual simulation results are presented in Sections 4.2.1 through 4.2.7 and the predictive simulations summary along with the cumulative risk of all simulated COPCs is presented in Section 4.2.8. Figures 4-5 and 4-6 illustrate well locations for comparison of simulated and measured contaminant concentrations.

Table 4-1 Simulated beta/gamma radiation emitting contaminants.

Contaminant	Half-life (years)	Sediment K_d (ml/g)	Basalt K_d (ml/g)	10^{-6} Risk Concentration (pCi/L)	Federal Drinking Water Standard* (pCi/L)
Iodine 129 (I-129)	1.57e+7	0.	0.	0.261	1.0
Cobalt 60 (Co-60)	5.27	10.	0.4	2.54	100.
Cesium 137 (Cs-137)	30.2	500.	20.	1.52	200.
Tritium (H-3)	12.3	0.	0.	671.	20,000.
Plutonium 241 (Pu-241)	14.4	22.	0.88	0.145	63.**
Strontium 90 (Sr-90)	29.1	12.	0.48	0.859	8.
Technetium 99 (Tc-99)	2.11e+5	0.2	0.008	34.3	900.

*Based on the 4mrem/yr critical organ dose as listed in the National Bureau of Standards Handbook 69 (HB69) and 2l/d 365d/yr consumption rate.

**Not listed in NBS 69. 1991 proposed limits at 4mrem/yr effective dose equivalent, which corresponds to 4.66e-6 risk.

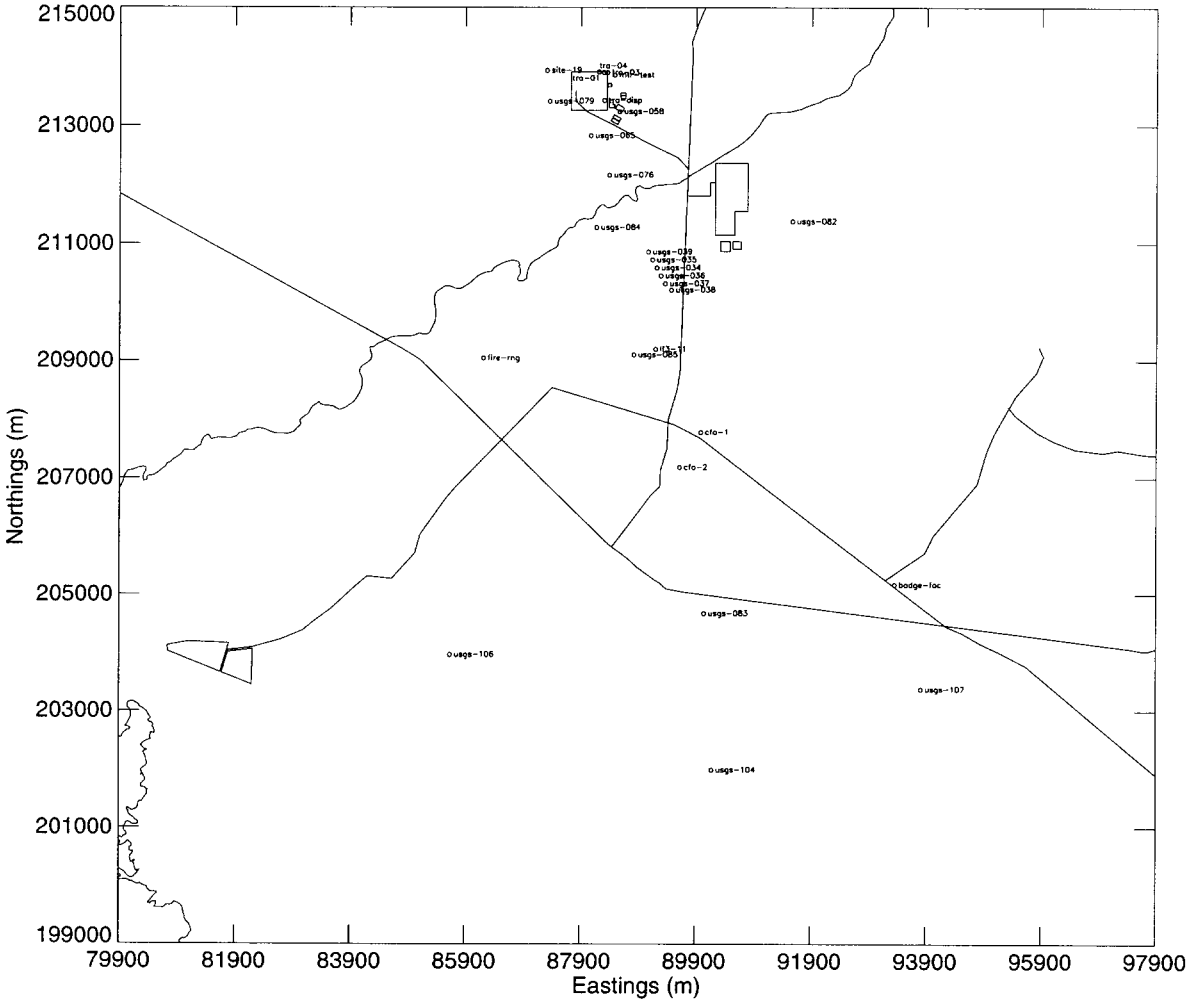

Figure 4-5 Well locations used for comparison of simulated and measured contaminant concentration.

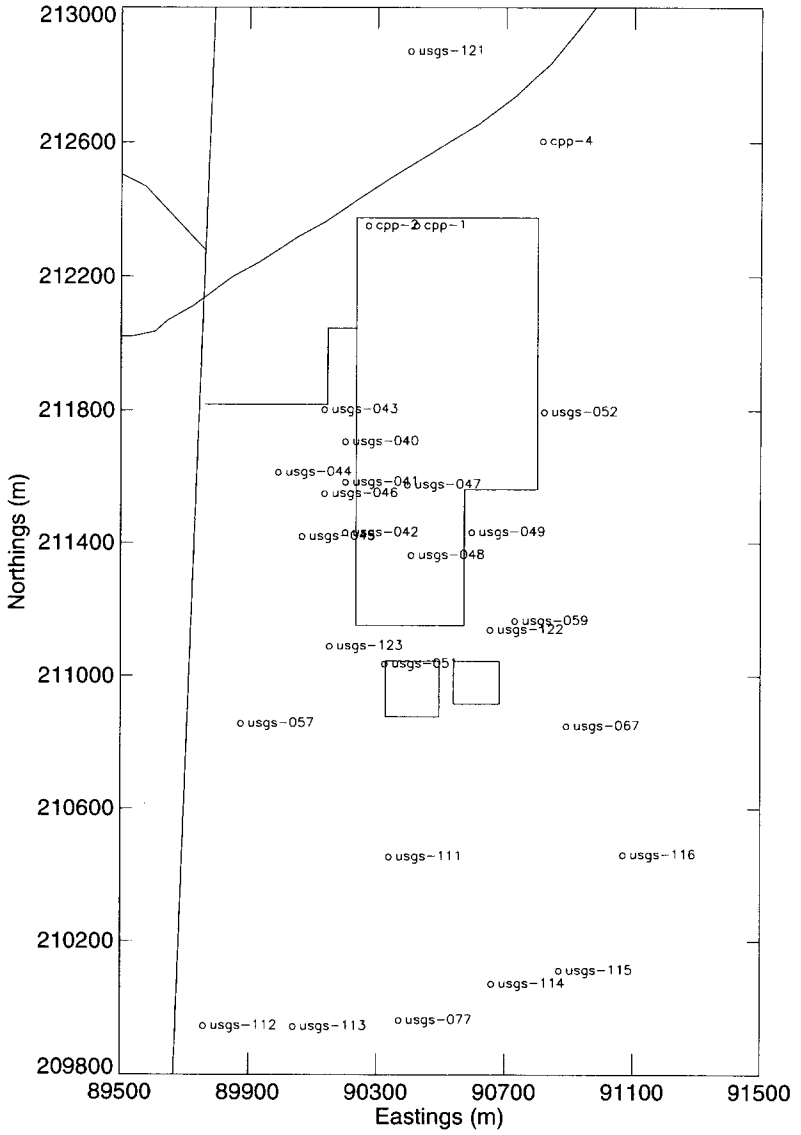

Figure 4-6 Well locations used for comparison of simulated and measured contaminant concentration near the INTEC.

4.2.1 Iodine-129

I-129 concentrations are predicted to remain above the 0.26 pCi/L 10^{-6} risk throughout the simulation period and remain above the 1 pCi/L federal drinking water standard until just before the year 2095. Figure 4-7 illustrates peak I-129 concentrations anywhere in the aquifer model domain and Figure 4-8 compares simulated and measured I-129 concentrations in monitoring wells. The model overpredicted the I-129 concentrations in most of the calibration wells. The relatively good match between simulated and measured tritium concentrations obtained from the recalibration effort and the high simulated I-129 concentrations suggests the 0 K_d for I-129 may have been too low.

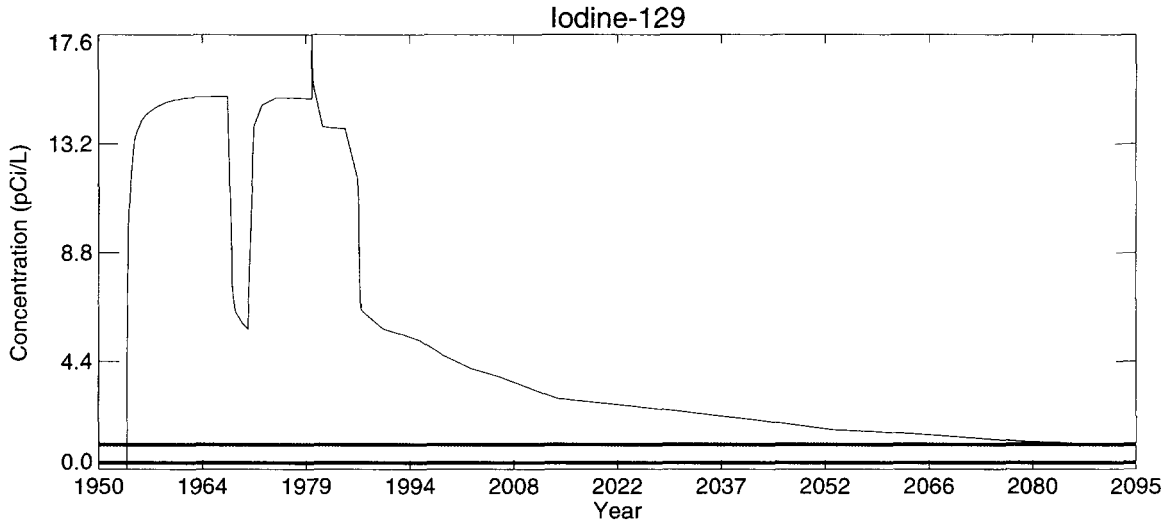

Figure 4-7 Peak aquifer concentration for I-129 (red line is 10^{-6} risk and blue line is MCL concentration).

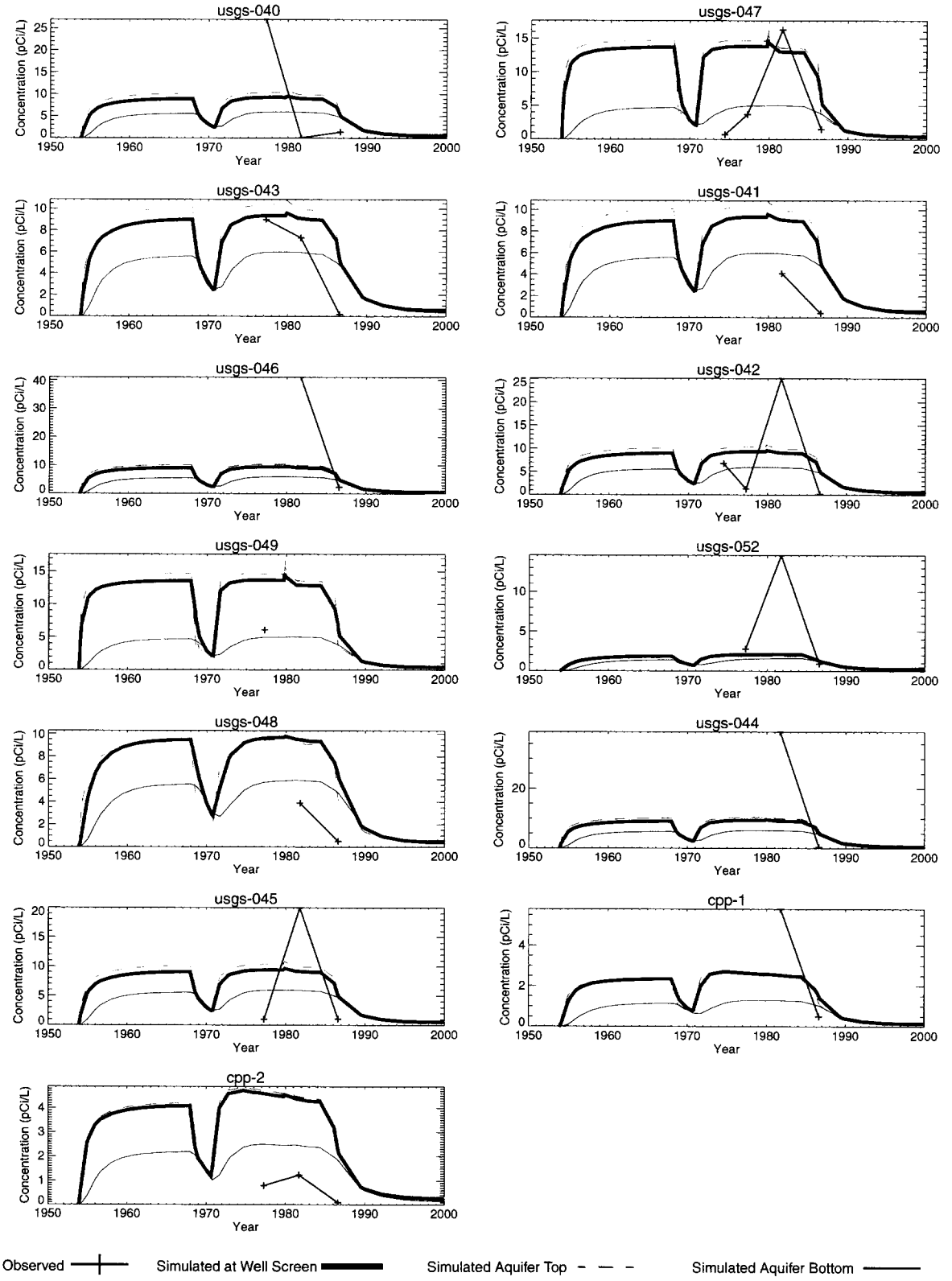

Figure 4-8 Comparison of simulated and measured I-129 concentrations.

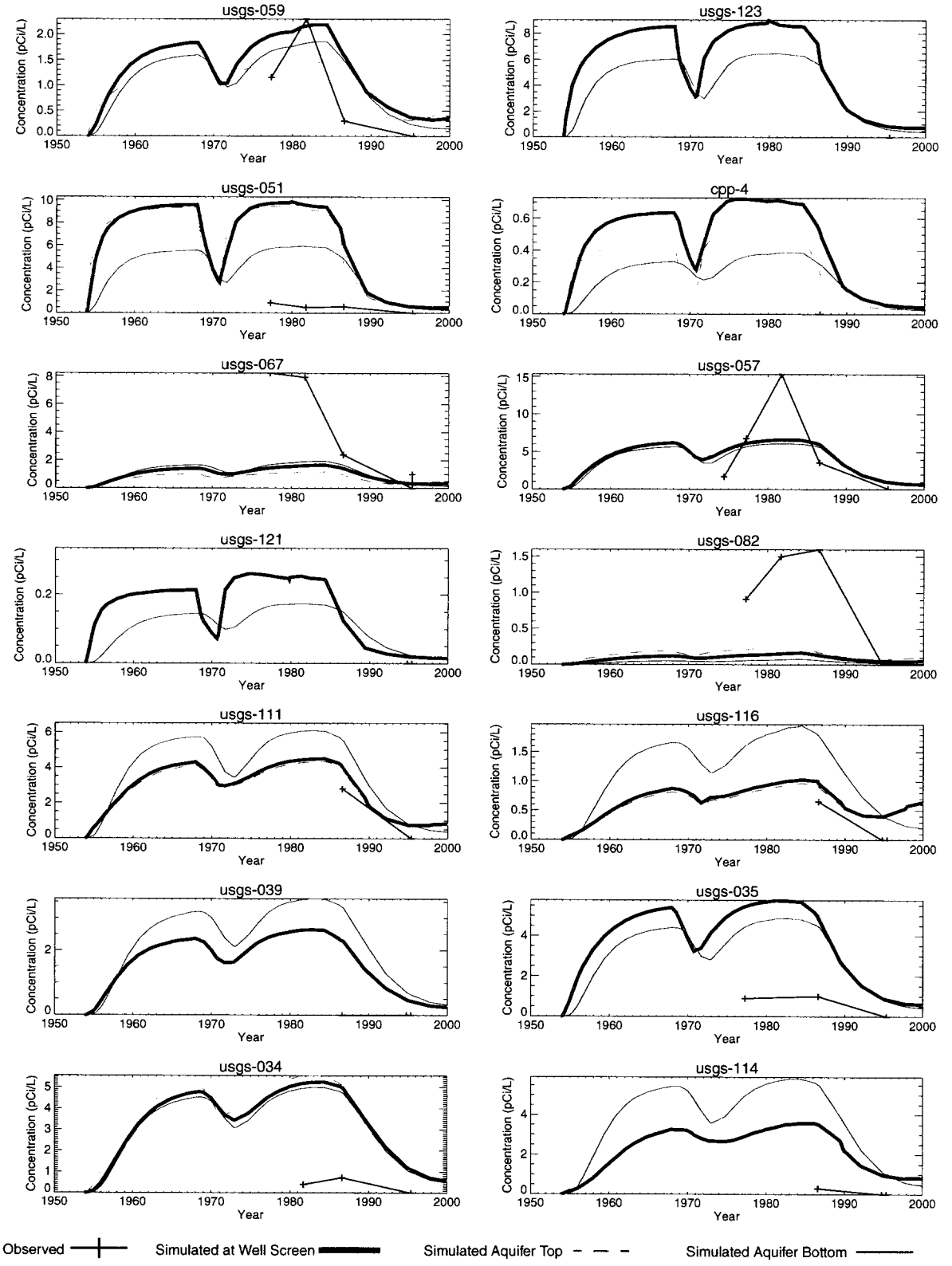

Figure 4-8 continued Comparison of simulated and measured I-129 concentrations.

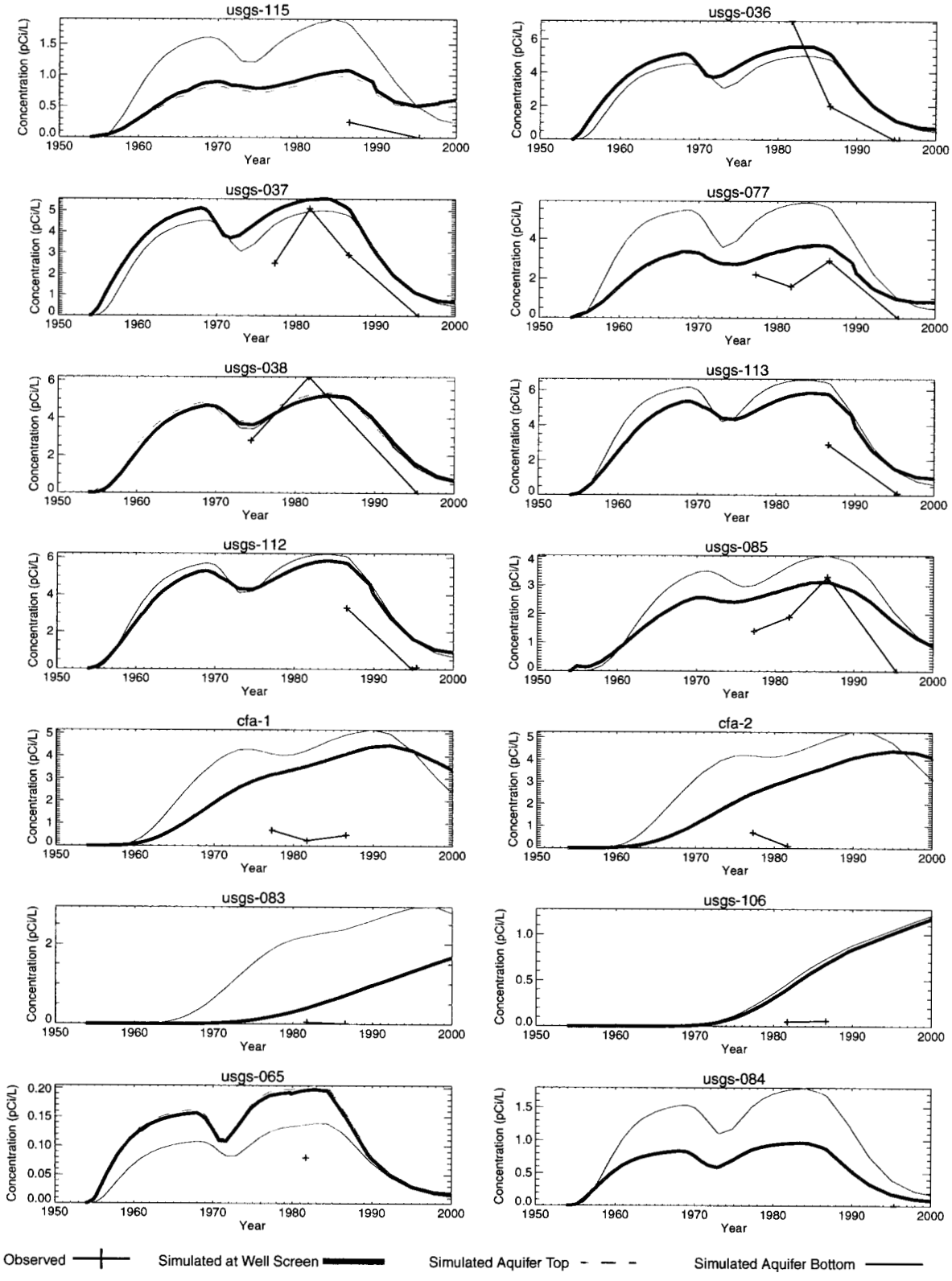

Figure 4-8 continued Comparison of simulated and measured I-129 concentrations.

4.2.2 Cobalt-60

The Co-60 concentrations exceeded the 10^{-6} risk concentration during the period 1954 through 1980, but always remained below the MCL concentration. Figure 4-9 illustrates peak aquifer concentration anywhere in the aquifer and Figure 4-10 compares the simulated and measured Co-60 concentrations in monitoring wells. The model underpredicts concentrations in wells near the INTEC (USGS-40, USGS-43, USGS-44 and USGS-37), which indicates the fractured basalt K_d was too high. The simulated concentrations near the TRA are zero, which contradicts the observed concentrations. The updated and the RI/BRA models did not include Test Reactor Area (TRA) Co-60 sources and the simulated groundwater gradient does not allow a significant amount of the INTEC contamination to reach the TRA.

The WAG-7 preliminary RI/BRA model (Magnuson and Sondrup, 1998) calculated fractured basalt contaminant K_ds from fracture surface area rather than the mass of the rock matrix. The fracture surface area based K_ds basalt/sediment ratios were much less than the 1/25 ratio assumed in the INTEC RI/BRA analysis. For example, the WAG-7 Co-60 sediment K_d was 1,000 ml/g and the fractured basalt K_d was 6.5e-3 ml/g.

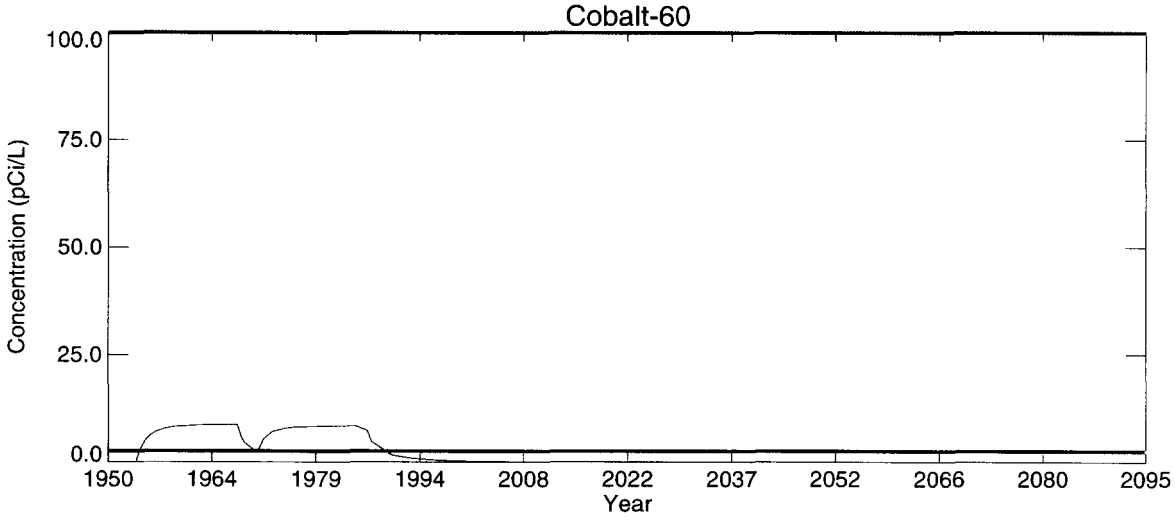

Figure 4-9 Peak aquifer concentration for Co-60 (red line is 10^{-6} risk and blue line is MCL concentration).

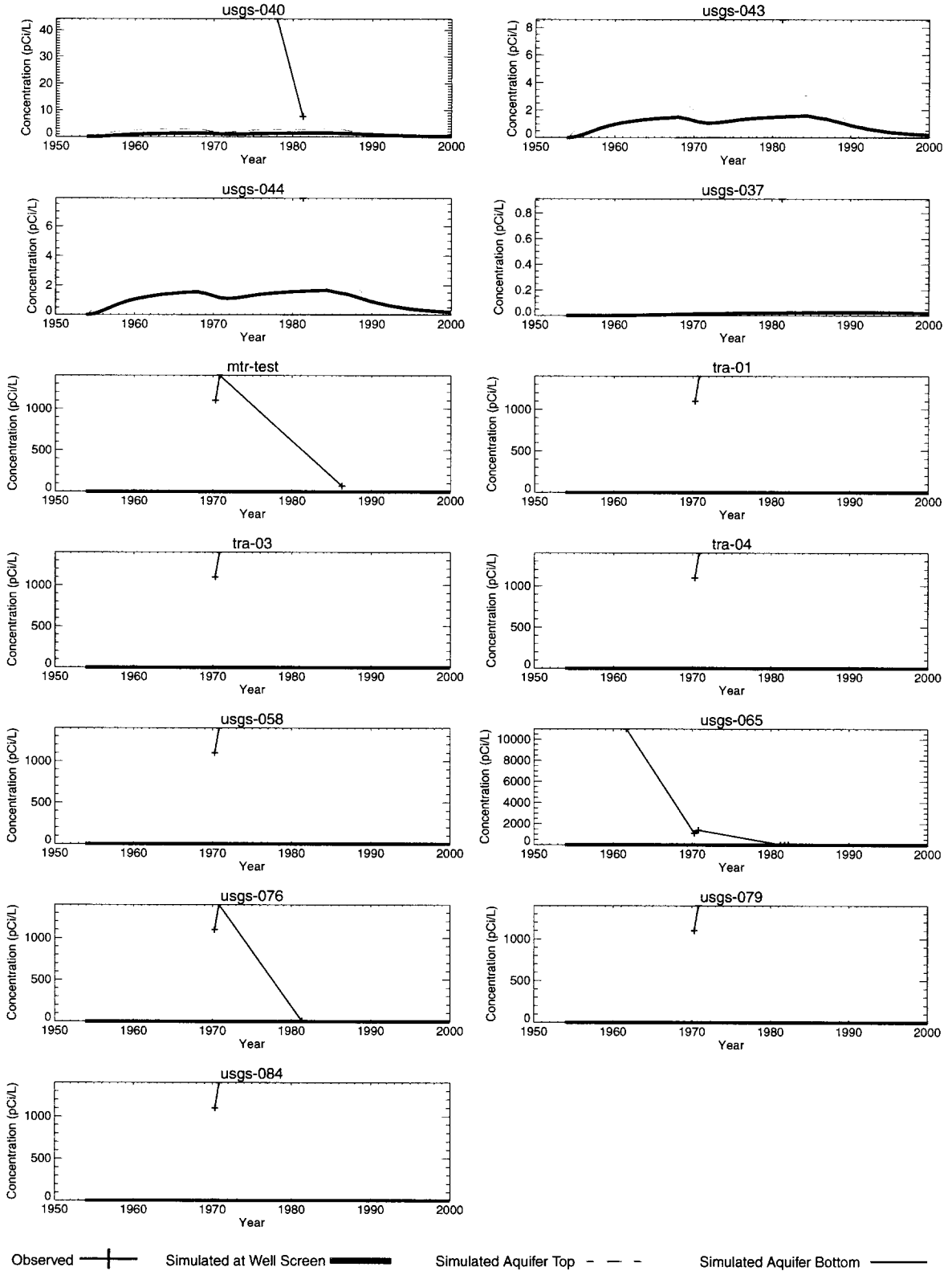

Figure 4-10 Comparison of simulated and measured Co-60 concentrations.

4.2.3 Cesium-137

Cs-137 concentrations remained above the 10^{-6} risk concentrations from 1954 through 2074, but did not exceed the MCL concentration. Figure 4-11 illustrates peak aquifer concentrations anywhere in the aquifer during the simulation period and Figure 4-12 compares simulated and measured Cs-137 concentrations in monitoring wells. As with the Co-60, the model under-predicts Cs-137 concentrations near the INTEC and concentrations are underpredicted by a greater extent than with Co-60. The large sediment K_d for Cs-137 (500 ml/g) and corresponding large fracture basalt K_d (20 ml/g) resulted in a more drastic overestimation of the fractured basalt K_d.

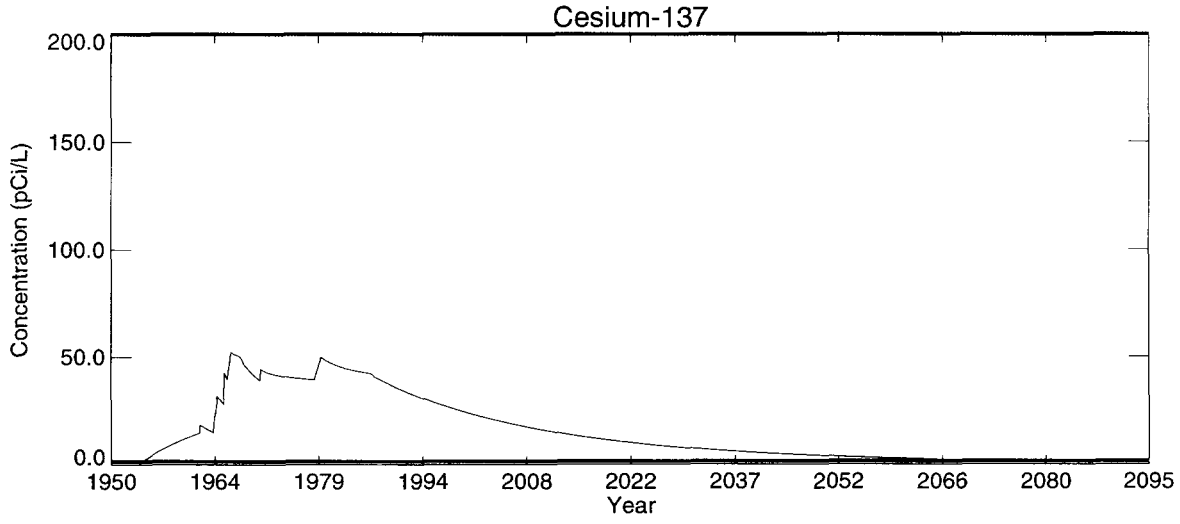

Figure 4-11 Peak aquifer concentration for Cs-137 (red line is 10^{-6} risk and blue line is MCL concentration).

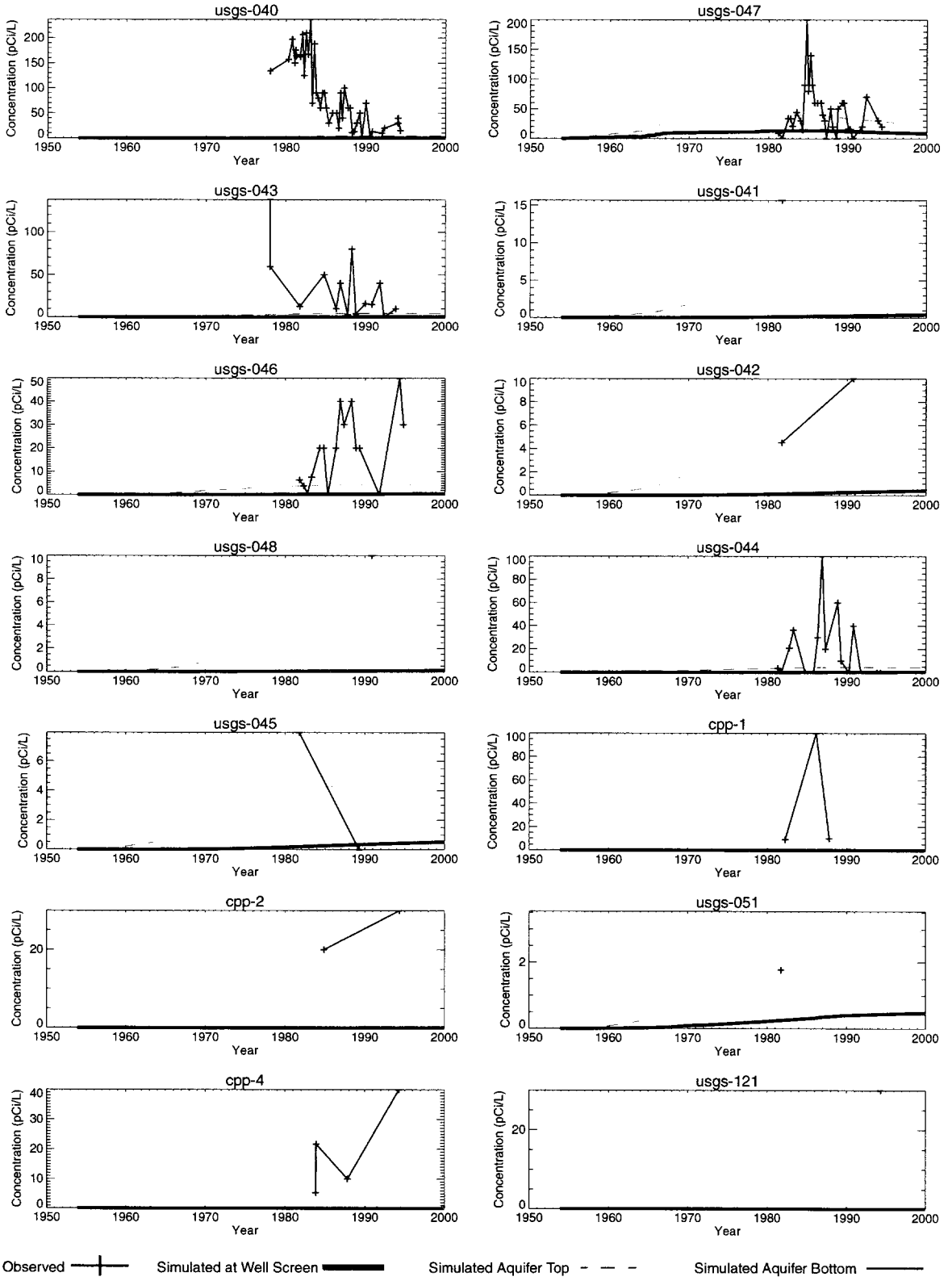

Figure 4-12 Comparison of simulated and measured Cs-137 concentrations.

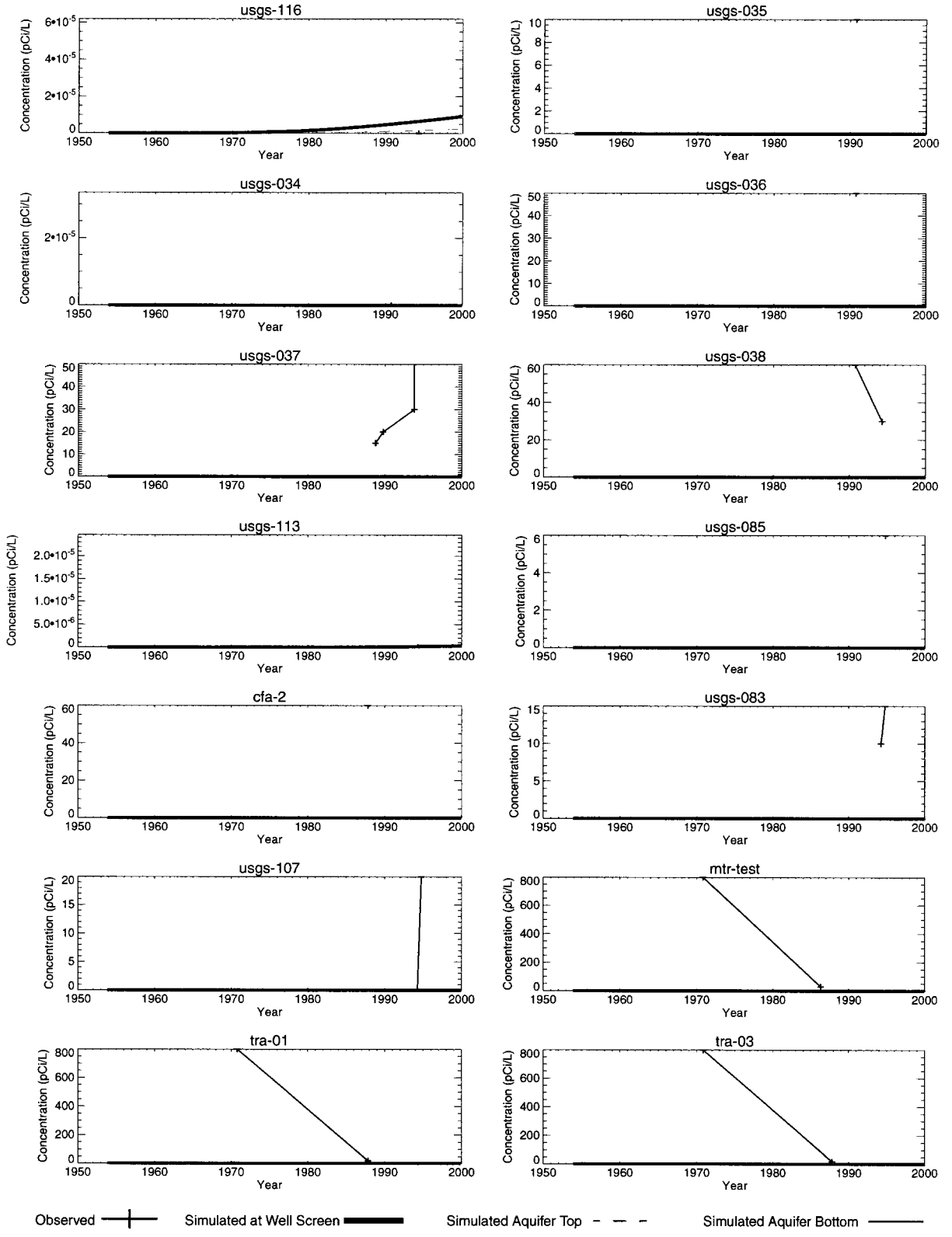

Figure 4-12 continued Comparison of simulated and measured Cs-137 concentrations.

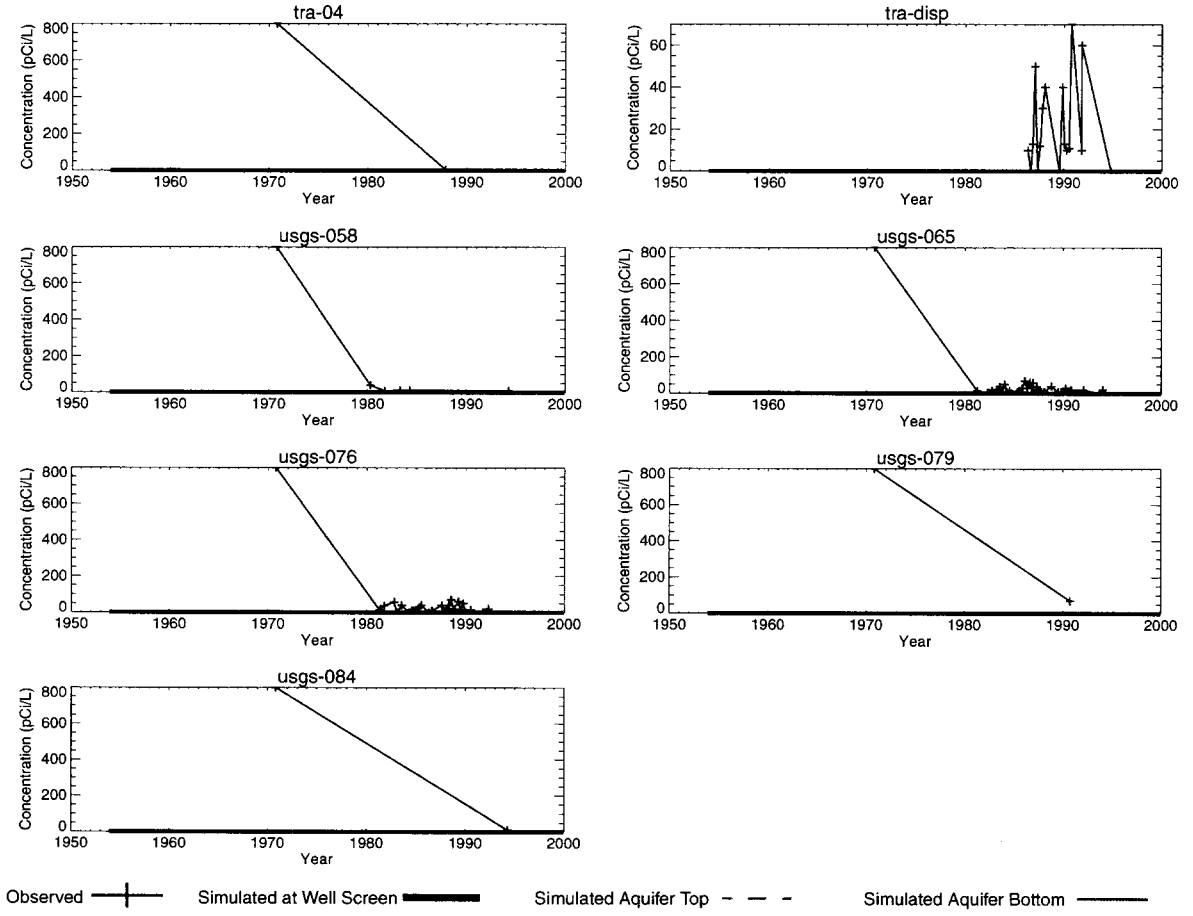

Figure 4-12 continued Comparison of simulated and measured Cs-137 concentrations.

4.2.4 Tritium

Tritium concentrations remained above the 10^{-6} risk concentration from 1954 through 2036 and remained above the MCL from 1954 through 2005. Figure 4-13 illustrates peak aquifer concentrations anywhere in the aquifer and Figure 4-14 compares simulated and measured tritium concentrations in observation wells. Tritium matches measured concentrations better than the other contaminants because it was the transport calibration contaminant and tritium does not chemically interact with the subsurface, thereby eliminating any error from estimating the fractured basalt and HI interbed partition coefficient.

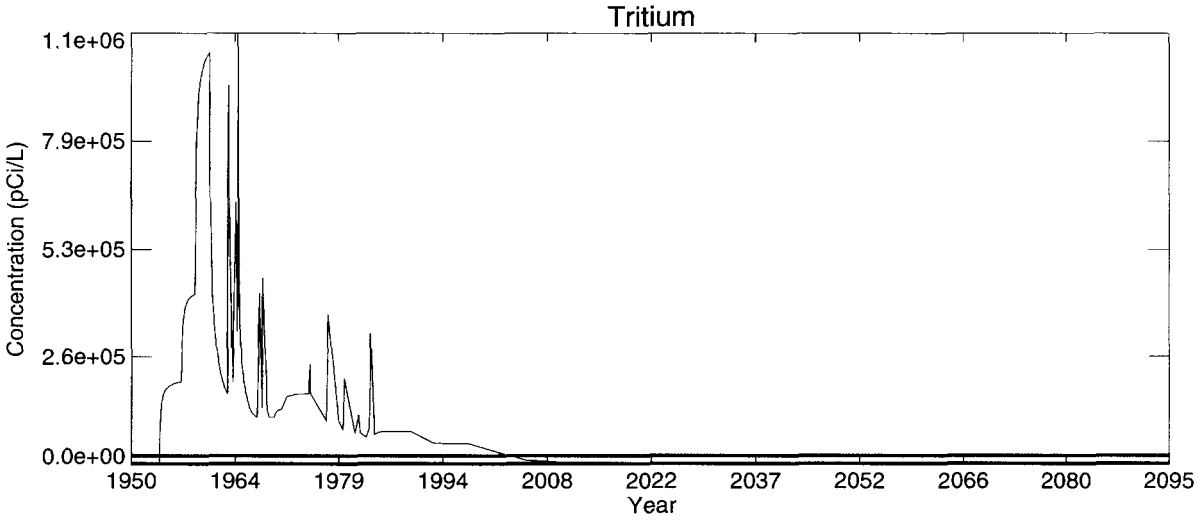

Figure 4-13 Peak aquifer concentration for H-3 (red line is 10^{-6} risk and blue line is MCL concentration).

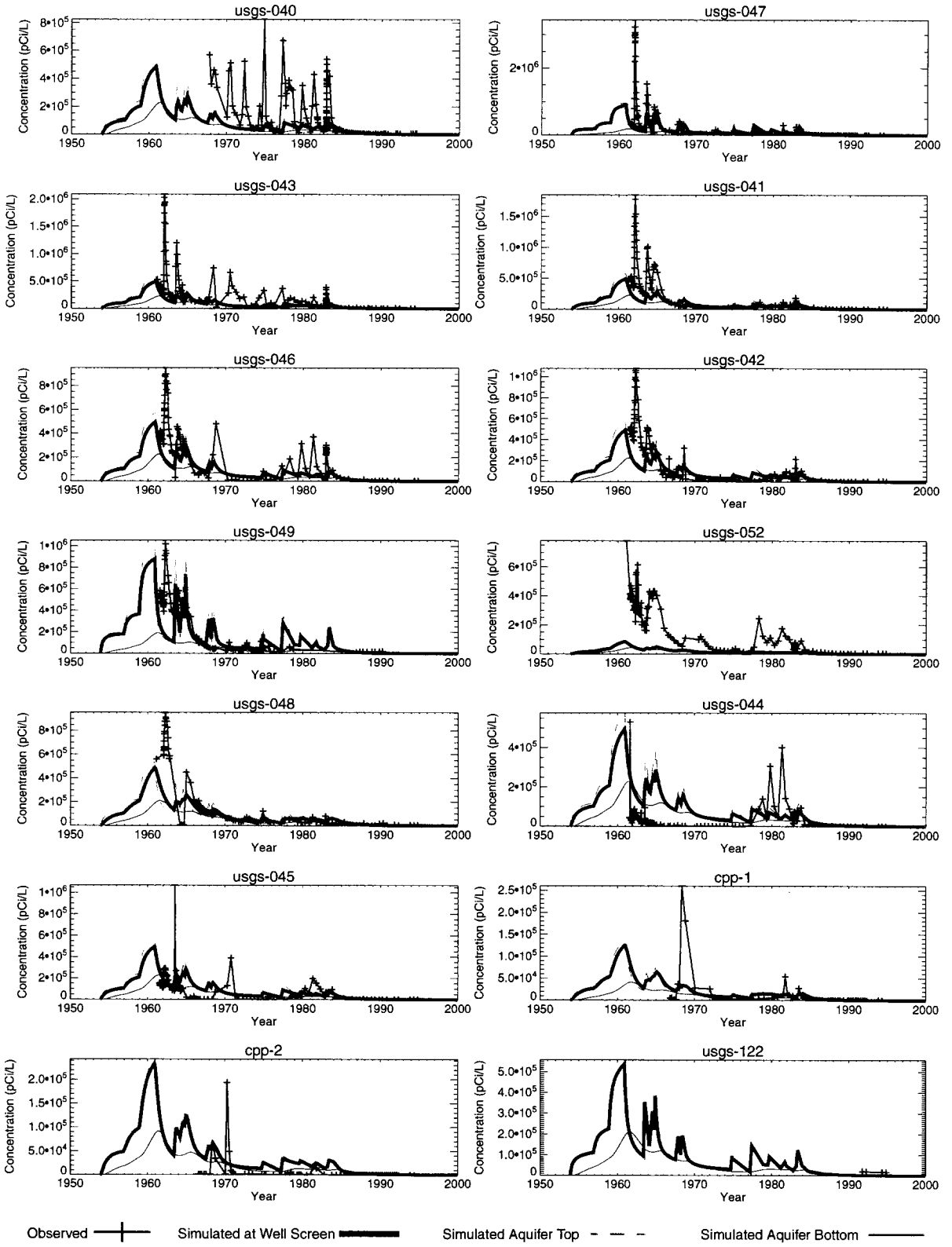

Figure 4-14 Comparison of simulated and measured H-3 concentrations.

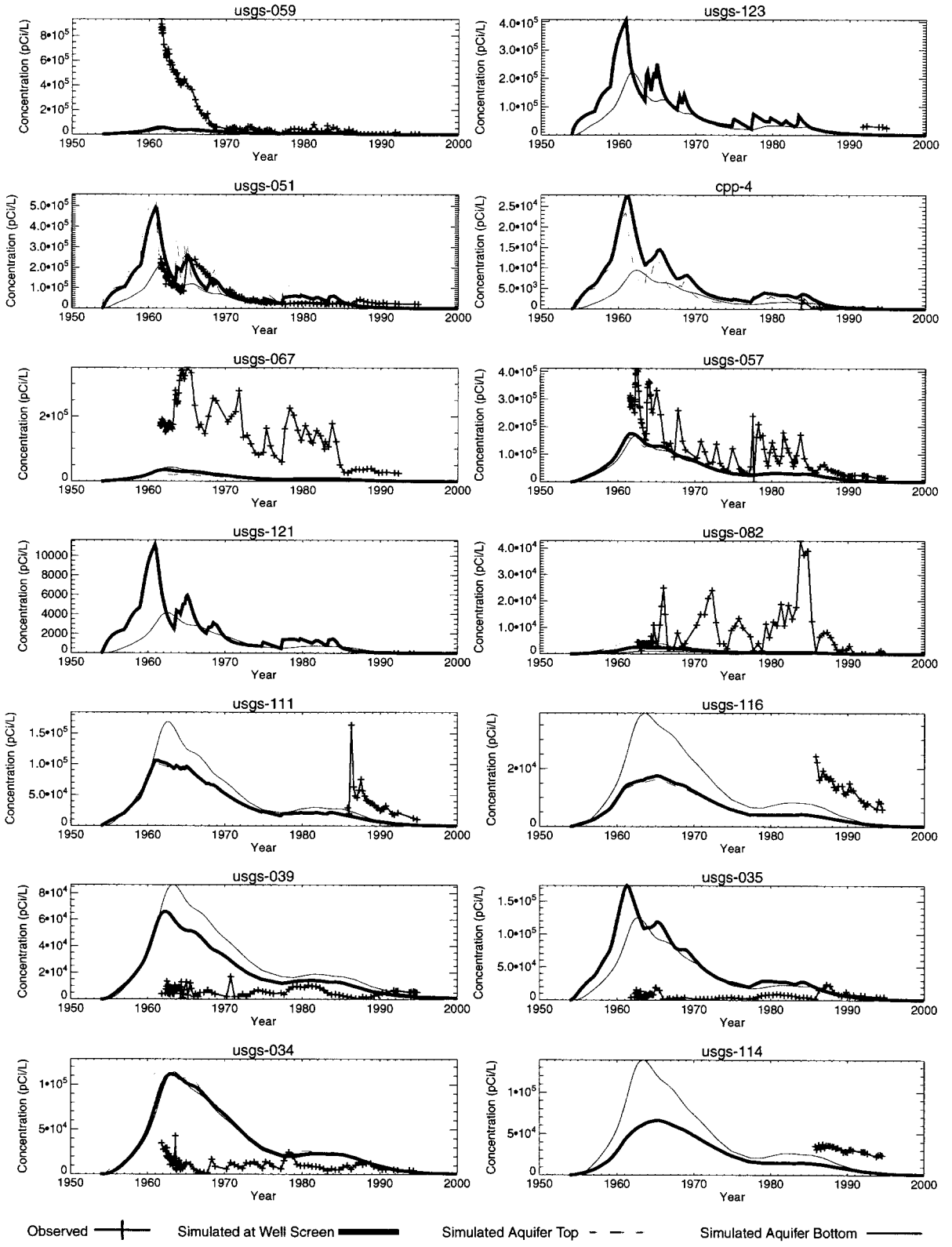

Figure 4-14 continued Comparison of simulated and measured H-3 concentrations.

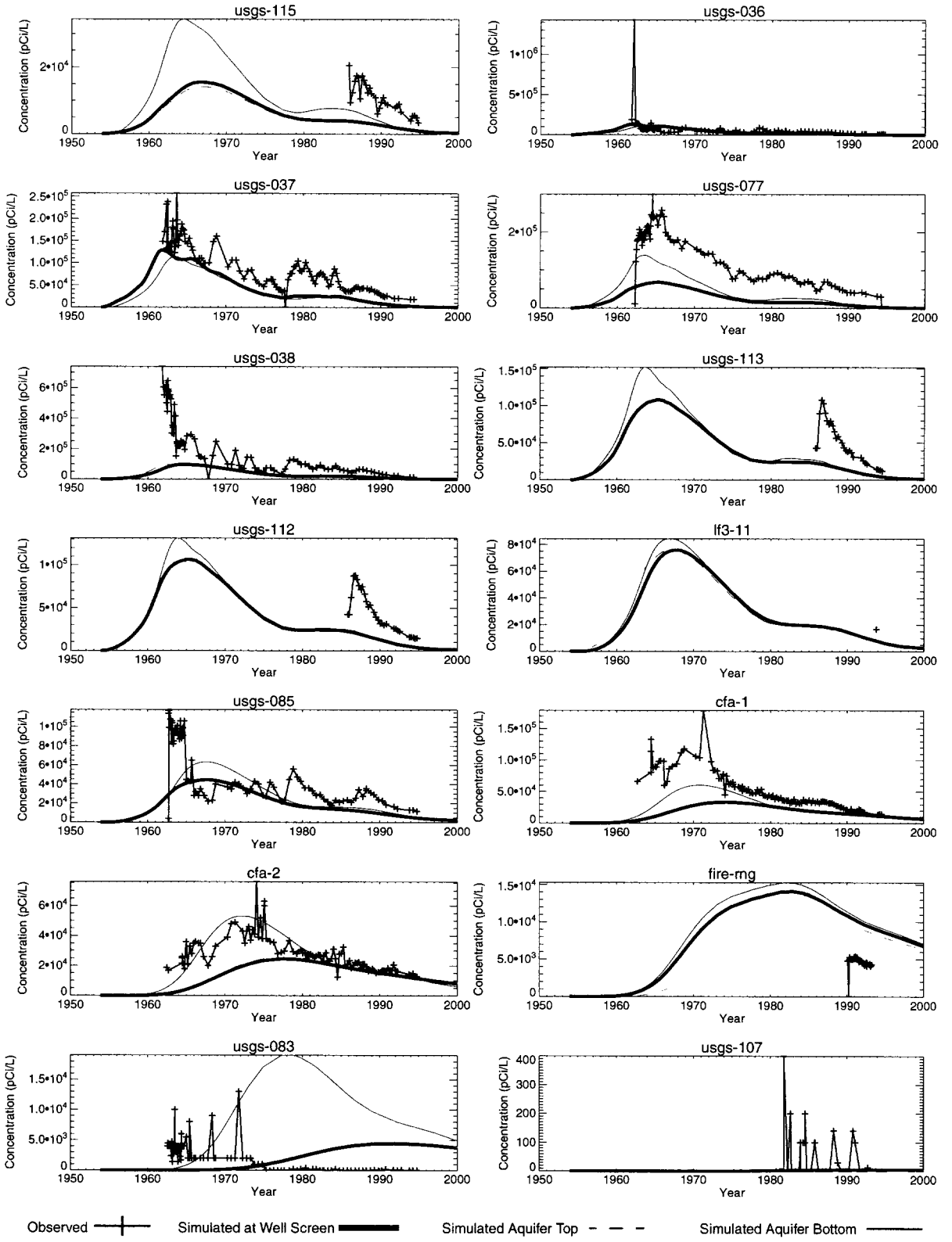

Figure 4-14 continued Comparison of simulated and measured H-3 concentrations.

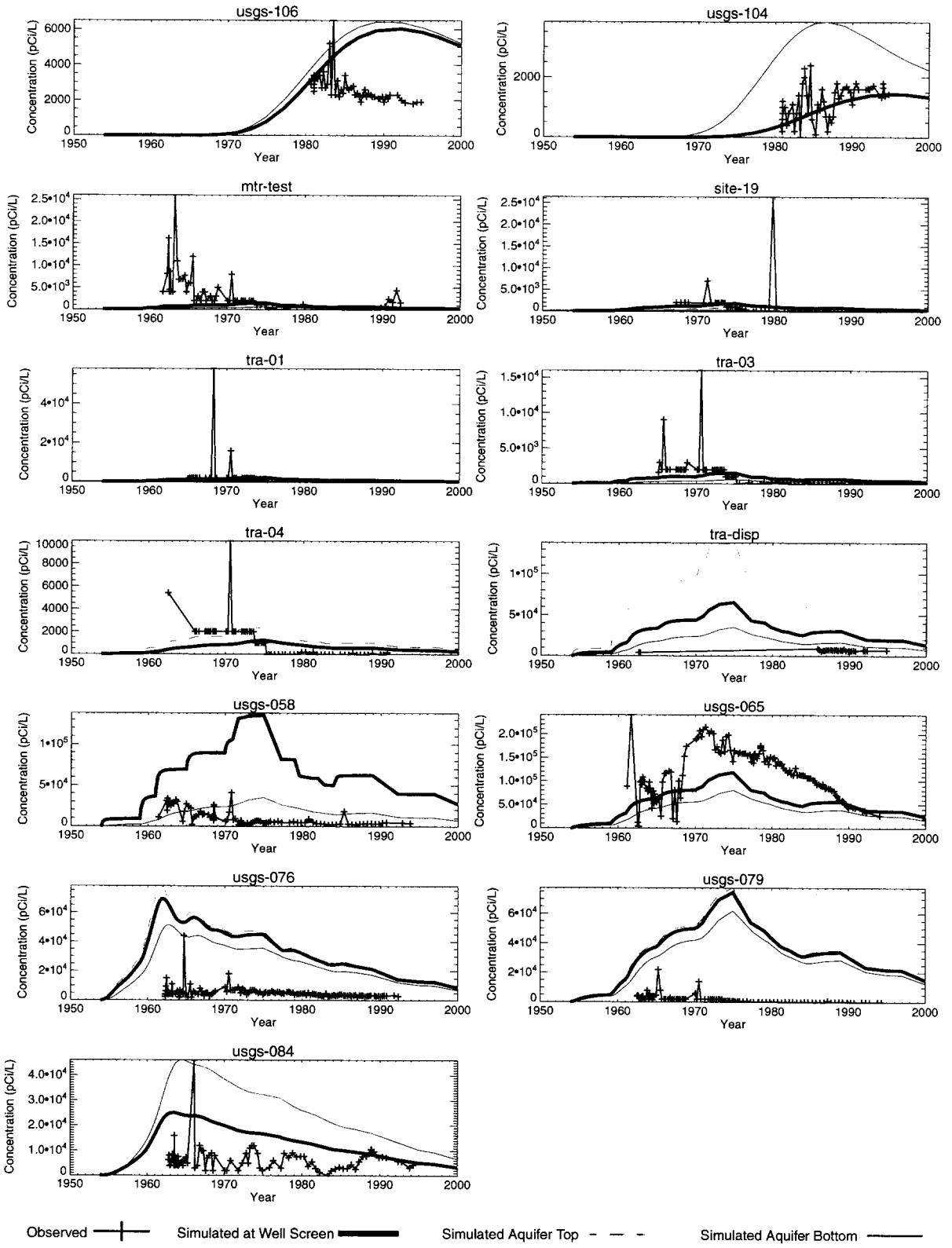

Figure 4-14 continued Comparison of simulated and measured H-3 concentrations.

4.2.5 Plutonium-241

Pu-241 concentrations exceeded the 0.145 pCi/L 10^{-6} risk concentration twice during the period 1959 through 1986, but always remained below the 63 pCi/L MCL during the simulation period. The RI/BRA analysis predicted the highest aquifer total plutonium concentrations would be a result of the vadose zone tank farm contamination and the peak aquifer concentration would occur in the year 3585. However, the short half-life of Pu-241 (14.4 years) and large K_d (20 ml/g) would result in the majority of the vadose zone Pu-241 decaying before entering the aquifer. Figure 4-15 illustrates peak aquifer concentrations anywhere in the aquifer. A comparison of simulated and observed because Pu-241 has not been reported in the aquifer.

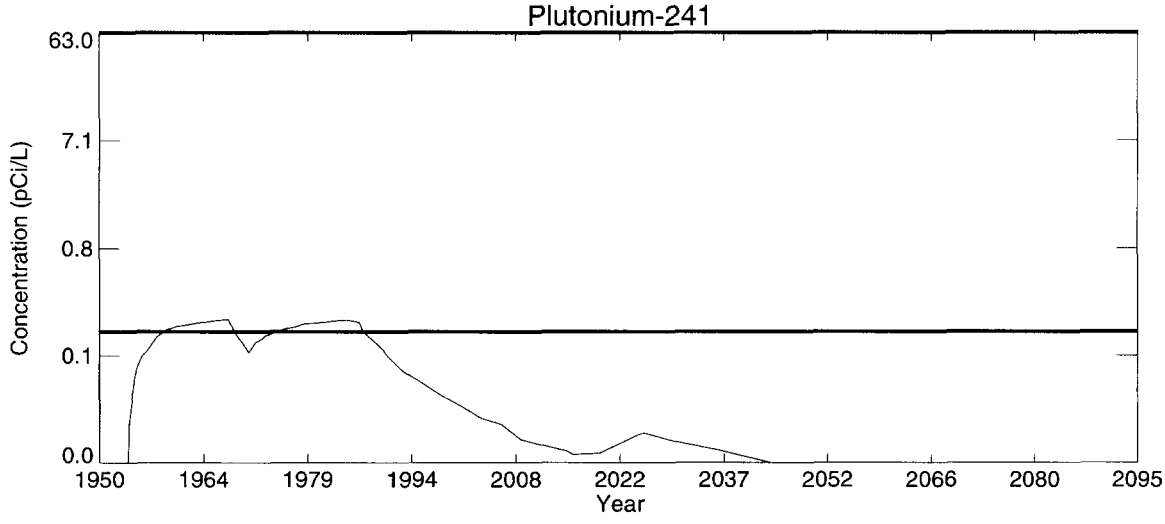

Figure 4-15 Peak aquifer concentration for Pu-241 (log scale, red line is 10^{-6} risk and blue line is MCL concentration).

4.2.6 Strontium-90

Sr-90 concentrations exceeded the 0.86 pCi/L 10^{-6} risk concentration from 1959 through the simulation period and remained above the 8 pCi/L MCL from 1959 through 2019. Figure 4-16 illustrates peak concentrations anywhere in the aquifer and Figure 4-17 compares simulated and measured Sr-90 concentrations in aquifer monitoring wells. The model both overpredicted and underpredicted aquifer concentrations, but underpredicted concentrations more often than not, lending more evidence that estimating fractured basalt sorption coefficients from 1/25 the sediment may overestimate the K_d value.

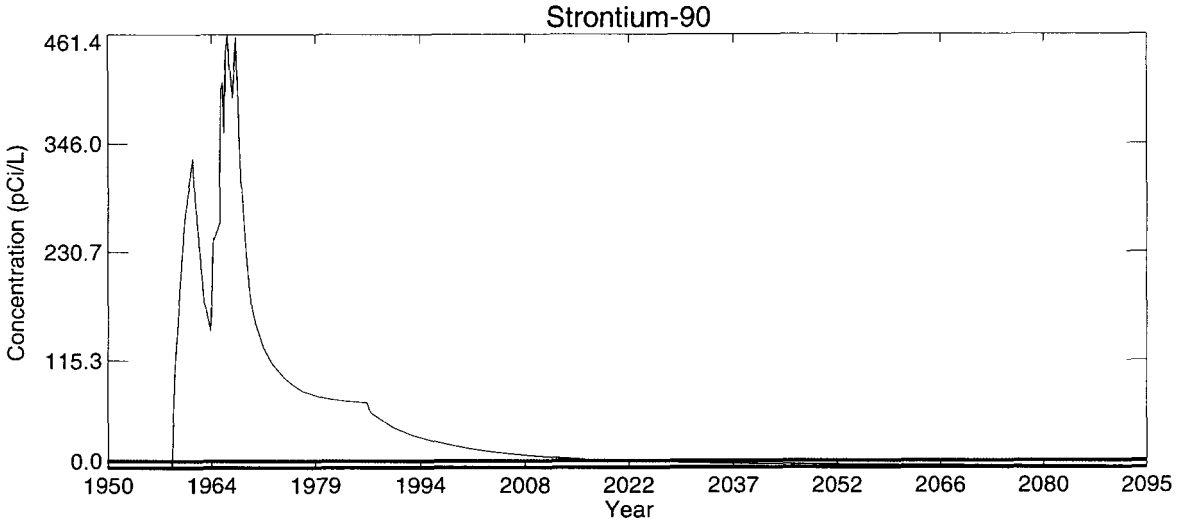

Figure 4-16 Peak aquifer concentration for Sr-90 (red line is 10^{-6} risk and blue line is MCL concentration).

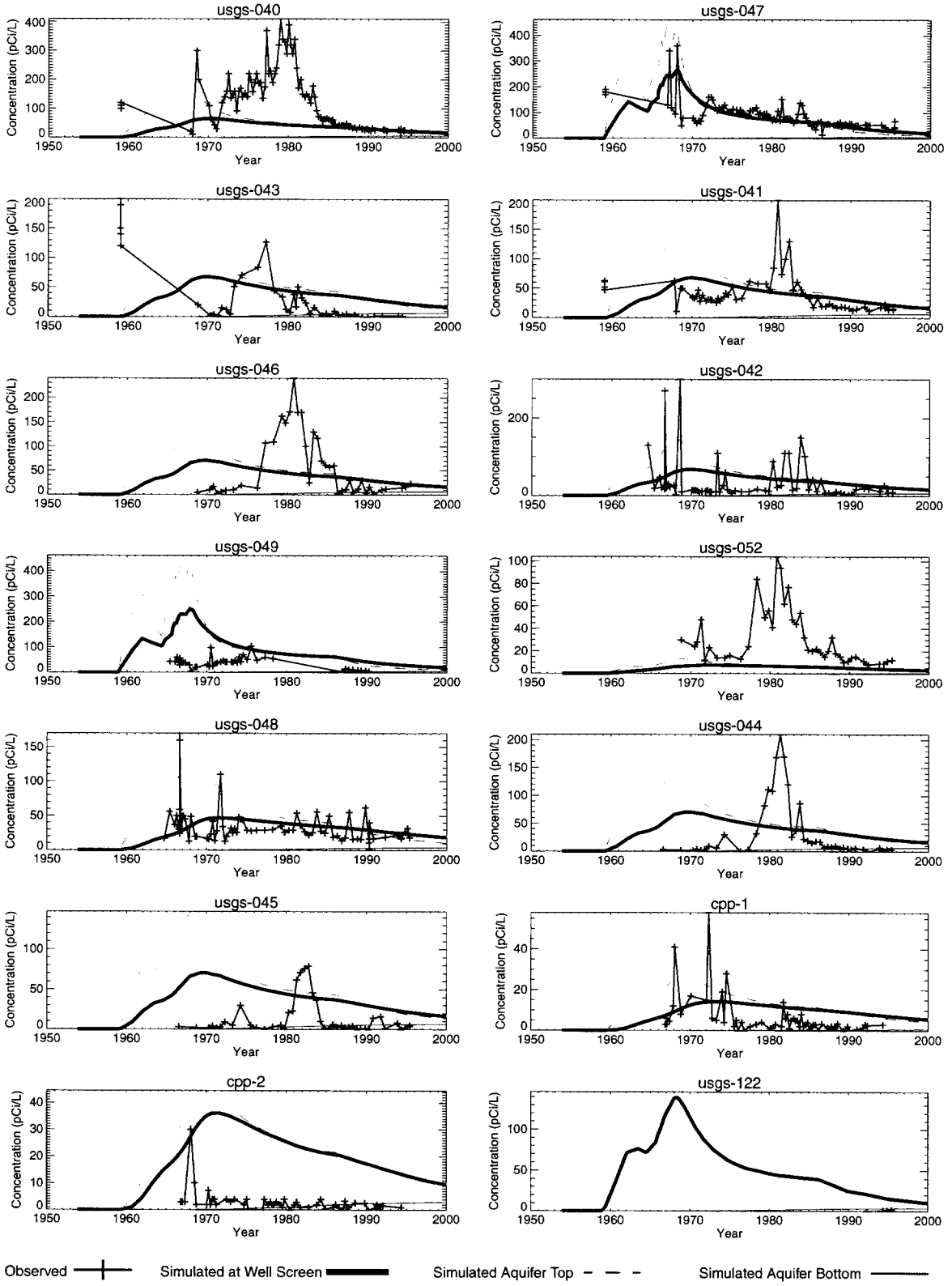

Figure 4-17 Comparison of simulated and measured Sr-90 concentrations.

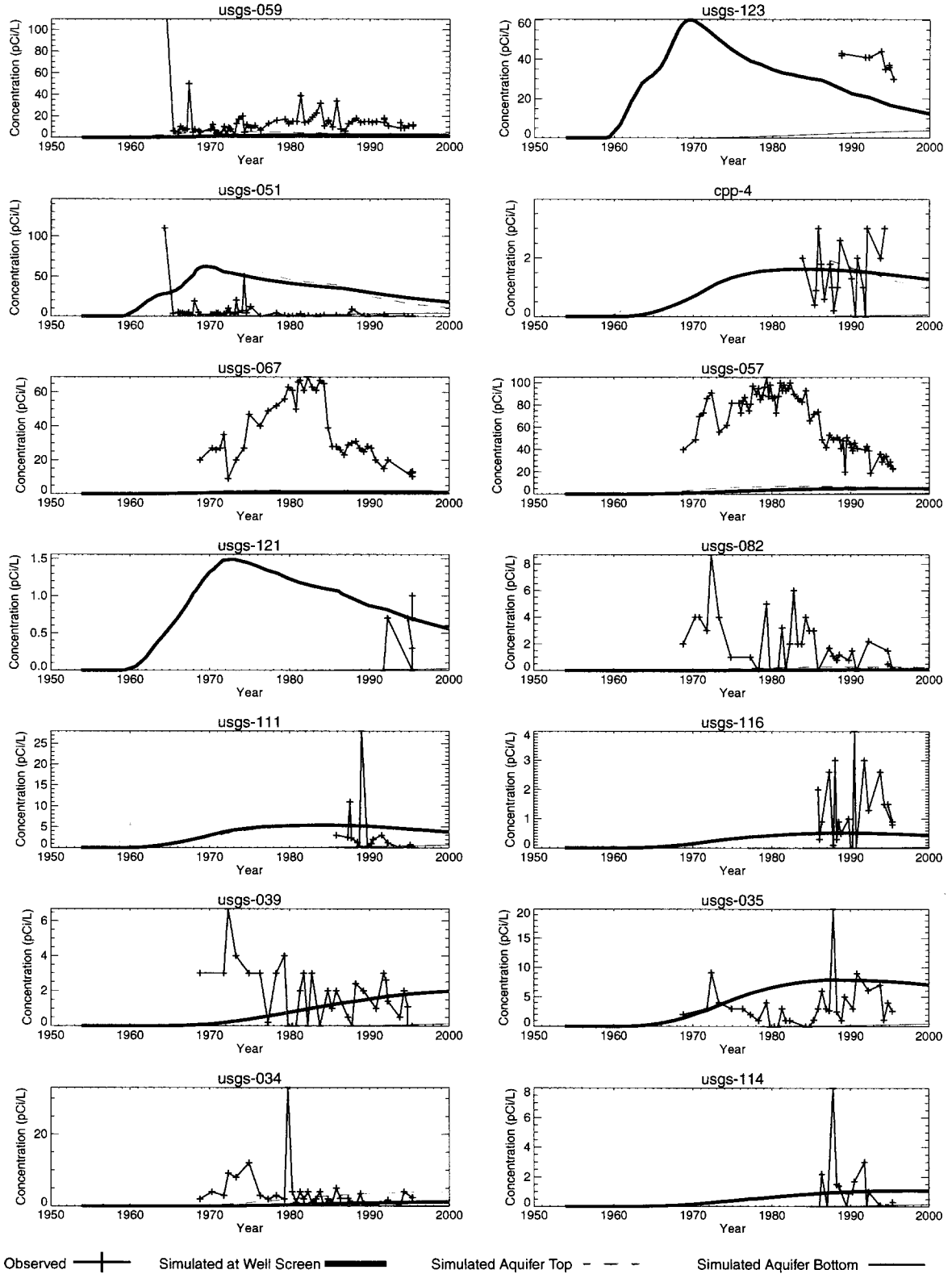

Figure 4-17 continued Comparison of simulated and measured Sr-90 concentrations.

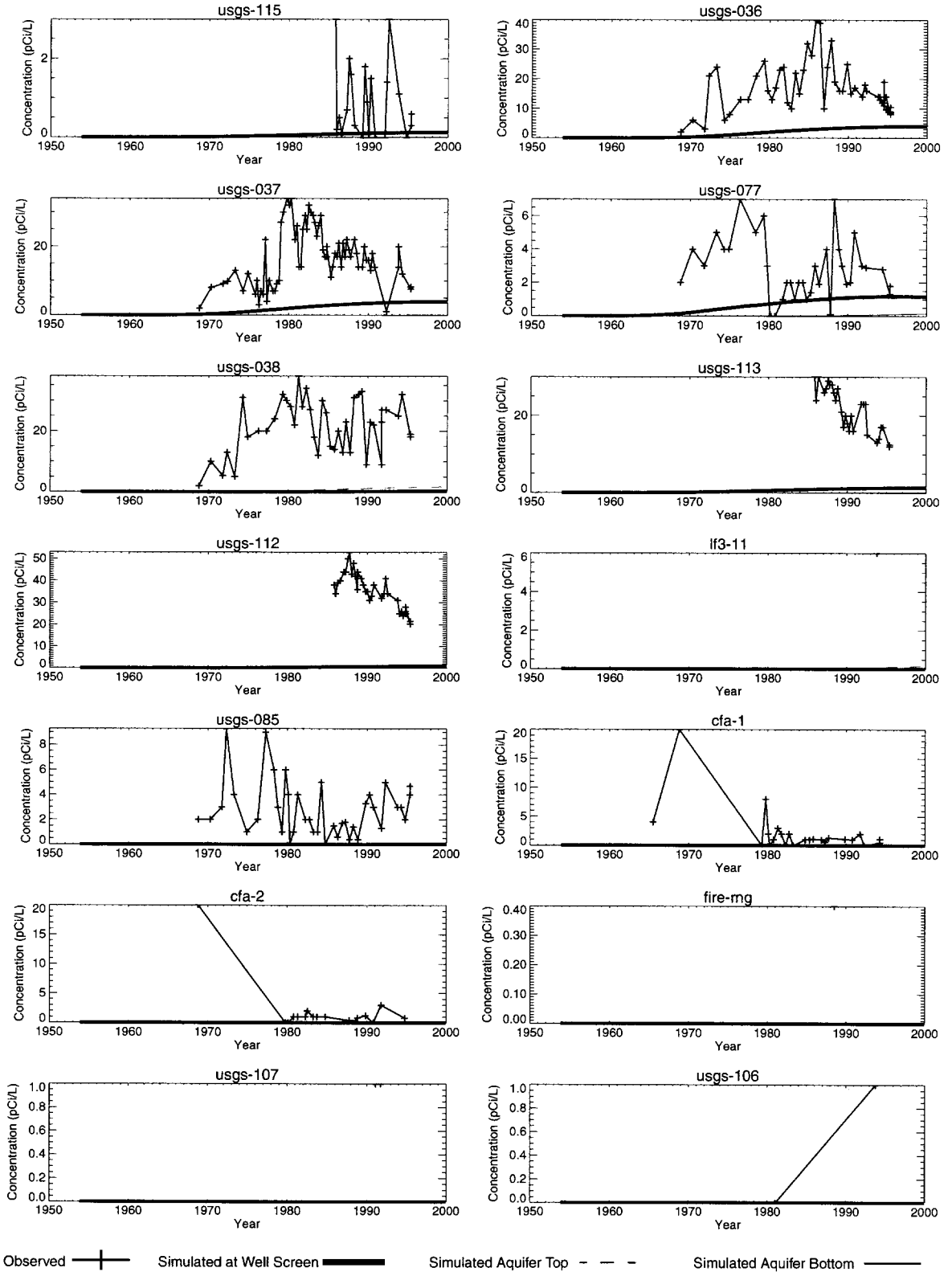

Figure 4-17 continued Comparison of simulated and measured Sr-90 concentrations.

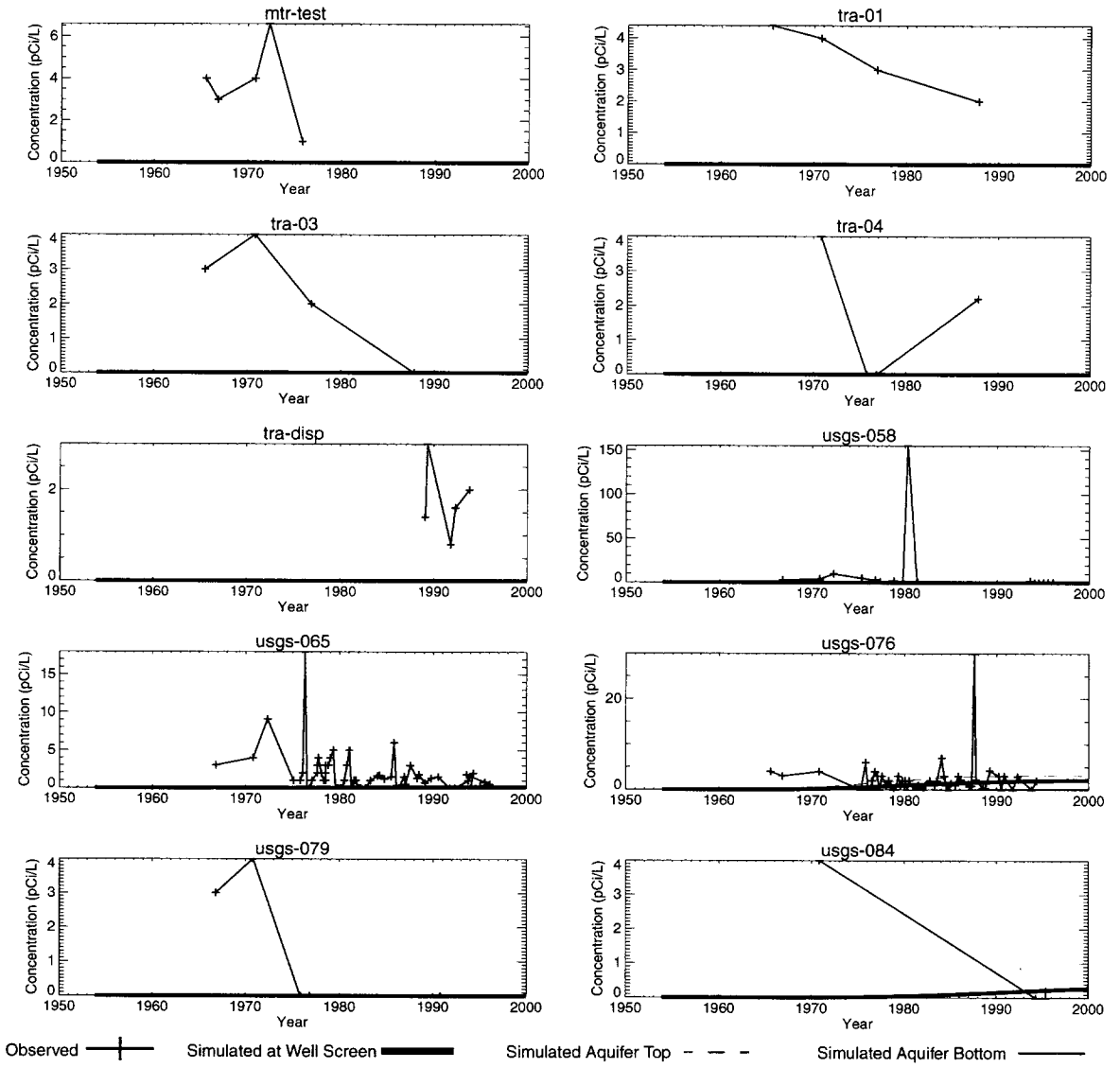

Figure 4-17 continued Comparison of simulated and measured Sr-90 concentrations.

4.2.7 Technetium-99

Tc-99 concentrations remained below the 34 pCi/L 10^{-6} risk and the 900 pCi/L MCL concentrations throughout the simulation period. Figure 4-18 illustrates peak aquifer concentrations anywhere in the aquifer and Figure 4-19 compares simulated and measured concentrations in aquifer monitoring wells. As with Sr-90, the model underpredicted aquifer concentrations more often than overpredicted aquifer concentrations, which again suggests the partition coefficients were overestimated. There is very little Tc-99 data and all measured concentrations were below MCL. All measured concentrations were also below the 10^{-6} risk concentration with the exception of wells USGS-47 and USGS-52.

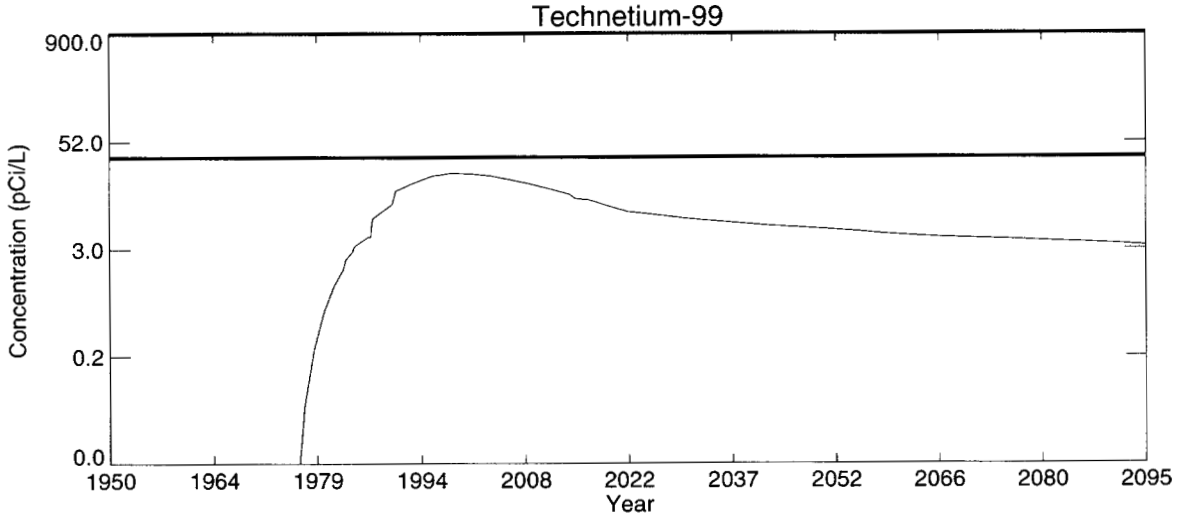

Figure 4-18 Peak aquifer concentration for Tc-99 (log scale, red line is 10^{-6} risk and blue line is MCL concentration).

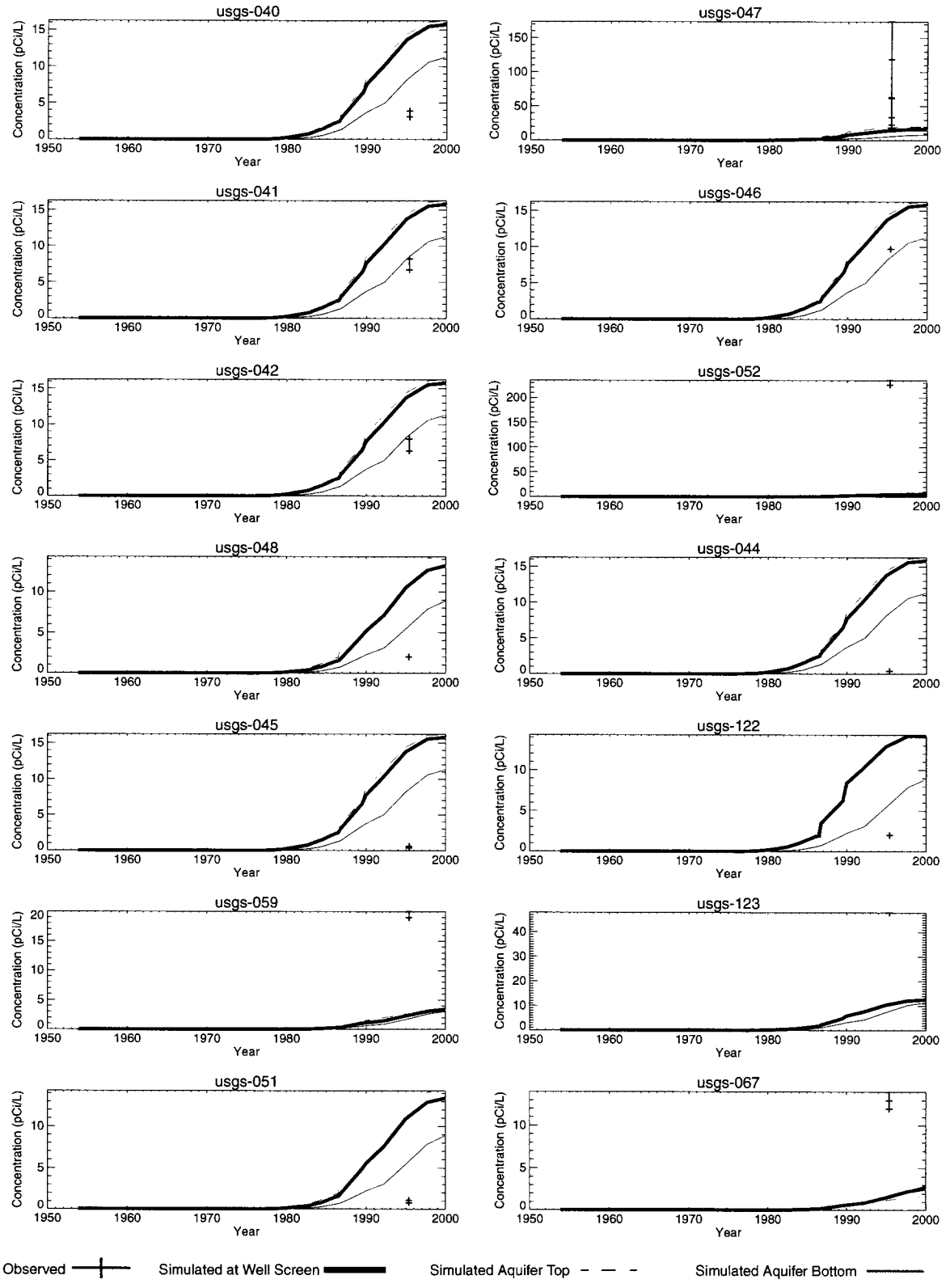

Figure 4-19 Comparison of simulated and measured Tc-99 concentrations.

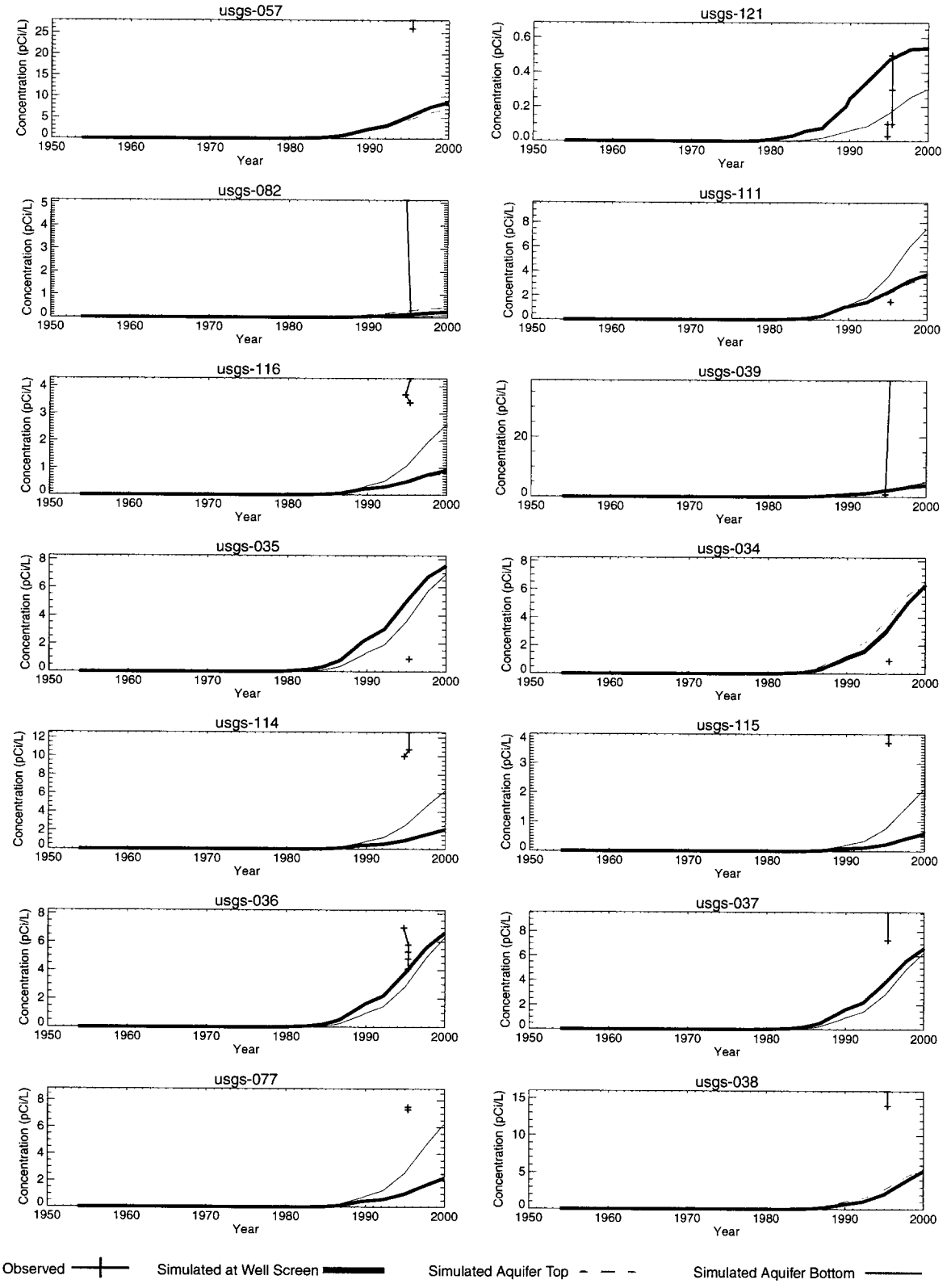

Figure 4-19 continued Comparison of simulated and measured Tc-99 concentrations.

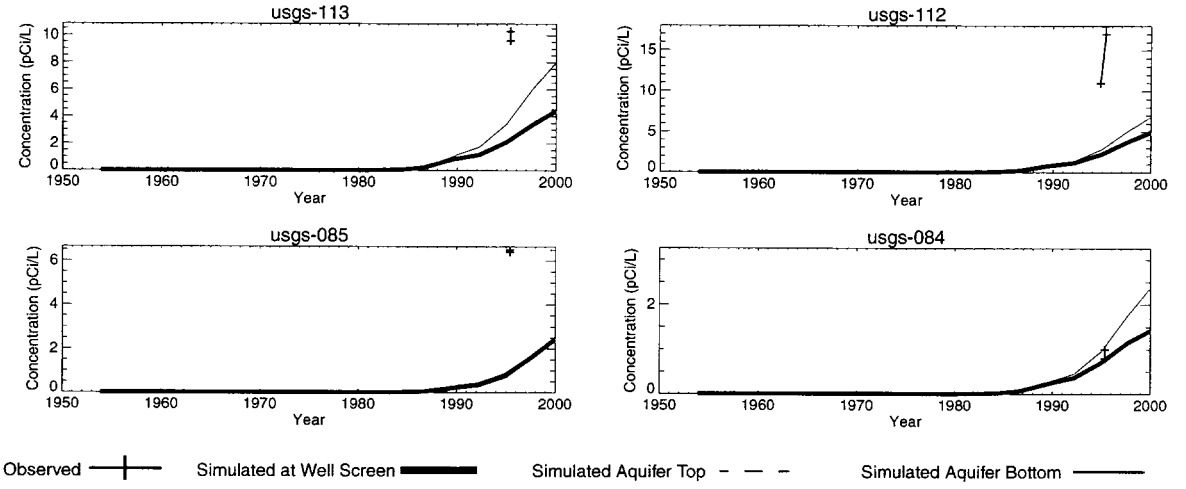

Figure 4-19 continued Comparison of simulated and measured Tc-99 concentrations.

4.2.8 Predictive Simulation Summary

Six out of the seven simulated COPCs had concentrations above the 10^{-6} risk concentration at some time between 1954 and 2095, and three contaminants had concentrations above the MCL. I-129, Co-60, Cs-137, H-3, Pu-241, and Sr-90 all had concentrations above the 10^{-6} risk concentration. I-129, H-3, and Sr-90 had concentrations above the MCL concentration. Table 4-2 summarizes the predictive simulation results and presents the peak contaminant concentration, time of peak during simulation period, peak concentration in 2095, 10^{-6} risk concentration, and MCL concentration.

Tritium, Sr-90, and I-129 dominated the cumulative aquifer beta/gamma risk. Figure 4-20 illustrates the cumulative aquifer risk at the southern INTEC fence line for all simulated COPCs. The black line in Figure 4-20 illustrates cumulative risk over time and the red, blue, and green lines illustrate the individual risk from tritium, Sr-90, and I-129, respectively. Figure 4-21 illustrates the cumulative dose rate at the southern INTEC fence line.

Table 4-2 Predictive simulation peak aquifer concentrations.

Contaminant	Peak Aquifer Concentration (pCi/L)	Time of Peak Aquifer Concentration (Year)	Peak Aquifer Concentration in 2095 (pCi/L)	10^{-6} Risk Concentration (pCi/L)	Federal Drinking Water Standard* (pCi/L)
Iodine 129 (I-129)	17.6	1979	0.99	0.261	1.0
Cobalt 60 (Co-60)	8.76	1968	0.023 in 2063***	2.54	100.
Cesium 137 (Cs-137)	52.4	1966	0.85	1.52	200.
Tritium (H-3)	1.06e+6	1964	7.21	671.	20,000.
Plutonium 241 (Pu-241)	0.186	1967	0.003	0.145	63.**
Strontium 90 (Sr-90)	461.	1966	2.01	0.859	8.
Technetium 99 (Tc-99)	22.5	1997	3.22	34.3	900.

*Based on the 4 mrem/yr critical organ dose as listed in the National Bureau of Standards Handbook 69 (HB69) and 2l/d 365d/yr consumption rate.

**Not listed in HB69. 1991 proposed limits at 4 mrem/yr effective dose equivalent, which corresponds to 4.66e-6 risk.

***Simulation ended before 2095.

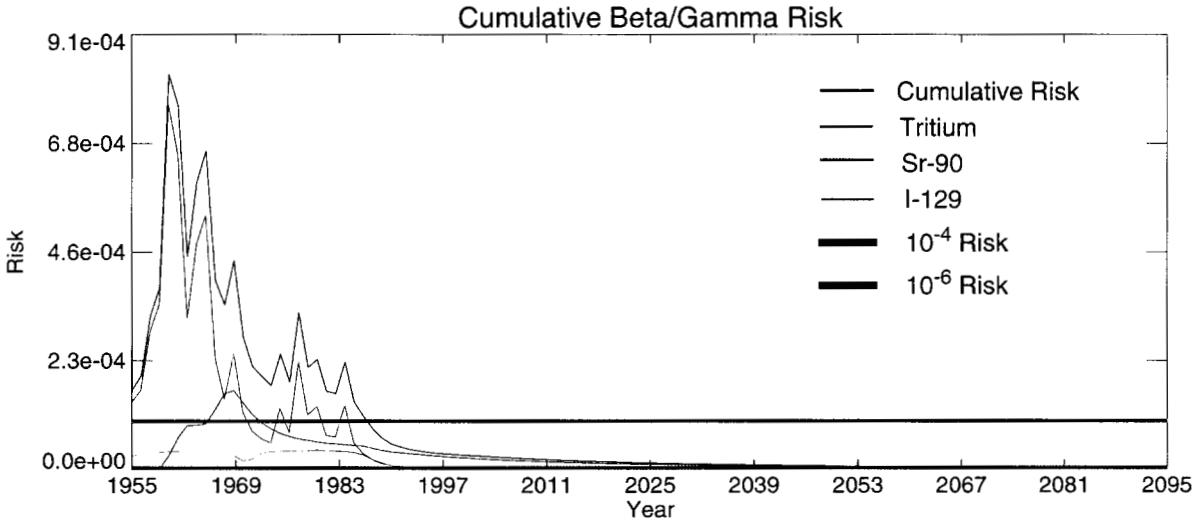

Figure 4-20 Cumulative risk for all simulated COCs.

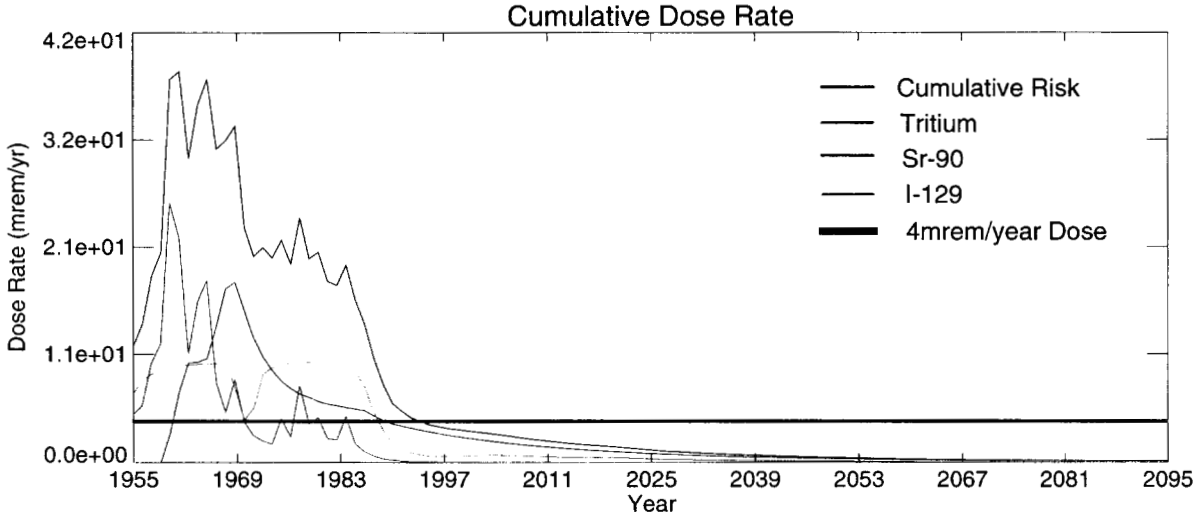

Figure 4-21 Cumulative dose rate for all simulated COCs.

5 MODELING DATA NEEDS

Contaminant concentration data in the aquifer basalt and HI interbed are needed to verify whether modeling is correctly simulating the interaction of the basalt and HI interbed. At this time, elevated I-129 and other contaminant concentrations in the interbed are hypothetical and are based on modeling. Answering this data need can best be accomplished by gathering a vertical profile of aquifer concentrations above, within and below the HI interbed at several locations. The area immediately south of the INTEC percolation ponds and the area near the Central Facilities Area are of particular interest because these areas are predicted to have elevated HI interbed I-129 concentrations now and retain these high concentrations in the year 2095.

The areal extent of contamination in the year 2095 was very sensitive to permeability in both the rediscretized and RI/BRA models, thereby indicating interbed permeability on a field scale at several locations is needed to verify the RI/BRA model's homogeneous 4 mD (0.01 ft/d) and the recalibrated model's 70 mD (0.17 ft/d) HI interbed permeability. HI interbed permeability investigations should not be limited to evaluation of retrieved core because hydrological properties of INEEL core rarely represent INEEL conditions on a field scale. The most useful HI interbed permeability measurements would be obtained from a straddle packer type pumping test of the insitu HI interbed.

Additional HI interbed elevation, interbed thickness, aquifer thickness data are also needed. However, it may not be feasible to gather enough data to adequately describe the HI interbed elevation, interbed thickness, and aquifer thickness with statistical confidence because of the variability of the data and the large area of interest.

There also is a need for better partition coefficients for the contaminants that interact chemically with the aquifer matrix. The RI/BRA analysis was very conservative and probably underestimated the sediment values, but may have overestimated the fractured basalt values. The fractured basalt partition coefficients were estimated from 1/25 of the sediment value and the result may have been to overestimate the amount attenuation from sorption in the aquifer. The approach used by the WAG-7 preliminary RI/BRA modeling (Magnuson and Sondrup, 1998) to estimate fracture basalt K_d values should be used to evaluate WAG-3 contaminant K_d values. Magnuson and Sondrup calculated fractured basalt contaminant K_ds from fracture surface area rather than the mass of the rock matrix, because the contaminant's chemical interaction with the rock is a surface area phenomena.

6 MODELING PATH FORWARD

In the event that sampling of the Snake River Plain Aquifer HI interbed indicates I-129 concentrations significantly exceed the specified action level of 11.4 pCi/L, characterization of the HI interbed should be performed. Data gathered during the characterization effort should be incorporated into the updated model and the model should be used to reassess long term risk and help guide remediation efforts.

The modeling presented in this document represents a first effort in refining the RI/BRA model to more accurately represent the Snake River Plain Aquifer and the interaction of contaminants with the aquifer's HI interbed. However, the model calibration is not complete and needs to incorporate contaminant sampling and characterization data from the HI interbed before predictive simulations can be relied upon. Furthermore, partition coefficients for the fractured basalt need to be reassessed.

7 REFERENCES

Anderson, S. R. and B. D. Lewis, 1991, *Stratigraphy of the Unsaturated Zone at the Radioactive Waste Management Complex, Idaho National Engineering Laboratory, Idaho*, USGS Water-Resource Report 89-4065 (IDO-22080).

DOE-ID, 1997, *Comprehensive RI/FS for the Idaho Chemical Processing Plant OU 3-13 at the INEEL - Part A*, RI/BRA Report, DOE/ID-10534, Nov.

Frederick, D. B and G. S. Johnson, *Estimation of Hydraulic Properties and Development of a Layered Conceptual Model for the Snake River Plain Aquifer at the Idaho National Engineering Laboratory, Idaho*, State of Idaho INEL Oversite Program, Idaho Water Resources Research Institute, Feb. 1996.

Magnuson, S. O., and A. J. Sondrup, 1998, *Development, Calibration and Predictive Results of a Simulator for Subsurface Pathway Fate and Transport of Aqueous- and Gaseous-Phase Contaminants in the Subsurface Disposal Area at the Idaho National Engineering and Environmental Laboratory*, INEEL/EXT-97-00609, Idaho Falls, ID.

Magnuson, S. O., 1995, *Inverse Modeling for Field-Scale Hydrologic and Transport Parameters of Fractured Basalt*, INEL-95/0637, Idaho Falls, ID.

Martian, P., 1997, *Numerical Modeling Support of the Natural Attenuation Field Evaluation for Trichloroethene at the Test Area North, Operable Unit 1-07B, Idaho National Engineering and Environmental Laboratory*, INEEL/EXT-97-01284 Revision 1, Idaho Falls, ID.

McCarthy, J.M., R. C. Arnett, R. M. Neupauer, M. J. Rohe, and C. Smith, 1995, *Development of a Regional Groundwater Flow Model for the Area of the Idaho National Engineering Laboratory, Eastern Snake River Plain Aquifer*, INEL-95/0169, EG&G Idaho Inc., Idaho Falls, ID.

NCRP, 1959, National Committee on Radiation Protection and Measurement , *Maximum Permissible Body Burdens and Maximum Permissible Concentrations of Radionuclides in Air and in Water for Occupational Exposure*, NCRP Report No. 22, National Bureau of Standards Handbook 69 (U.S. Government Printing Office, Washington D.C.).

Robertson, J. B., 1974, Digital Modeling of Radioactive and Chemical Waste Transport in the Snake River Plain Aquifer at the National Reactor Testing Station, Idaho, IDO-22054, U.S. Geological Survey Open File Report, U.S. Geological Survey.

Smith, R. P., 2000, Personal Communication to obtain the active depth of the Snake River Plain Aquifer in the vicinity of the INEEL., Integrated Earth Sciences, Bechtel BWXT Idaho LLC, Idaho Falls, ID.

Vinsome, P. K. W. and G. M. Shook, 1993, Multi-Purpose Simulation, *Journal of Petroleum Science and Engineering*, 9, 29-38, Elsevier Science Publishers B. V., Amsterdam.

Appendix C-1

TETRAD Changes from Version 12.2 to Version 12.7

Version 12.3 Improved wellbore calculation for geothermal simulations

TETRAD uses analytic models of well production rates given well bottom hole pressures, grid block pressures, and fluid properties. This modification implements an improved model for the geothermal simulation mode. The environmental simulations performed for WAG-3 used the multicomponent simulation mode and this change does not affect the WAG-3 simulations.

Version 12.4 Input keywords PERFS, QMULT, ELIMW, BVMYLAY, TMULYLAY, PERMMXYZ, PCMULT, PCUMLXYZ added

These keywords perform the following functions:

(1.) PERFS sets well productivity indices from well screen perforations, which are used in the well production/injection models.

(2.) QMULT allows a specified well constraint (pressure or flux rate) to be multiplied by a specified factor.

(3.) ELIMW sets production rate economic limits. If the production rate falls below the specified value, the well is closed.

(4.) BVMYLAY multiplies the grid block volumes in an entire model layer.

(5.) TMULYLAY multiplies the transmissibility in a specified Y direction plane.

(6.) PERMMXYZ multiplies permeability in a specified rectangular region.

(7.) PCMULT multiplies the capillary pressure by a specified factor. The capillary pressures are calculated from the relative permeability vs. pressure table and multiplied by PCMULT. This is equivalent to specifying a new capillary pressure vs. permeability curve.

(8.) PCUMLXYZ multiplies the capillary pressures in a rectangular region. All of these keywords were not used in the WAG-3 model and these changes do not affect the WAG-3 simulations.

Version 12.5 Input keyword RKREGXYZ added

RKREGXYZ defines which relative permeability table a rectangular region of the model will use. This keywords was not used in the WAG-3 model and this change does not affect the WAG-3 simulations.

Version 12.6 Interlease component mass flows and cumulatives are calculated

Different regions of a model can be defined as "leases" and the amount of water or other component moving between different leases is reported in the output file. The term "lease" is from the oil an gas industry and originates from leasing mineral rights for a specified area. This update only changes what is reported in the output file and does not change the simulation results.

Version 12.7 Molecular diffusion boundary conditions options added and dispersion restart file parameter initialization error corrected

The option for simulating component diffusion in and out of the model by specifying a concentration outside of the model domain was added. The RI/BRA model did not simulate molecular diffusion and the update does not change the WAG-3 RI/BRA result. Correcting the restart file did have an affect the WAG-3 simulations because all the RI/BRA transport simulations were performed from a common restart file which specified the initial aquifer pressure.